THE

LONDON, EDINBURGH, AND DUBLIN

PHILOSOPHICAL MAGAZINE

AND

JOURNAL OF SCIENCE.

[SEVENTH SERIES.]

SUPPLEMENT, NOVEMBER 1932.

XCIII. *Experiments with Capillary Jets.*

By E. TYLER, *D.Sc., F.Inst.P., and* F. WATKIN, *B.Sc., Physics Dept., College of Technology, Leicester* *.

[Plates XXIV.–XXVII.]

Introduction.

THE present investigation is a continuation of the work contained in an earlier paper † entitled "The Characteristic Curves of Liquid Jets," in which examination has been made of the behaviour of different liquids issuing vertically downwards from a capillary tube under varying experimental conditions, an extension also of the work of Smith and Moss ‡.

When a capillary jet falls vertically from a cylindrical orifice, the salient feature is the relation between the continuous part of the cylindrical column, known as the jet-length L, and the velocity of efflux V of the fluid at the orifice. Characteristic curves showing the relation between these quantities reveal the existence of two critical velocities at which discontinuity in the jet-length occurs :

(1) A lower value appearing in the early stage of the jet's existence.

(2) An upper value at a much higher speed of flow.

* Communicated by the Authors.

† Proc. Phys. Soc. xxxvii. (Aug. 1925).

‡ Proc. Roy. Soc. A, xciii. (1917).

These critical velocities owe their origin to different causes; the former is ascribed by Smith and Moss as due to the counterpart of a phenomenon observed by Allen* with falling spheres at low velocities, but a tentative suggestion may be preferred in respect of the possibility of the drop formation occurring at the smaller jet-lengths influencing the initial disturbances producing disintegration at the orifice, causing the jet to break up at unusual small lengths.

The upper critical velocity is due to turbulence as a result of excessive radial velocity within the jet, and represents the stage of the jet's existence where streamline motion within it breaks down.

The general features of a jet-length velocity curve consist of three distinct effects or phases superimposed:

(1) A linear relation between L and V due to streamline motion within the jet, controlled primarily by surface tension, and representing the jet's existence between the critical velocities.

(2) At small jet-lengths, L increases more rapidly with increase in V, due to drop formation occurring near the orifice.

(3) A hyperbolic relation between L and V, the breaking up being due to turbulence controlled by viscosity, corresponding to speeds greater than the upper critical.

Smith and Moss confined their attention in the main to mercury jets of different diameters and surface tensions, falling vertically into aqueous solutions, the density and viscosity of the jet fluid remaining constant, and in their experiments the effect of viscosity of the jet fluid is shown to have very little influence on the critical velocities, simplicity arising from the fact that the inertia forces were predominant, but there are no doubt other cases in which viscosity has an influence, and the viscous forces are no longer negligible. From this point of view, Richardson and one of us (E. T.) have examined some of the properties of jets of different liquids falling vertically through air, in which viscosity is shown to have a marked influence on the upper critical velocity. Furthermore, this upper critical speed is also dependent on surface tension, and at this speed, either of these properties (viscosity and surface tension) operating alone would effect disruption of the jet at the same critical length. Dimensional formulæ have been given to interpret

* Phil. Mag., Sept. 1900.

the results. With regard to viscosity affecting the streamline parts of the curve, experimental evidence suggests that with moderately viscous liquids there is very little influence, but with a highly viscous liquid there might be some modification.

An attempt has therefore been made in the present work to examine further the properties of capillary jets from the following aspects :—

(*a*) Liquid jets in air, more viscous than hitherto used.

(*b*) Liquid jets in different liquids, and the effects of the surrounding medium.

Experimental Arrangement.

The apparatus for producing the jets differed from that previously used in some respects. An inverted glass bottle supported vertically was connected to a large reservoir provided with an air manometer and a valve through which air could be pumped. With the liquid in the bottle and the nozzle attached at the lower end, the pressure in the reservoir was gradually increased step by step, and at each stage, with the liquid issuing freely downwards, the jet-length was measured by means of a cathetometer microscope, and the corresponding velocity of efflux determined by collecting the volume of liquid in a known time, and weighing. The pressure during each set of operations remaining constant because of the large reservoir used.

The jet was illuminated in such a way as to produce two bright vertical bands of reflected light, one down each side, and the end of the continuous portion was taken to be the position at which the two bands merged into the diffused light throughout the section of the jet. In the case of the mercury jets in another liquid, it was found convenient to allow the jet to fall into an inner tube during the time of collecting, provided with an outlet with a fine constriction and tap. The lower part of the collecting apparatus was tilted, when not requiring the measured volume to allow the jet to fall into the outer vessel. For the lighter liquid jets an overflow vessel with side outlet near the top was used.

The nozzles were constructed as before by drawing out narrow bore tubing (1 mm.) and cutting at right angles at the middle section. To ensure cylindricality at the orifice, both halves were tested with water and any pair not giving similar L-V curves was rejected. This condition is most important, as pointed out in the earlier paper, for conicality

or divergence of the nozzle considerably modifies the jet's characteristic.

Results for Jets of Different Liquids formed in Air.

Typical L-V curves are shown in figs. 1 and 2, each curve exhibiting the aforementioned upper and lower critical velocities. Between these points the streamline parts for all the liquids, with the exception of mercury, are straight lines passing through the origin. The slopes, however, vary for the different liquids, and are consistent with previous results obtained by one of us.

Fig. 1.

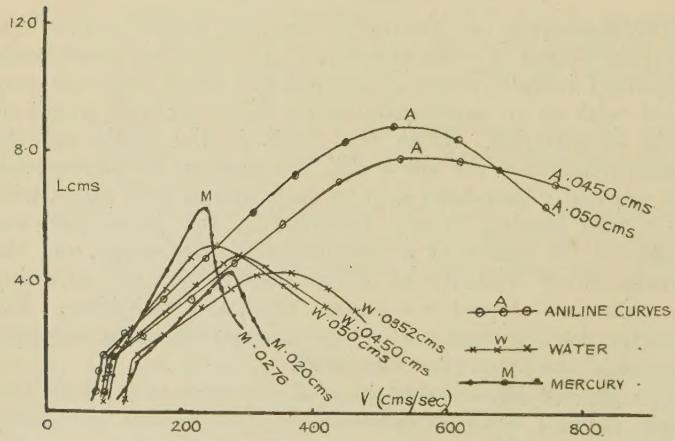

It is possible, following Smith and Moss's application of Lord Rayleigh's theory of instability of liquid jets, to reduce the curves to a single straight line, if the viscosities are of the same order. Information can, however, be obtained from dimensional considerations as follows.

Reduction Formula for Streamline part of L-V *Curves, Viscosity neglected.*

Ignoring for the present the effect of the surrounding medium and the viscosity of the jet, L may depend on the velocity of efflux, V, the diameter of the nozzle, d, the density of the fluid, ρ, its surface tension, σ, and gravity, g.

Instantaneous photographs of mercury jets show very little

tapering, if any, due to the action of gravity, therefore we can neglect the effect of g and put

$$L = K.\rho^x.d^y.\sigma^z.V^n,$$

whence, equating exponents of mass, length, and time,

$$\frac{L}{d} = K\left(V\sqrt{\frac{\rho d}{\sigma}}\right)^n,$$

and since L is proportional to V for a given jet, except in the case of mercury, $n=1$, *i. e.*,

$$\frac{L}{d} = \text{constant}.V\sqrt{\frac{\rho d}{\sigma}}. \quad . \quad . \quad . \quad . \quad (1)$$

Fig. 2.

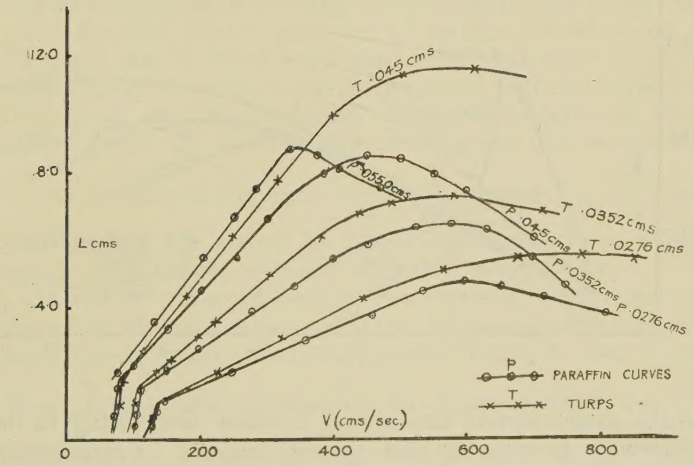

In the case of mercury, $n=\sqrt{2}$, giving

$$\frac{L}{d} = \text{constant}\left(V\sqrt{\frac{\rho d}{\sigma}}\right)^{\sqrt{2}} \quad . \quad . \quad . \quad . \quad (2)$$

To further test these relations, the results in figs. 1 and 2 were obtained, and $\frac{L}{d}$ plotted against $V\sqrt{\frac{\rho d}{\sigma}}$, as shown in fig. 3. With the liquids used it is not possible to represent the streamline parts of all the curves by one straight line passing through the origin when produced. In the case of

mercury the discrepancy between it and the water results is unlikely to be due to viscosity, since the values for both the liquids are approximately the same. The upper and lower critical values of $V\sqrt{\frac{\rho d}{\sigma}}$ are, however, approximately the same.

The possibility of the non-wetting effect of mercury with glass has also been shown to be non-valid as the cause of this discrepancy.

Accepting Smith and Moss's explanation, it may be that the initial disturbance producing disintegration at the orifice is influenced by pulsations of pressure occuring within the jet as each drop forms and breaks away, and the effects are not

Fig. 3.

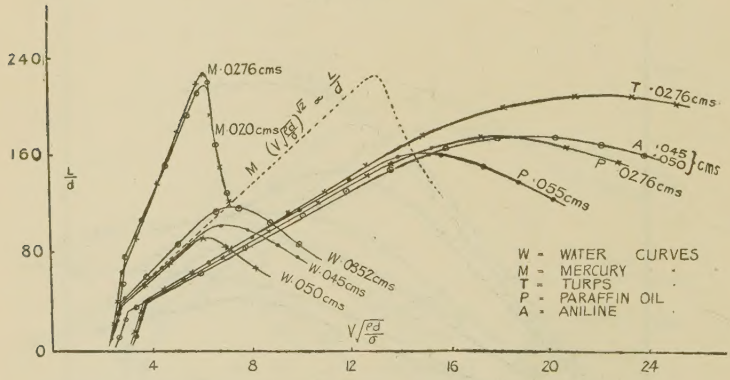

of the same relative importance in each case owing to the difference in density and surface tension. Furthermore, the disturbance occuring at the point of disruption may not readily reach the orifice when the velocity of capillary waves travelling up the jet is considered in the different cases.

Referring to the results for aniline, turps, and paraffin in air, it will be seen that the slopes of the linear parts of the streamline curves are not the same as for water; moreover, the upper critical $V\sqrt{\frac{\rho d}{\sigma}}$ is about 20 for these liquids, compared with 7 for water.

The higher critical value of $V\sqrt{\frac{\rho d}{\sigma}}$ is an attribute of the higher viscosity of the liquids, and is consistent with the

theory given in the earlier paper, in which the effect of viscosity on the upper critical $V\sqrt{\frac{\rho d}{\sigma}}$ is represented by the relation

$$V\sqrt{\frac{\rho d}{\sigma}} = A + B\frac{\mu}{\sqrt{\sigma\rho d}},$$

where A and B are constants, and μ = the viscosity of the liquid.

A summary of the upper and lower critical $V\sqrt{\frac{\rho d}{\sigma}}$ is included in Table I.

Effect of Viscosity on the Jet's Streamline Characteristic.

The non-coincidence of the aniline, paraffin, and turps results with water values given in fig. 3, was thought to be due to differences in viscosity of the liquids, and to test this point further, treacle solutions of various viscosities up to 16 times that of water were used, it being known that very little change of surface tension occurred with the concentrations used, and the maximum change in density was about 20 per cent. To test for any modification due to viscosity it was considered sufficient to plot $\frac{L}{d}$ against $V\sqrt{\frac{\rho d}{\sigma}}$, and such results are shown in figs. 4 and 5 and Table II. for nozzles of diameter ·450 and ·501 mm. respectively.

It will be observed that as the viscosity is increased, the slopes of the streamline parts of the curves decrease, but each curve when produced passes through the origin. There is the usual increase in the upper critical $V\sqrt{\frac{\rho d}{\sigma}}$ with increase in viscosity, and with the more viscous liquids it was not always possible to reach these points with the apparatus used.

Application of Lord Rayleigh's Theory of Liquid Jets, with Modification for Viscosity, to account for the Streamline parts of the L-V *Curves for Jets formed in Air.*

In attempting to explain the breaking-up of a cylindrical column of liquid in the light of Savart's results *, Plateau † has shown that when a disturbance acts upon such a column, alternate swellings and contractions are produced under the

* *Ann. Chim. Phys.* vol. liii.

† 'Statique des liquides,' p. 354 (1873).

Table I.

Results for Jets in Air.—Critical Velocities.

Liquid.	Diameter of nozzle d cm.	Temperature °C.	σ dynes/cm.	ρ gm./cc.	Lower critical velocity V_1 cm./sec.	Upper critical velocity V_2 cm./sec.	$V_1\sqrt{\frac{\rho d}{\sigma}}$.	$V_2\sqrt{\frac{\rho d}{\sigma}}$.	$\frac{\mu}{\sqrt{\sigma\rho d}}\times 10^4$.
Paraffin (*a*) ...	·0550	20	26·4	·804	—	240	—	13·9	140
	·0276	20	26·4	·804	110	590	3·19	17·1	199
Paraffin (*b*) ...	·0352	17·5	26·0	·790	100	600	3·26	19·6	212
	·0450	17·7	26·0	·790	75	450	2·76	16·6	188
Aniline	·050	21·5	40·0	1·028	85	560	3·04	20·0	230
	·045	22·0	40·0	1·028	98	575	3·34	19·6	238
Water	·050	20	72·0	1·00	95	245	2·50	6·45	53·0
	·045	19	72·0	1·00	100	290	2·50	7·25	56·8
	·0352	16	72·0	1·00	110	350	2·44	7·74	70·4
Mercury	·0276	20	547	13·55	106	240	2·78	6·29	—
	·0200	20	547	13·55	130	280	2·89	6·22	—
Turpentine ...	·0352	14·5	27·0	·87	100	550	3·43	18·9	205
	·0450	14·5	27·0	·87	80	490	3·10	19·0	182
	·0276	16·5	27·0	·87	115	725	3·50	22·0	220

influence of surface tension, and if the "wave-length" of these appearances exceeds the circumference of the column, instability is produced, and the column is resolved into drops.

Fig. 4.

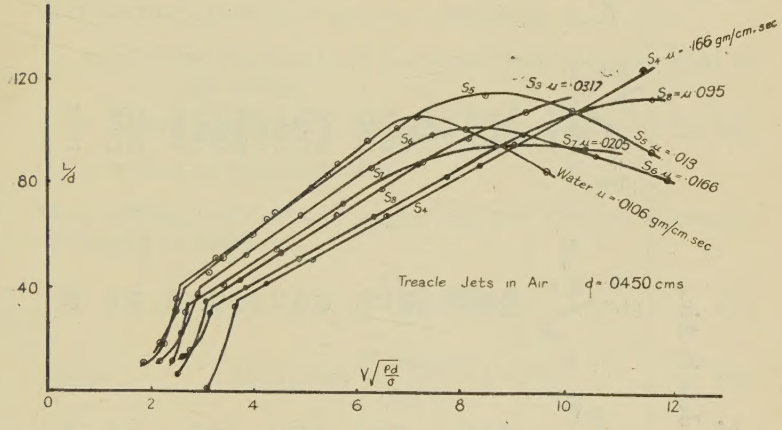

Fig. 5.

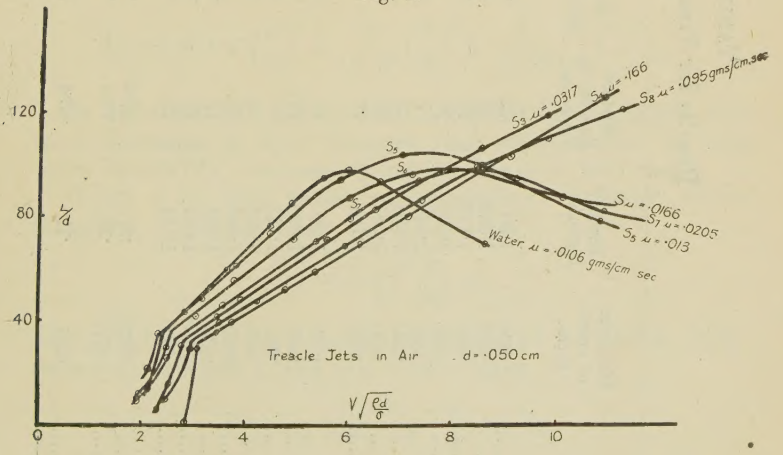

Rayleigh *, adopting this criterion of instability to a liquid jet, points out that any disturbance impressed upon the liquid column at the orifice will, if the wave-length exceeds

* 'Sound,' ii. p. 360.

Table II.

Results for Treacle Jets in Air.

Liquid.	Diameter of nozzle d cm.	Density ρ gm./cc.	Surface tension σ dynes/cm.	Viscosity gm./cm. sec.	$\frac{L}{d}$ at $V\sqrt{\frac{\rho d}{\sigma}} = 6.$	$\frac{L}{d} \div V\sqrt{\frac{\rho d}{\sigma}}$ for streamline curves.	$\left[\frac{\sqrt{\sigma\rho d}}{\mu}\right]^{\frac{3}{2}} \div 4095.$
Water	·050	1·00	72	·0106	100	16·66	2400
Aniline	·050	1·028	40	·0346	68	11·33	264
Solution 3	·050	1·118	72	·0317	73	12·16	505
Solution 4	·050	1·221	72	·166	65	10·83	45
Solution 5	·050	1·040	72	·013	95	15·83	1820
Solution 6	·050	1·064	72	·0166	84	14·0	1280
Solution 7	·050	1·081	72	·0205	77	12·83	940
Solution 8	·050	1·184	72	·0950	67	11·16	102
Water	·045	1·00	72	·0106	97	16·16	2220
Aniline	·045	1·028	40	·0346	68	11·33	249
Solution 3	·045	1·118	72	·0317	71	11·83	465
Solution 4	·045	1·221	72	·166	62	10·33	41
Solution 5	·045	1·040	72	·013	92	15·33	1685
Solution 6	·045	1·064	72	·0166	82	13·66	1190
Solution 7	·045	1·081	72	·0205	75	12·50	870
Solution 8	·045	1·184	72	·095	64	10·66	94
Turpentine	·0276	·87	27·0	·0177	64	10·66	306
Paraffin	·0276	·79	26·4	·0180	68	11·33	366
Paraffin	·055	·79	26·4	·0180	73	12·16	604

the circumference of the jet, produce waves which travel down the jet; at the same time the amplitude of the disturbance grows exponentially until finally the continuity of the jet is destroyed.

The time of disintegration of such a column will depend on the magnitude of the initial disturbance at the orifice, and the rate at which it grows. Assuming

a_0 = initial amplitude of the wave disturbance created at the orifice,

a = final amplitude at the point of breaking-up of the jet,

t = time of disintegration,

then putting $a = a_0 e^{qt}$ and neglecting the effect of viscosity, according to Rayleigh

$$q = \sqrt{\frac{8\sigma}{\rho d^3}} \cdot \mathrm{F}(z), \quad \ldots \ldots \quad (1)$$

where

$$[\mathrm{F}(z)]^2 \equiv \frac{iz \cdot \mathrm{J}_0'(iz)}{\mathrm{J}_0(iz)} (1 - z^2), \quad \ldots \ldots \quad (2)$$

in which $z = \dfrac{\pi d}{\lambda}$ and

$$\mathrm{J}_0(iz) = 1 + \left(\frac{z}{2}\right)^2 + \frac{1}{(2\,!)^2}\left(\frac{z}{2}\right)^4 + \frac{1}{(3\,!)^2}\left(\frac{z}{2}\right)^6 + \ldots$$

In equation (2), $i\mathrm{J}_0'(iz)$ and $\mathrm{J}_0(iz)$ are both positive, and as z decreases, q first becomes real when $z = 1$. At this point instability commences, but its degree is very small.

When z is very small, corresponding to large wave-lengths,

$$q = 2\sqrt{\frac{\sigma}{\rho d^3}} \cdot z,$$

so that q is again very small, hence q has a maximum value between $z = 0$ and 1, and this occurs when

$$\mathrm{F}(z) = \cdot 343 \quad \text{or} \quad \frac{\lambda}{d} = 4 \cdot 51.$$

Attempting now to include viscosity μ, we may express q in terms of σ, ρ, d, and μ from dimensional considerations.

It can easily be shown that

$$q \propto \frac{1}{t} \text{ or } \propto \sqrt{\frac{\sigma}{\rho d^3}} \left(\frac{\mu}{\sqrt{\sigma \rho d}}\right)^n, \text{ where } n \text{ is an unknown index.}$$

Equation (1) may therefore be modified as

$$q = \sqrt{\frac{8\sigma}{\rho d^3}}\left(\frac{\mu}{\sqrt{\sigma\rho d}}\right)^n . \mathrm{F}(z). \quad . \quad . \quad . \quad . \quad (3)$$

Remembering that

$$q = \frac{1}{t}\log_e \frac{a}{a_0} \quad \text{and} \quad \mathrm{L} = \mathrm{V}t$$

(supposing V constant during descent of the liquid), then substituting for q and t in equation (3), we get

$$\frac{\mathrm{L}}{d} = \mathrm{V}\sqrt{\frac{\rho d}{\sigma}} \cdot \left(\frac{\sqrt{\sigma\rho d}}{\mu}\right)^n \cdot \frac{1}{2\sqrt{2}\mathrm{F}(z)} \cdot \log_e \frac{a}{a_0}.$$

The unknown term $\left(\frac{\sigma\rho d}{\mu}\right)^n$ being non-dimensional, its general form may be expressed as $f\left(\frac{\sqrt{\sigma\rho d}}{\mu}\right)$, and putting $y = 2\sqrt{2}\,\mathrm{F}(z)$, we derive as a general relationship,

$$\frac{\mathrm{L}}{d} = \mathrm{V}\sqrt{\frac{\rho d}{\sigma}} \cdot f\left(\frac{\sqrt{\sigma\rho d}}{\mu}\right) \cdot \frac{1}{y} \cdot \log \frac{a}{a_0},$$

which is the simplest theoretical relation between the variables involved. The value of $f\left(\frac{\sqrt{\sigma\rho d}}{\mu}\right)$ must be derived from experimental data.

We may, however, expand $f\left(\frac{\sqrt{\sigma\rho d}}{\mu}\right)$ as a series of terms putting

$$f\left(\frac{\sqrt{\sigma\rho d}}{\mu}\right) = \mathrm{A} + \mathrm{B}\left(\frac{\sqrt{\sigma\rho d}}{\mu}\right)^x + \text{higher power terms},$$

in which A, B, and x are constants to be evaluated. Neglecting the higher power terms, this leads finally to the relation

$$\frac{\mathrm{L}}{d} = \mathrm{V}\sqrt{\frac{\rho d}{\sigma}}\left[\mathrm{A} + \mathrm{B}\left(\frac{\sqrt{\rho\sigma d}}{\mu}\right)^x \frac{1}{y}\right] \cdot \log \frac{a}{a_0}.$$

Simplicity now arises from the experimental results shown in figs. 4 and 5, as a result of plotting $\frac{\mathrm{L}}{d}$ against $\mathrm{V}\sqrt{\frac{\rho d}{\sigma}}$, for it will be observed that each graph, for the streamline parts, consist of straight lines passing through the origin, the slopes decreasing as the viscosity increases. The

physical significance of this criterion leads us to assume that, provided maximum instability exists, giving y a maximum constant value (and photographic evidence supports this), $\log \frac{a}{a_0}$ is also constant for a given fluid, which simplifies the deduction of x.

It is found that $x = \frac{3}{2}$ in order to satisfy the linear relationship of equation (5), for a plot of $\frac{L}{d}$ $\left(\text{at constant } V\sqrt{\frac{\rho d}{\sigma}} = 6\right)$ and $\left(\frac{\sqrt{\sigma\rho d}}{\mu}\right)^{3/2}$ produces a straight line graph as shown in fig. 6, the values of A and B being 1 and $\frac{1}{4095}$ respectively.

Fig. 6.

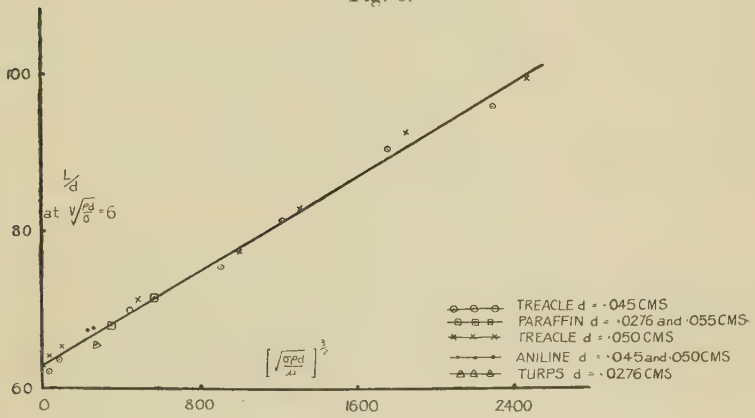

Thus the experimental results for the streamline parts are well represented by the equation

$$\frac{L}{d} = V\sqrt{\frac{\rho d}{\sigma}}\left[1 + \frac{1}{4095}\left(\frac{\sqrt{\sigma\rho d}}{\mu}\right)^{3/2}\right]\frac{1}{y}.\log\frac{a}{a_0}, \quad . \quad (6)$$

the term in the brackets being the correction necessary to account for the influence of viscosity.

In order to test the validity of this expression, assuming constancy of $\frac{1}{y}.\log\frac{a}{a_0}$, we should expect to be able to reduce the family of curves for all the liquids to one single curve by plotting $\frac{L}{d}$ against $V\sqrt{\frac{\rho d}{\sigma}}\left[1 + \frac{1}{4095}\left(\frac{\sqrt{\sigma\rho d}}{\mu}\right)^{3/2}\right]$, and the

results of this are shown in figs. 7 and 8, where verification is clearly established.

A simple relation and physical significance is suggested by such results as follows :—

Denoting the variables for two different liquids by the

Fig. 7.

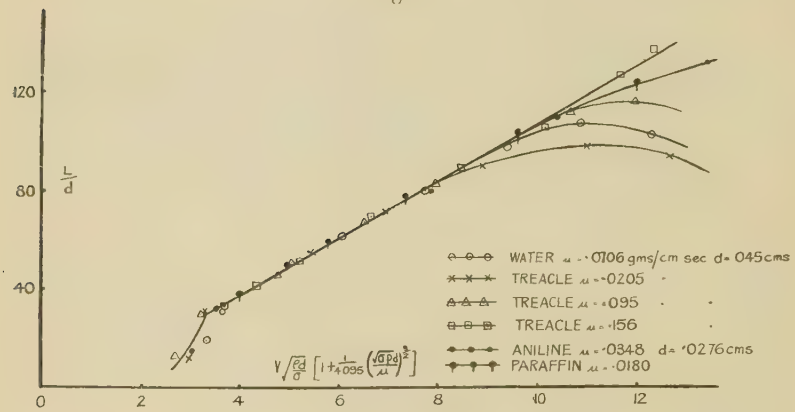

Fig. 8.

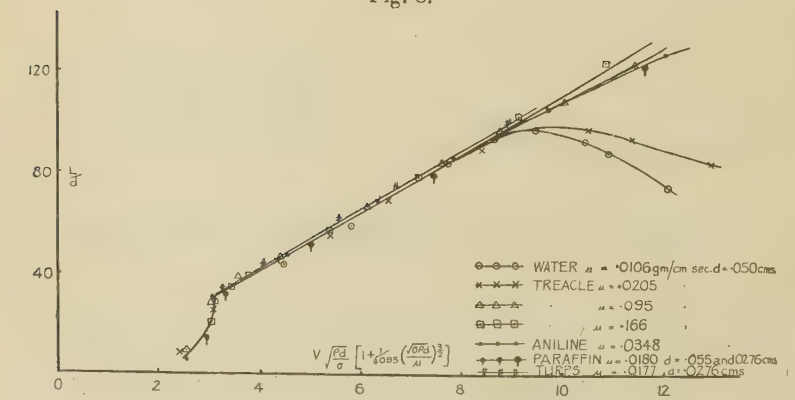

suffixes 1 and 2 respectively, and supposing different nozzles are used, we have, by equation (6),

$$\frac{L_1}{d_1} = V_1\sqrt{\frac{\rho_1 d_1}{\sigma_1}}\left[1+\frac{1}{4095}\left(\frac{\sqrt{\sigma_1\rho_1 d_1}}{\mu_1}\right)^{3/2}\right]\left[\frac{1}{y}\log\frac{a}{a_0}\right]_1$$

and

$$\frac{L_2}{d_2} = V_2\sqrt{\frac{\rho_2 d_2}{\sigma_2}}\left[1+\frac{1}{4095}\left(\frac{\sqrt{\sigma_2\rho_2 d_2}}{\mu_2}\right)^{3/2}\right]\left[\frac{1}{y}\log\frac{a}{a_0}\right]_2$$

Since all the results in figs. 6 and 7 fall on a single reduced curve, it follows that

$$\left[\frac{1}{y}\log\frac{a}{a_0}\right]_1 = \left[\frac{1}{y}\log\frac{a}{a_0}\right]_2$$

provided that $\frac{L_1}{d_1} = \frac{L_2}{d_2}$ when

$$V_1\sqrt{\frac{\rho_1 d_1}{\sigma_1}}\left[1+\frac{1}{4095}\left(\frac{\sqrt{\sigma_1\rho_1 d_1}}{\mu_1}\right)^{3/2}\right] = V_2\sqrt{\frac{\rho_2 d_2}{\sigma_2}}\left[1+\frac{1}{4095}\left(\frac{\sqrt{\sigma_2\rho_2 d_2}}{\mu_2}\right)^{3/2}\right].$$

Furthermore, if y is constant, we obtain the condition that the ratio of the initial and final amplitudes of disintegrating disturbance is the same for any pairs of liquids when the velocities V_1 and V_2 are in the ratio

$$\sqrt{\frac{\sigma_1}{\rho_1 d_1}}\left[1+\frac{1}{4095}\left(\frac{\sqrt{\sigma_2\rho_2 d_2}}{\mu_2}\right)^{3/2}\right] : \sqrt{\frac{\sigma_2}{\rho_2 d_2}}\left[1+\frac{1}{4095}\left(\frac{\sqrt{\sigma_1\rho_1 d_1}}{\mu_1}\right)^{3/2}\right].$$

Concerning the possible complex nature of the initial disturbance produced at the orifice, we can regard it as resolved into components of different wave-lengths and amplitudes whose effects are superimposed, and the relation between the wave-length and amplitude of these components, we may suppose, determines the degree of instability of the jet.

The time of disintegration of such jets for streamline characteristics where the viscosity effect is considered will be given by

$$t = \sqrt{\frac{\rho d^3}{\sigma}}\left[1+\frac{1}{4095}\left(\frac{\sqrt{\sigma\rho d}}{\mu}\right)^{3/2}\right]\frac{1}{y}\log\frac{a}{a_0}.$$

Liquid Jet in a Liquid. Effect of the Surrounding Medium on the Jet-length.

Examination of the properties of jets of different liquids falling into other liquids affords an opportunity of extending the range of this work further than hitherto attempted, and enables the controlling influence of the surrounding medium upon the jet's characteristics to be investigated.

In the earlier work of Smith and Moss, mercury jets of different diameters fell into aqueous solutions of potassium

cyanide and mercurous nitrate, the density and viscosity of the jet liquid remaining constant. Under such conditions the effect of the viscosity of the surrounding fluid is approximately constant, and therefore exerts a constant controlling influence on the jet.

Any attempt to increase the viscosity of the surrounding liquid, keeping the surface tension constant with respect to the jet fluid, should result in reducing the rate of growth of the initial amplitude of the disturbance created at the orifice, with a consequent increase in the time of disintegration for a given jet speed. Also the greater the viscosity of the

Fig. 9.

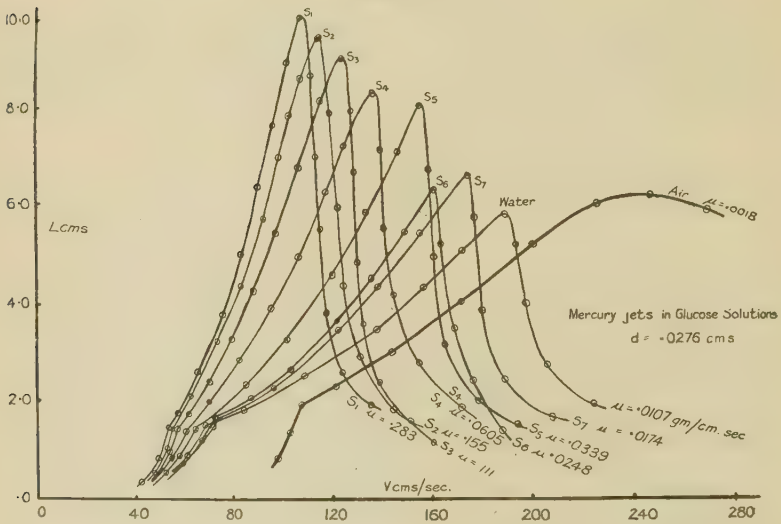

surrounding fluid, the less will be the disturbed motion at the orifice, and hence the initial amplitude will be smaller, and therefore a longer time will be taken for the jet to break up. Since $t = \frac{L}{V}$, it follows that for a more viscous liquid medium, a longer jet will be produced for a given speed of flow. Rayleigh noticed this, but made no quantitative observations.

In order to test such inference, the surface tension between the jet and the surrounding fluid was maintained constant by allowing mercury jets to fall vertically downwards into glucose solutions of varying viscous strengths. The viscosity

was increased to as much as 28 times that of water, while the change in density was only about 21 per cent.

In figs. 9 and 10 and Table III. results are shown for nozzles of diameters ·20 and ·276 mm. respectively, and confirm the foregoing suggestions. It is evident that the properties of the surrounding medium in respect of viscosity and density do considerably modify the jet's characteristics. To further bring out this point, pairs of liquids, such as water and paraffin, water in turps and benzene, were used, each in turn as the jet with the other as the surrounding medium, the surface tension * between the two liquids remaining constant (if time effects are inappreciable). Any differences

Fig. 10.

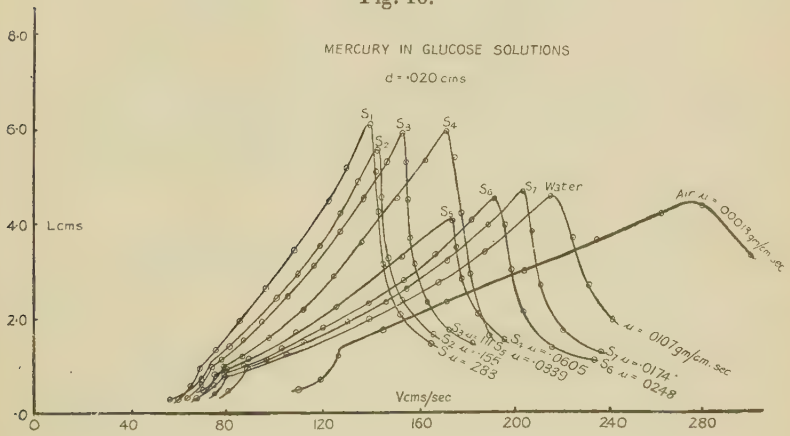

in the results could only be due to either the viscosity or the density of the liquids.

Furthermore, in view of the lighter liquids used, we should expect to find more marked changes than with mercury in respect of the influence of the surrounding medium.

Other liquids, such as aniline in water, mercury in normal and $\frac{N}{4}$ potassium hydroxide, and in $\frac{N}{4}$ mercurous nitrate were used as special cases in which the interfacial surface tensions were of different values and did not vary much with time.

* Measured by (1) Drop method, (2) Capillary Rise method.

Table III.

Results for Mercury Jets in Glucose Solutions of Different Viscosities.

σ=427 dynes/cm. ρ=13·59 gm./c.c. } For Hg.			Nozzle d = ·0276 cm.				Nozzle d = ·020 cm.			
Surrounding medium.	Viscosity of medium μ_m gm./cm. sec.	Density of medium ρ_m gm./c.c.	Lower critical velocity V_1 cm./sec.	Upper critical velocity V_2 cm./sec.	$V_1\sqrt{\frac{\rho d}{\sigma}}$.	$V_2\sqrt{\frac{\rho d}{\sigma}}$.	Lower critical velocity V_1 cm./sec.	Upper critical velocity V_2 cm./sec.	$V_1\sqrt{\frac{\rho d}{\sigma}}$	$V_2\sqrt{\frac{\rho d}{\sigma}}$
Air	·00018	·00129	106	240	2·78	6·29	130	280	2·89	6·22
Solution 1 ...	·283	1·215	54	107	1·60	3·18	70	140	1·76	3·53
Solution 2 ...	·155	1·205	56	114	1·66	3·37	73	142	1·84	3·58
Solution 3 ...	·111	1·185	57	124	1·69	3·67	75	154	1·89	3·88
Solution 4 ...	·0605	1·153	61	137	1·81	4·05	78	173	1·96	4·36
Solution 5 ...	·0339	1·110	66	156	1·96	4·62	76	175	1·92	4·41
Solution 6 ...	·0248	1·089	74	164	2·19	4·85	80	194	2·02	4·89
Solution 7 ...	·0174	1·06	75	178	2·21	5·28	82	205	2·06	5·17
Water	·0107	1·00	70	187	2·07	5·55	90	218	2·26	5·50

Fig. 11 *a*.

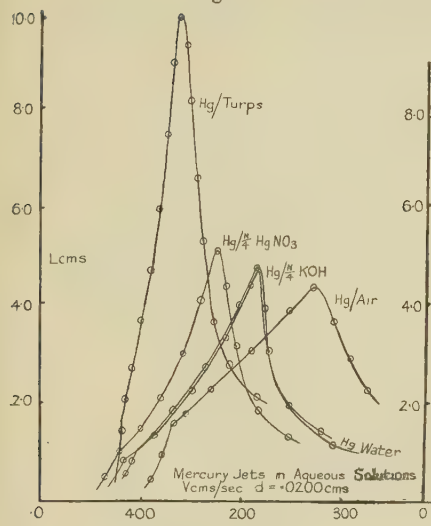

Fig. 11 *b*.

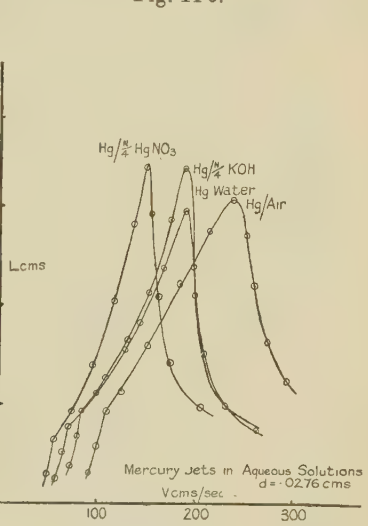

Fig. 12.

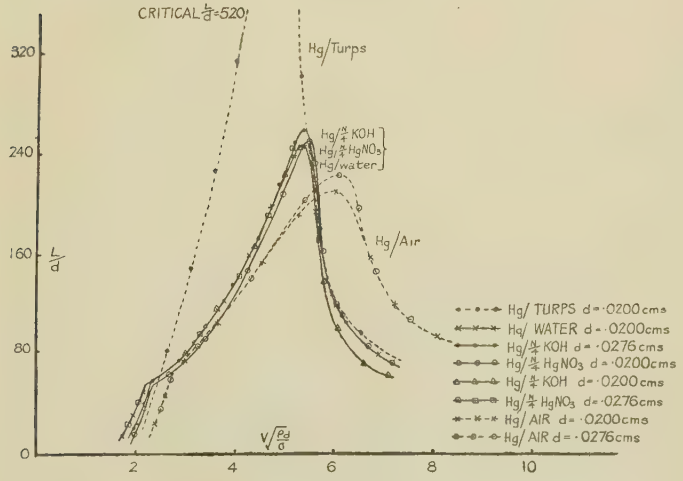

Results for Liquid Jets in Different Liquids.

Typical families of the L-V curves are included in figs. 13, 14, and 15, and exhibit some peculiar and very interesting effects.

In the case of the lighter liquids it will be observed that the speeds of the jets are very much less than in the case of

Fig. 13.

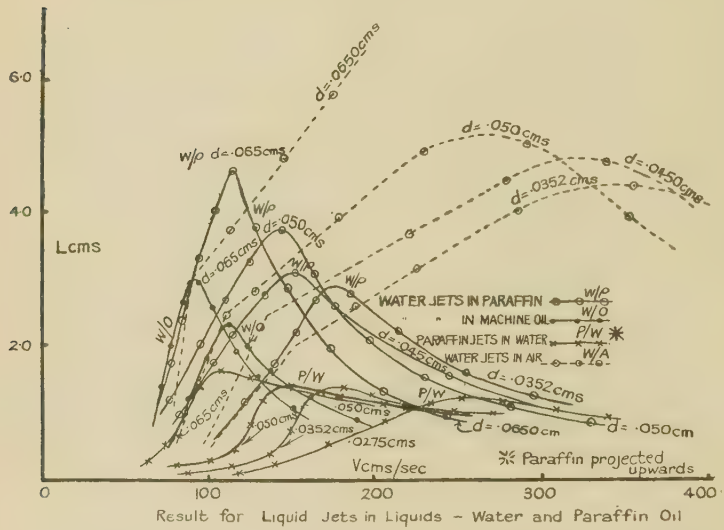

Result for Liquid Jets in Liquids – Water and Paraffin Oil

Fig. 14.

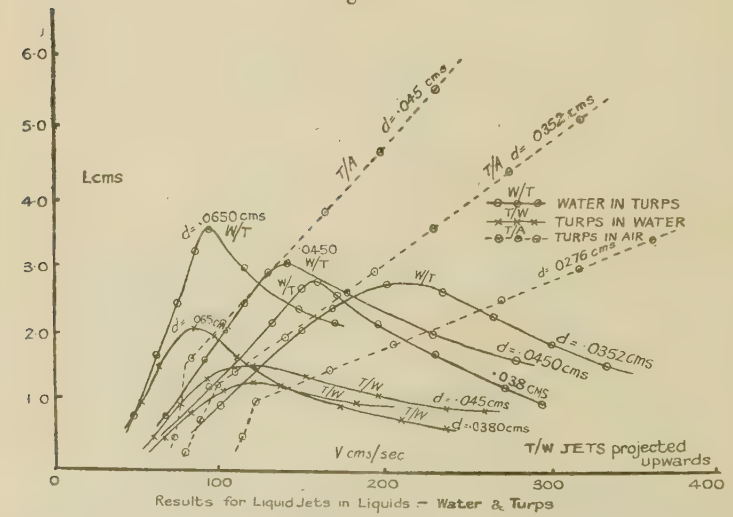

Results for Liquid Jets in Liquids – Water & Turps

jets formed in air with the same nozzles, and the jet-lengths never reach anything like the values attained in air. While

the upper critical velocity is still in evidence, the lower seems to be non-existant or comes in at the drop formation stage.

With mercury falling into liquids of constant surface tension but of varying viscosity, we have previously seen that longer jet-lengths are obtained, with correspondingly smaller critical velocities, for increased viscosity of the medium surrounding the jet. When the surface tension between the mercury and the surrounding fluid is changed, generally a reduction, there is also a reduction in the critical velocity, though not of the same extent as with the lighter liquids, the change is, however, in the right direction, and is in accordance with the predictions outlined by Smith and Moss from application of Rayleigh's theory.

Fig. 15.

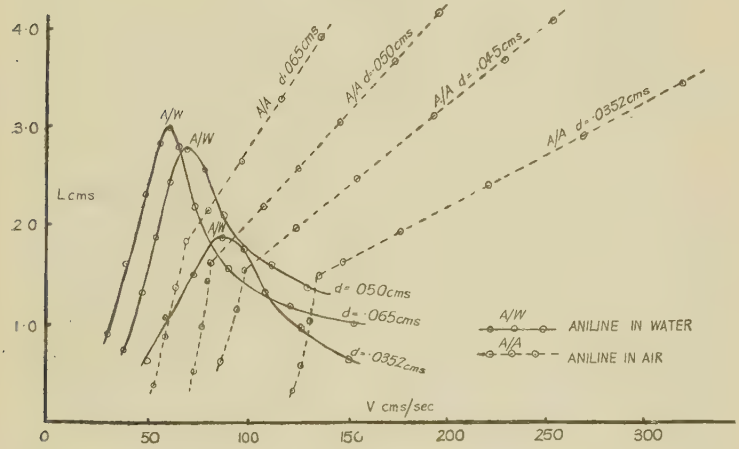

This increased jet-length phenomenon exhibited by the mercury jets is also characteristic of the lighter liquids, for it will be observed (figs. 13, 14, and 15) that even with the pairs of liquids selected, one acting as the jet and the other as the surrounding medium (*i. e.*, surface tension constant), for a given nozzle, longer jets are produced when the liquid with the higher viscosity is the surrounding medium. Furthermore, the greater the viscosity of the fluid surrounding the jet, the longer are the jet-lengths corresponding to the upper critical velocities.

A possible cause of the shorter jet-length in the case of the less dense liquids may be the large reduction in surface tension produced generally with most of the liquids. The drops formed at the point of disruption of the jet are very

much larger than those formed in air, and will therefore produce a greater reaction on the jet, the disturbance of which will get back more readily to the orifice (as a result of the smaller jet speeds).

In order to confirm this point, instantaneous photographs were taken, using the spark discharge of a Leyden jar as illuminant.

Figs. 1 & 2 (Pl. XXIV.) are typical exposures for mercury jets falling through air from a cylindrical nozzle and from a diverging nozzle. Figs. 3 & 4 (Pl. XXV.) are for aniline falling through air and through water for the same nozzle $d = \cdot 501$ mm. Figs. 5, 6, & 7 (Pl. XXVI.) are for water, coloured with Meldola's Blue, falling through air, paraffin, and turpentine respectively, also for the nozzle $d = \cdot 501$ mm. The exposures on figs. 6 & 7 (Pl. XXVI.) are of particular interest, since they were taken at different jet speeds less than and greater than the upper critical value. It is evident that in both cases of a rapidly diverging nozzle and liquid jets in other liquids the size of the drops are very much greater, and the bigger the reduction in the surface tension between the liquids, the larger the drops formed.

This increased predominence of drop formation disturbance will therefore tend to increase the turbulence within the jet, which controls the upper critical velocity, with consequent shortening of the jet-length, and it is of interest to compare these results with those for mercury jets * in air using a rapidly diverging nozzle, where excessive drop formation is encouraged, and its disturbance easily gains access to the nozzle. There is some analogy in the two cases.

Viscosity of Surrounding Medium Large.

In the case where the viscosity of the medium is very large compared with that of the jet, and particularly where there is a marked reduction in the surface tension between the liquids, considerable slowing up of the jet will take place as it leaves the orifice, with consequent broadening of its cross-section. As a result of this, much larger drops will be formed at the end of the jet, and hence greater reaction effect at the orifice. Under such conditions, this reaction of drop formation should manifest itself throughout the entire existence of the jet for all speeds.

By way of confirmation of this point, water jets were allowed to fall vertically into machine oil, whose viscosity was about 90 times that of water, and density ·91 gm./c.c.

* Proc. Phys. Soc. xxxvii. p. 301 (Aug. 1925).

Results obtained for nozzles $d = \cdot 50$ and $\cdot 65$ mm. are included in fig. 13 and prove the validity of the foregoing conclusion.

Very large drops were formed at the end of the jet, which were very much retarded. In fact, at the lower speeds it was possible to produce standing waves or undulations on the jet similar in character to those obtained by Brinkworth *, using a solid obstacle in the path of a slowly-moving jet of water.

In the liquid drop case, the large drop about to be detached from the lower end of the jet acts as the obstacle, since it moves much slower than the jet elements impinging on it. Typical stages of such formation in castor oil are shown in figs. 9 & 10 (Pl. XXVII.). Fig. 8 (Pl. XXVII.) shows the corresponding water jets in air for same nozzle.

It will also be observed that the L-V curves for water falling into machine oil coincide with the L-V curves for water falling through air, using the same nozzles (see fig. 13), and the maximum jet-lengths obtainable are those corresponding to the lower critical velocities in the water-air case. This coincidence clearly indicates the cause of the existence of these lower critical velocities, namely, the speed at which any disturbance due to drop formation at the disruption point in the jet ceases to gain access to the orifice owing to the predominance of the surface tension forces controlling the streamline motion within the jet.

Examining the results for mercury falling into different liquids, from this point of view of drop formation, since the surface tension forces between the mercury and the surrounding media are generally much larger than with the lighter liquids, the drops formed will not be so large. The amplitude of disturbance due to drop formation will therefore be less at the disruption point (*i. e.*, apart from the difference in density).

Moreover, with an increase in viscosity of the surrounding medium, such disturbances tending to travel back to the orifice will become damped out, and in view of the already existing longer jet lengths, will not reach the nozzle.

Since with mercury we are dealing with a liquid of high density, the jets will not be retarded to anything like the same extent as with the lighter liquids, and this also tends to prevent these reaction disturbances from reaching the orifice. The main effect on a heavy liquid like mercury therefore appears to be either a reduction of the initial amplitude of the disintegrating disturbance created at the

* Proc. Roy. Soc. xliv. pt. 2 (March 1932).

orifice, or retardation in its rate of growth, possibly both simultaneously. Accepting either explanation, both effects operate in the same direction, resulting in the production of longer jets for a given speed.

Adhesion of Jet Liquid at the Orifice.

The condition of escape of the jet from the orifice when using the pairs of different liquids for comparison purposes must not be overlooked. Whereas in the case of water-jets issuing into lighter non-miscible liquids, considerable adhesion of the water to the lower end and sides of the nozzle is exhibited, thus producing a marked contraction of the jet. With the lighter liquids (oil and turpentine) projected upwards into water, this property is practically negligible, the jets travelling straight out from the nozzle with none or very small contraction. The effective diameter of the jet at the orifice in the former case is thus increased, and it is therefore conceivable that the tendency of the water to adhere to the nozzle will act as a protecting influence on the initial amplitude of disturbance at the orifice, freeing it to a greater degree from extraneous reactions, particularly that due to drop formation at the end of the jet, which is more effective with the lighter liquids projected upwards into water. We should therefore expect to obtain longer jets with water in either paraffin or turpentine than when either paraffin or turpentine are projected into water, which is what is found.

Examination of the oscillating nature of the jets revealed greater suction back into the orifice immediately after disruption of a drop from the end of the jet, when the oils are projected into water, than in the reverse case.

The magnitude of drop formation reaction reaching the orifice appears to be controlled by the adhesive property of the jet liquid to the nozzle, and such reactions are more effective with the lighter oils projected into water than with water-jets formed in them. Increase in the adhesion of the jet to the nozzle thus operates in the same way as increase in viscosity of the surrounding medium, namely, the production of longer jets.

Theoretical Discussion of Results for Liquid Jets in Liquids.

Case 1.—*Viscosity of Jet and Surrounding Medium Constant.*

Ignoring for the moment the controlling influence of viscosity of the jet and the surrounding medium, and

referring to the theory for liquid jets in air, equation (6), when simplified, may be written as

$$\frac{L}{d} = V\sqrt{\frac{\rho d}{\sigma}} \cdot \frac{1}{y} \cdot \log \frac{a}{a_0}, \quad . \quad . \quad . \quad . \quad (7)$$

where, in the case of a liquid jet in a liquid, σ is the surface tension between the liquids, and ρ is the density of the jet fluid. This is the equation developed and tested qualitatively by Smith and Moss, employing their mercury jets, in which the viscosity of the surrounding medium was kept constant.

Since only relative data was given by these authors, we have applied our results quantitatively for mercury jets falling into various solutions, the viscosity and density of which were also constant.

(a) *L-V Characteristics of Mercury Jets in Aqueous Solutions (Viscosity Small).*

It was considered sufficient from the above equation to plot $\frac{L}{d}$ against $V\sqrt{\frac{\rho d}{\sigma}}$, the upper and lower critical values being included in Table IV. for comparison purposes.

Fig. 12 shows such results and confirms the validity of equation.

All the results fall on a single reduced curve, which, as pointed out by Smith and Moss, suggests a simple criterion of the physical conditions existing.

Again denoting the variables for two different liquids surrounding the mercury jets by the suffixes 1 and 2 respectively, and supposing different nozzles are used, we have, by equation (7),

$$\frac{L_1}{d_1} = V_1\sqrt{\frac{\rho d_1}{\sigma_1}}\left[\frac{1}{y}\log\frac{a}{a_0}\right]_1$$

and

$$\frac{L_2}{d_2} = V_2\sqrt{\frac{\rho d_2}{\sigma_2}}\left[\frac{1}{y}\log\frac{a}{a_0}\right]_2,$$

ρ being the density of the jet fluid.

Since all the results in fig. 12 fall on one curve, it follows that

$$\left[\frac{1}{y}\log\frac{a}{a_0}\right]_1 = \left[\frac{1}{y}\log\frac{a}{a_0}\right]_2,$$

provided $\frac{L_1}{d_1} = \frac{L_2}{d_2}$ when $V_1\sqrt{\frac{\rho d_1}{\sigma_1}} = V_2\sqrt{\frac{\rho d_2}{\sigma_2}}$.

Furthermore, if y is constant, we obtain the condition that the ratio of the initial and final amplitudes of disintegrating disturbance is the same for any pair of liquids when the velocities V_1 and V_2 are in the ratio

$$\sqrt{\frac{\sigma_1}{\rho d_1}} : \sqrt{\frac{\sigma_2}{\rho d_2}}.$$

Also, since for mercury jets $\frac{L}{d} \div V\sqrt{\frac{\rho d}{\sigma}}$ increases as V increases, the ratio of the initial and final amplitudes of disintegrating disturbance increases with increase in V.

The slight deviation between the mercury jets in air results is no doubt due to the surrounding medium, whose effects are emphasized to a greater degree by the mercury jets in glucose solution.

(b) *Critical Velocities for Mercury Jets in Aqueous Solutions (Viscosity Small).*

Analysis of the upper and lower critical velocities reveal constancy in the corresponding values of $V\sqrt{\frac{\rho d}{\sigma}}$ (*vide* Table IV.), although slightly lower than the upper critical values for mercury jets in air.

The same average value of the upper $V\sqrt{\frac{\rho d}{\sigma}}$ is obtained with the lighter liquid jets formed in water, or *vice versa*. It therefore appears that the viscosity of the jet fluid for liquid jets in liquid has very little effect on the upper critical $V\sqrt{\frac{\rho d}{\sigma}}$ quite different from jets formed in air. The inertia forces are now no longer predominant.

(c) *Streamline Characteristics for Lighter Liquid Jets in Liquids.*

Analyzing from the same point of view as outlined for the mercury jets, by plotting $\frac{L}{d}$ against $V\sqrt{\frac{\rho d}{\sigma}}$ it is possible to reduce all the graphs for the oil jets in water (where surface tension is considerably reduced) such that their streamline parts all coincide, falling on a single straight line not going through the origin (fig. 16). The slopes of the

TABLE IV.—Results for Mercury Jets in Different Solutions (Viscosity constant).

Medium.	Diameter of nozzle d cm.	Density of mercury gm./c.c.	Surface tension mercury/liquid dynes/cm.	Lower critical velocity V_1 cm./sec.	Upper critical velocity V_2 cm./sec.	$V_1\sqrt{\frac{\rho d}{\sigma}}$.	$V_2\sqrt{\frac{\rho d}{\sigma}}$.
$\frac{N}{4}$ KOH	·0200	13·59	459	100	220	2·43	5·34
Water	·0200	13·59	427	86·0	217	2·16	5·46
Air	·0200	13·59	547	130	275	2·86	6·05
$\frac{N}{4}$ $HgNO_3$ ...	·0200	13·59	295	80	180	2·42	5·46
Turpentine...	·0200	13·59	250	83	155	2·74	5·10
$\frac{N}{4}$ KOH	·0276	13·59	459	83·0	190	2·37	5·43
$\frac{N}{4}$ $HgNO_3$ ...	·0276	13·59	295	60·0	150	2·14	5·34
Water	·0276	13·59	427	70·0	190	2·07	5·63
Air	·0276	13·59	547	110·0	240	2·85	6·20
$\frac{N}{4}$ KOH	·0219	13·59	459	96·0	205	2·45	5·22
NKOH	·0219	13·59	383	105·0	187	2·90	5·19
$\frac{N}{4}$ $HgNO_3$ ...	·0219	13·59	295	75·0	169	2·38	5·36
Air	·0219	13·59	547	120·0	272	2·76	6·28
Water	* ·0172	13·59	427	—	233	—	5·45
Water	* ·0248	13·59	427	—	170	—	4·77
$\frac{N}{4}$ KCN	* ·0237	13·59	463	110	254	2·93	6·77
$\frac{N}{4}$ $HgNO_3$ ...	·0237	13·59	295	70·0	207	2·30	6·84
Air	·0237	13·59	547	125 approx.	400	3·03	9·70

* Smith and Moss values.

reduced graphs are approximately the same as for the corresponding jets formed in air.

Instead of equation (7), we now have

$$\frac{L}{d} = V\sqrt{\frac{\rho d}{\sigma}} \cdot \frac{1}{y} \cdot \log \frac{a}{a_0} - C \quad . \quad . \quad . \quad (8)$$

(C being a constant) as representative of the lighter oils in water.

Water in paraffin and benzene shows exception to the case of oil jets in water, the slopes of the streamline parts being greater. In these cases, the reduction in surface tension is much less than for most of the liquids, and drop formation disturbances will have less access to the orifice, thus giving characteristics intermediate between the oil jets in water, and oil jets in air.

Application of equation (8) to such jets formed in water indicates a similar type of controlling influence as with the jets formed in air, namely, the streamline characteristics controlled mainly by the surface tension forces, and in addition by drop formation reaction at the orifice, this being of constant magnitude. Furthermore, it follows, from equation (8), that $\dfrac{\frac{L}{d} + C}{V\sqrt{\frac{\rho d}{\sigma}}} = \frac{1}{y} \log \frac{a}{a_0}$ is the same for all the oil jets in water over the streamline range, which also suggests a simple relationship between the existing physical conditions.

If the suffixes denote corresponding values for any two liquids and nozzles, the factor $\left[\frac{1}{y} \cdot \log \frac{a}{a_0}\right]$ is constant provided the jet-lengths and velocities are related by the following equality

$$\frac{\left[\frac{L_1}{d_1} + C\right]_1}{\left[\frac{L_2}{d_2} + C\right]_2} = \frac{V_1\sqrt{\frac{\rho_1 d_1}{\sigma_1}}}{V_2\sqrt{\frac{\rho_2 d_2}{\sigma_2}}}.$$

Again, if y is considered constant, we arrive at the simple condition that the ratio of the initial to the final amplitude of disturbance $\frac{a}{a_0}$ is the same for the oil jets formed in water, provided that the foregoing relationship is satisfied.

TABLE V.—Results for Liquid Jets in Liquids.

Jet liquid.	Medium.	Diameter of nozzle d cm.	Density of jet ρ gm /cc.	Density of medium gm./c.c.	Surface tension σ dynes/cm.	Viscosity of medium gm./cm. sec.	Upper critical velocity V_2 cm./sec.	$V_2\sqrt{\frac{\rho d}{\sigma}}$.	Upper critical $\frac{L}{d}$.
Aniline	Water	·050	1·027	1·00	6·59	·0107	66	5·80	52
		·045	1·027	1·00	6·59	·0107	70	5·88	—
		·065	1·027	1·00	6·59	·0107	60	6·06	46·0
		·0352	1·027	1·00	6·59	·0107	87	6·50	54·0
Paraffin	Water	·050	·790	1·00	39·0	·0107	155	4·98	30·0
		·045	·790	1·00	39·0	·0107	170	5·12	—
		·065	·790	1·00	39·0	·0107	110	4·00 *	25·0
		·0352	·790	1·00	39·0	·0107	175	4·80	38·0
		·0275	·790	1·00	39·0	·0107	240	5·66	44·0
Water	Paraffin	·050	1·00	·790	39·0	·0190	145	5·20	76·0
		·065	1·00	·790	39·0	·0190	120	4·90	72·0
		·045	1·00	·790	39·0	·0190	155	5·26	73·0
		·0352	1·00	·790	39·0	·0190	175	5·25	82·0
Turpentine	Water	·065	·87	1·00	17·9	·0107	92	5·17	32·0
		·045	·87	1·00	17·9	·0107	120	5·60	34·0
		·038	·87	1·00	17·9	·0107	125	5·35	36·0
Water	Turpentine	·065	1·00	·87	17·9	·018	93	5·61	56·0
		·045	1·00	·87	17·9	·018	132	6·60	67·0
		·038	1·00	·87	17·9	·018	158	(7·10)	78·0
Water	Machine oil ...	·050	1·00	·91	34·6	·99	112	4·26 *	47·0
		·065	1·00	·91	34·6	·99	95	4·12 *	45·0
Water	Benzene	·050	1·00	·879	30·0	·0069	128	5·24	52·0
		·045	1·00	·879	30·0	·0069	145	5·60	55·6
Benzene	Water	·050	·879	1·00	30·0	·0108	120	4·59	70·0
		·045	·879	1·00	30·0	·0108	130	4·72	73·3

* Cases where excessive drop formation reaction is predominant. Lower values of $V_2\sqrt{\frac{\rho d}{\sigma}}$ are obtained.

CASE 2.—*Effect of Viscosity of Medium.*

(a) *Upper Critical Jet-lengths for Lighter Liquids.*

Referring to Table V. and fig. 16, it is noteworthy that the viscosity of the medium has very little effect on the upper critical values of $V\sqrt{\frac{\rho d}{\sigma}}$ for the light liquid jets, but the critical values of $\frac{L}{d}$ are, however, controlled by the viscosity of the surrounding medium.

Fig. 16.

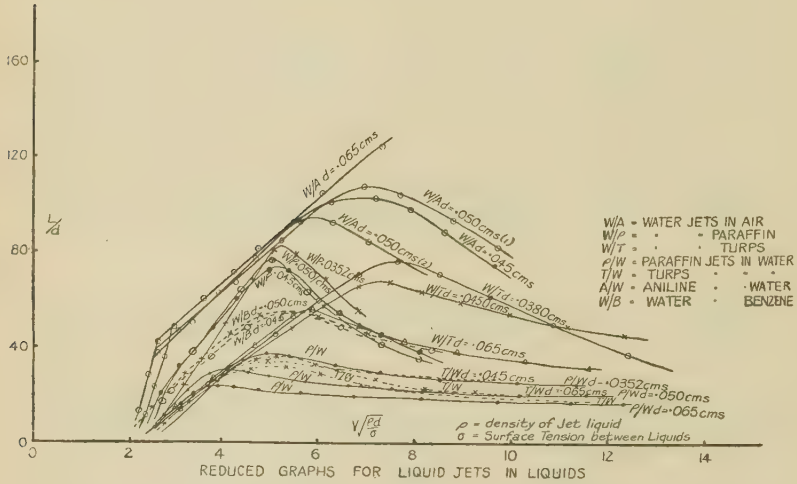

Analysis shows that with a given pair of liquids, greater values of $\frac{L}{d}$ are produced at the upper critical $V\sqrt{\frac{\rho d}{\sigma}}$ using the less viscous liquid as the jet, with the other as the surrounding medium. There appears to exist a simple relation between the jet-lengths L_1, L_2 at the upper critical velocities V_1, V_2 for any pair of liquids so used.

At such points for a given nozzle, the following relation is satisfied :

$$\frac{\frac{L_1}{d} \div V_1\sqrt{\frac{\rho_1 d}{\sigma}}}{\frac{L_2}{d} \div V_2\sqrt{\frac{\rho_2 d}{\sigma}}} = \frac{\mu_2}{\mu_1},$$

μ_1 and μ_2 being the viscosities of the two liquids.

Now, remembering that $V_1\sqrt{\frac{\rho_1 d}{\sigma}} \doteq V_2\sqrt{\frac{\rho_2 d}{\sigma}}$ for such jets, we have

$$\frac{L_1}{L_2} = \frac{\mu_2}{\mu_1},$$

i. e., the ratio of the jet-lengths produced at the upper critical velocities for a given pair of non-miscible liquids is equal to the ratio of the viscosities of the surrounding media, for a given nozzle.

It is not possible to apply the same treatment to the mercury jets falling into glucose owing to the relatively large difference in density and opacity of the mercury; neither is one able to fix with any certainty the jet-lengths at the upper critical velocities, since in this region the jets are very unstable.

The upper values of $V\sqrt{\frac{\rho d}{\sigma}}$ can, however, be obtained with greater precision, and information derived in respect of the viscosity of the surrounding medium modifying same.

(b) *Upper Critical Velocities for Mercury Jets in Glucose Solutions. Suggested Dimensional Theory to Account for the Upper Critical Points.*

Attempting to include the viscosity of the surrounding medium as a controlling factor on the upper critical velocity, it is easy to show by dimensional considerations that the upper critical velocity V_c may be expressed as

$$V_c = K\sqrt{\frac{\sigma}{\rho d}} f\left(\frac{\sqrt{\sigma\rho_m d}}{\mu_m}\right),$$

where K is a constant involving $\frac{1}{y} \cdot \log \frac{a}{a_0}$, ρ_m is the density, and μ_m the viscosity of the surrounding medium. The viscosity of the jet fluid is supposed negligible.

Expanding the function f as a series of power terms, we derive the expression

$$V_c = K\sqrt{\frac{\sigma}{\rho d}}\left[a + b\left(\frac{\sqrt{\sigma\rho_m d}}{\mu_m}\right)^x + \text{other terms}\right]$$

or

$$V_c\sqrt{\frac{\rho d}{\sigma}} = A + B\left(\frac{\sqrt{\sigma\rho_m d}}{\mu_m}\right)^x, \text{ neglecting the other terms.}$$

The deduction of $x=\frac{1}{5}$ can be shown by logarithmic plotting of $V_c\sqrt{\frac{\rho d}{\sigma}}$ against $\frac{\sqrt{\sigma\rho_m d}}{\mu_m}$.

For mercury jets formed in glucose solutions of various viscous strengths, the relation

$$V_c\sqrt{\frac{\rho d}{\sigma}} = A + B\left(\frac{\sqrt{\sigma\rho_m d}}{\mu_m}\right)^{1/5}$$

is found to satisfy the experimental conditions.

Fig. 17.

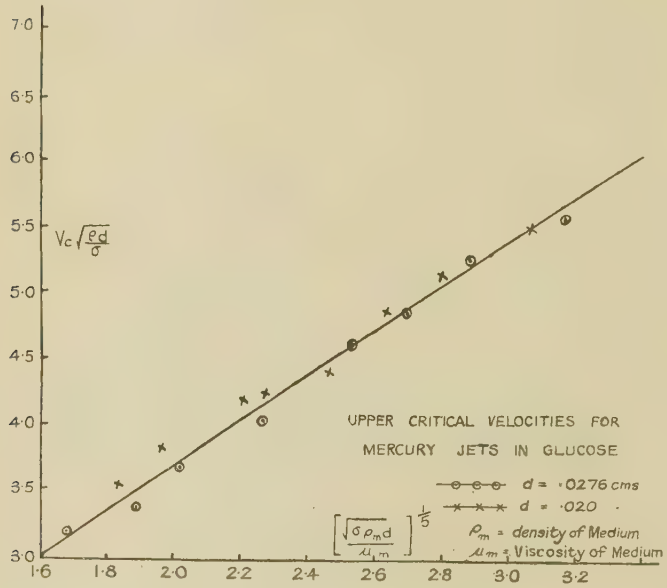

Further verification of this linear relationship is exhibited in fig. 17, where a plot of $V_c\sqrt{\frac{\rho d}{\sigma}}$ against $\left(\frac{\sqrt{\sigma\rho_m d}}{\mu_m}\right)^{1/5}$ for nozzles $d=\cdot200$ mm. and $\cdot276$ mm. produces a straight line graph, allowing for experimental errors. This result is also consistent with mercury jets falling into other solutions.

The possibility of obtaining a general theory covering all the stages examined seems remote, owing to the number of varying factors which predominate under the experimental conditions, for in one case where one condition is of main influence, in another it may be of negligible importance.

Summary.

Continuing the earlier work of one of us (E. T.) examination is made of the properties of capillary jets, concerning the causes which are of primary importance in controlling the relation between the continuous length of the jet (L) and its velocity of efflux (V) from a cylindrical nozzle.

Characteristic L-V curves exhibit upper and lower critical velocities, at which discontinuity in the jet-length occurs, with an L-V streamline part for intermediate speeds.

Whereas viscosity and surface tension of the jet fluid are the prime factors controlling the upper critical point, drop formation disturbance produced at the disruption point of the jet, gaining access to the nozzle, is the cause of the lower.

Particular cases of liquid jets formed in air more viscous than previously used, reveal modification of both the streamline characteristic and upper critical velocity, as a result of increased viscosity.

Liquid jets formed in other non-miscible liquids enabled the controlling influence of the surrounding medium with respect to viscosity and density to be investigated.

Photographs of capillary jets produced under varying conditions are included, together with dimensional formulæ covering the various phases examined.

We are much indebted to Messrs. E. Langton, B.Sc., and E. M. Heddle, M.C., M.A., B.Sc., of the Physics Staff, Leicester College of Technology, for the loan of the camera outfit with which the photographs were obtained.

XCIV. *A Simple Numerical Method for the Treatment of Elastic Stability Questions and similar "Characteristic Value" Problems.* *By* A. F. Cornock, *M.Sc.* (A Communication from the Staff of the Research Laboratories of the General Electric Company, Limited, Wembley, England *.)

Summary.

The solution of "Characteristic Value" problems, such as the determination of the crippling load of a strut or the whirling speed of a rotating shaft, has hitherto only been possible (except in simple cases) by the use of approximate

* Communicated by C. C. Paterson, M.I.E.E.

methods. The present paper describes a very simple method of successive approximations by which the numerical solution of such problems may readily be determined to any desired degree of approximation.

---

1. *Introduction.*

THE determination of the crippling load of a strut, or the whirling speed of a shaft, or the solution of any similar "characteristic value" problem can only be effected by the ordinary analytical methods for comparatively simple cases. In more complicated cases, recourse is usually had to Rayleigh's method, or, less frequently to Ritz's method. Rayleigh's method is so well known, that comment on it is almost unnecessary; it may, however, be remarked that the accuracy of the results obtained in practice is dependent upon the slowness of the variation of the ratios of the kinetic to the potential energy with variations of the assumed deflexion form from the true deflexion form, for if this ratio varies rapidly, it is obviously necessary for the assumed deflexion form to be very near the true form if accurate results are to be obtained. Temple [1], [2] has recently given an extremely elegant process by which Rayleigh's method may be carried to any desired degree of approximation; but the use of his method seems to be dependent upon the use of the Green's function for the equation of which the characteristic values are to be found, and where the Green's function cannot be expressed analytically, the numerical working appears to become somewhat complicated.

Ritz's method is also capable, in principle, of being carried to any desired degree of approximation, but it is sometimes difficult to find a suitable family of functions, satisfying the boundary conditions, by means of which the solution is to be constructed.

The object of the present paper is to provide a method whose great merits are, its simplicity (both of principle and performance), its ability to be readily carried to a degree of accuracy quite sufficient for ordinary engineering or physical purposes, and the fact that it indicates the order of the accuracy attained at each stage of the process.

The method does not pretend to "rigour," in the sense of the pure mathematician—it may even refuse to give a solution at all, if grossly abused—but it is not the less accurate for that, and may be applied with confidence where the functional nature of the solution required is already known—as is the case with engineering and physical problems.

2. *Principle of the Method.*

The basis of the new treatment is Picard's method for the solution of differential equations.

Picard has shown that an approximation to the solution of the equation

$$\frac{d^n y}{dx^n} = f_1(x)\frac{d^{n-1}y}{dx^{n-1}} + f_2(x)\frac{d^{n-2}y}{dx^{n-2}} + \ldots + \lambda f_n(x)y \quad (2.1)$$

in an interval $a_1 \leq x \leq a_2$ containing no singular points of y, and satisfying the terminal conditions

$$\left.\begin{aligned} x = a_1, \quad & y = b_1 \\ x = a_2, \quad & y = b_2 \end{aligned}\right\} \quad \ldots \ldots \quad (2.2)$$

(together with $n-2$ other terminal conditions) may be obtained by assuming for y any continuous function of x which satisfies the conditions (2.2), substituting this assumed function in the right-hand side of (2.1), integrating n times, and so determining the n constants of integration that the n boundary conditions are satisfied. He further showed that if the function of x thus determined be again substituted in the right-hand side of (2.1), and the process repeated, the new function thus obtained is a still better approximation, and that if the process be repeated m times, the function obtained as m tends to ∞, itself tends to the solution of the equation (2.1).

Taking the case of the second order equation, by way of example,

$$\frac{d^2y}{dx^2} = f_1(x)\frac{dy}{dx} + \lambda f_2(x)y \quad \ldots \ldots \quad (2.3)$$

with the two conditions

$$\left.\begin{aligned} x = a_1, \quad & y = b_1, \\ x = a_2, \quad & y = b_2, \end{aligned}\right\} \quad \ldots \ldots \quad (2.21)$$

the solution obtained will not be zero everywhere unless b_1 and b_2 are both zero, in which case the solution will be identically zero unless λ has certain special values—the "characteristic values" for the equation.

The problem may now be formally stated as follows: given a linear differential equation of even order (equations of *even* order will be particularly considered since they are the most common ones in physical questions),

$$\frac{d^{2r}y}{dx^{2r}} = f_1(x)\frac{d^{2r-1}y}{dx^{2r}} + \ldots + \lambda f_{2r}(x)y, \quad \ldots \quad (2.4)$$

together with $2r$ linear homogeneous boundary conditions of the form

$$\sum_{s=0}^{s=2r-1}\left[\alpha_{st}\left(\frac{d^s y}{dx^s}\right)_{x=a_1}+\beta_{st}\left(\frac{d^s y}{dx^s}\right)_{x=a_2}\right]=0, \quad . \quad (2.5)$$

(where $t=1, 2, 3, \ldots\ldots 2r$), it is required to find the characteristic values of λ.

Now, in the case of most engineering or physical problems, the general form of the function y (*e.g.* the deflexion form of a vibrating rod) is known approximately, either from physical intuition or by inference from the known solution of a simple problem of the same type.

Fig. 1.

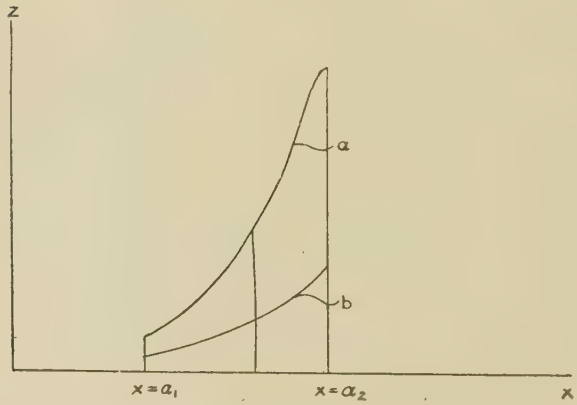

If, now, equation (2.4) be written in the form

$$\frac{d^{2r}y}{dx^{2r}}-f_1(x)\frac{d^{2r-1}y}{dx^{2r-1}}\cdot\ldots\ldots-f_{2r-1}(x)\frac{dy}{dx}=\lambda f_{2r}(x)y, \quad (2.41)$$

equation (2.41) expresses the fact that if the function y were known for one of the characteristic values λ, and from it the value of the left-hand side of equation (2.41) were calculated then, plotting the graph of the left-hand side (curve a in fig. 1), and the graph (curve b) of the right-hand side, the ratio of the ordinates z_a/z_b would be constant and equal to λ for all values of x in the interval a_1 to a_2. Or, if the value of λy be known, and from it the right-hand side of (2.41) be found and the equation integrated and the constants of integration determined from the boundary conditions thus giving the solution y_1, then (writing $\lambda y=y_0$) the ratio

y_0/y_1, will be similarly constant in the interval a_1 to a_2 and will be equal to λ.

Now it is found that if a "reasonable" form be assumed for y_0, and the process of integrating (2.41) performed, and the process repeated a number of times, using at each stage the newly derived form as the assumed form for y_0 for the next repetition, the ratio y_0/y_1 rapidly tends to constancy for all values of x within the interval a_1 to a_2. The rapidity with which this ratio tends to constancy—which may loosely but conveniently be called the rapidity of convergence—obviously depends on the nearness to truth of the initial assumption. Moreover, if, at any stage, the ratio y_0/y_1 be not constant, but varies between an upper bound P and a lower bound Q, it appears that the value of the ratio obtained from the next stage will lie between P and Q—thus giving a measure of the maximum error at each stage. No attempt will be made to demonstrate either of these statements analytically: in the first place, the "nearness to truth" of the initial assumption is a rather nebulous quantity, and in the second, it is felt that such demonstrations are of no particular physical interest—as remarked by Perry with regard to the somewhat similar question of delicate considerations of the convergence of series, "such considerations are unnecessary to the engineer; for him, a series must converge rapidly, or it is useless." In the same way here, the errors must rapidly and obviously become negligible—at least in a manner akin to the Remainder Term of an Asymptotic series—if the method is to be useful for the purposes for which it is intended; if it does not satisfy this requirement, the computer will abandon the use of the method, and he is therefore in no danger of being led astray by it. In the great majority of cases, it may be remarked, it is only necessary to make the second approximation, and where a number of similar cases have already been solved, the initial assumption can often be made so close that a single calculation is alone required.

In performing the calculations, it is usually convenient, when possible, to write equation (2.41) in the form

$$g_0(x)\frac{d}{dx}\left[g_1(x)\frac{d}{dx}\left\{g_2(x)\frac{d}{dx}\left(\quad\right)\right\}\right]y=\lambda f_{2r}(x)y. \quad (2.42)$$

Thus, for example, if, in the case of the second order equation the form be

$$g_0(x)\frac{d}{dx}\left[g_1(x)\frac{d}{dx}\{g_2(x)y\}\right]=\lambda f_2(x)y, \quad . \quad (2.6)$$

the integration can be very simply performed in the following steps:

$$\frac{d}{dx}\left[g_1(x)\frac{d}{dx}\{g_2(x)y\}\right]=\lambda f_2(x)y/g_0(x), \quad (2.61)$$

$$g_1(x)\frac{d}{dx}\{g_2(x)y\}=\int_{a_1}^{x}\frac{f_2(x)}{g_0(x)}\lambda y dx+\mathrm{A}, \quad (2.62)$$

$$\frac{d}{dx}\{g_2(x)y\}=\frac{1}{g_1(x)}\int_{a_1}^{x}\frac{f_2(x)}{g_0(x)}\lambda y dx+\mathrm{A}/g_1(x), \quad (2.63)$$

$$g_2(x)y=\int_{a_1}^{x}\frac{1}{g_1(x)}\int_{a_1}^{x}\frac{f_2(x)}{g_0(x)}\lambda y dx dx+\mathrm{A}\int_{a_1}^{x}\frac{dx}{g_1(x)}+\mathrm{B}, \quad (2.64)$$

where A and B are the constants of integration (provided that none of the g's vanish in the range of integration).

Fig. 2.

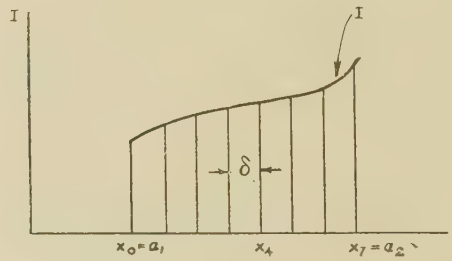

The integrations themselves may conveniently be effected numerically. Suppose, for example, the value of the quantity

$$\mathrm{I}=\frac{f_2(x)}{g_0(x)}\lambda y$$

in equation (2.61) is tabulated for suitable values of x (*e.g.* eight values). The tabulated values are graphically represented by the ordinates marked in fig. 2.

Then the value of the integral is

$$\int_{a_1}^{x}\mathrm{I}dx=\delta\Sigma\{\tfrac{1}{2}(x_0+x_1)+\tfrac{1}{2}(x_1+x_2)+\ \ldots\ldots\}$$

and the evaluation of the right-hand side may be readily carried out in tabular form. Where greater accuracy is required, the known methods of integrating by differences may be employed.

3. *Examples of the Use of the Method.*

Two examples of the use of the process will now be given, one being the determination of the whirling speed of a shaft, and the second the calculation of the frequency of vibration of a circular annulus of a flat plate, the annulus being clamped at its inner edge and free at its outer edge.

In the first case, consider a vertical shaft "encastré" at its lower end consisting of four cylindrical sections of radii of gyration k_1, k_2, k_3, k_4, the lengths from the base to the ends of the various sections being l_1, l_2, l_3, l_4, respectively, as shown in fig. 3. The shaft is supposed to rotate with angular velocity ω about the vertical.

Fig. 3.

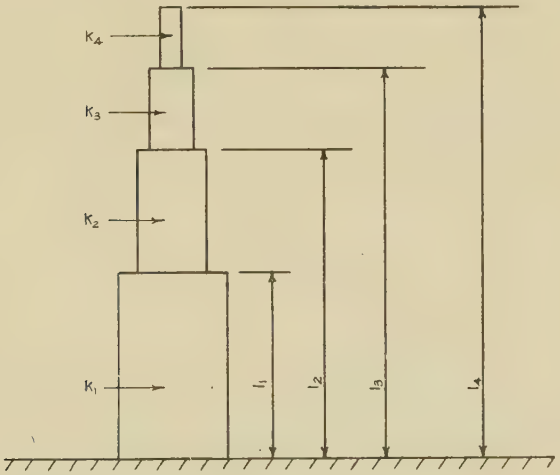

Let it be required to determine what the speed of rotation of this shaft must be in order that it may just attain its first unstable condition, *i. e.*, the lowest whirling speed.

Using the ordinary theory, the equation determining stability is

$$\mathrm{E}\frac{d^2}{dx^2}\left(\mathrm{I}\frac{d^2y}{dx^2}\right)=\frac{w}{g}\mathrm{A}\omega^2 y, \quad . \quad . \quad . \quad . \quad (3.1)$$

where

E = Young's modulus,
I = second moment of cross-section,
w = weight of rod per unit volume,
A = area of cross-section,
y = horizontal displacement of any point of rod,

and z is measured vertically from the base. The terminal conditions are that y and $\frac{dy}{dx}$ must vanish at the base, and that the bending-moment $\mathrm{I}\frac{d^2y}{dx^2}$ and shear force $\frac{d}{dx}\left(\mathrm{I}\frac{d^2y}{dx^2}\right)$ must vanish at the tip of the shaft.

If it be desired to determine the value of ω analytically in the ordinary way, the equation (3.1) is solved for each section of the rod, the necessary conditions of continuity at the ends of the sections are written down, and these conditions, with the terminal conditions, give a determinantal equation whose lowest root gives the required value of ω.

Performing this process in detail, since I and A are constant over each section of the rod, equation (3.1) may be written, for each section, in the form :

$$\frac{d^4y}{dx^4} = \frac{w}{g}\cdot\frac{\mathrm{A}\omega^2}{\mathrm{EI}}y = \frac{w}{g}\cdot\frac{\omega^2}{\mathrm{E}k_r^2}y, \quad . \quad . \quad . \quad (3.2)$$

where the appropriate value of k for each section is to be inserted. Writing

$$x = l_4\xi, \qquad \lambda^4 = \frac{w\omega^2 l_4^4}{g\mathrm{E}k_1^2}, \qquad \mu_r^4 = \frac{k_1^2}{k_r^2},$$

this becomes

$$\frac{d^4y}{d\xi^4} = \lambda^4\mu_r^4 y, \quad . \quad . \quad . \quad . \quad . \quad (3.3)$$

of which the solution is

$$y = \mathrm{A}_r\cosh\lambda\mu_r\xi + \mathrm{B}_r\sinh\lambda\mu_r\xi + \mathrm{C}_r\cos\lambda\mu_r\xi + \mathrm{D}_r\sin\lambda\mu_r\xi \quad (3.4)$$

(for $r=1, 2, 3, 4$).

The homogeneous terminal conditions to be satisfied are,

$$\xi = 0, \qquad y = \frac{dy}{d\xi} = 0, \quad . \quad . \quad . \quad (3.41)$$

$$\zeta = \frac{l_1}{l_4} = l', \qquad y_1 = y_2, \qquad \left(\frac{dy}{d\xi}\right)_1 = \left(\frac{dy}{d\xi}\right)_2,$$

$$\mathrm{I}_1\left(\frac{d^2y}{d\xi^2}\right)_1 = \mathrm{I}_2\left(\frac{d^2y}{d\xi^2}\right)_2, \qquad \mathrm{I}_1\left(\frac{d^3y}{d\xi^3}\right)_1 = \mathrm{I}_2\left(\frac{d^3y}{d\xi^3}\right)_2 \quad (3.42)$$

(the subscripts being used to indicate which section of the rod is under consideration), with four conditions similar to (3.42) at each of the other junctions, *i. e.*, when

$$\xi = \frac{l_2}{l_4} = l'', \quad \text{and when } \xi = \frac{l_3}{l_4} = l''',$$

and, finally, when

$$\xi=1, \qquad \frac{d^2y}{d\xi^2}=\frac{d^3y}{d\xi^3}=0, \quad . \quad . \quad . \quad (3.43)$$

Writing

$$I_2/I_1=\rho', \qquad I_3/I_2=\rho'', \qquad I_4/I_3=\rho''',$$

these become, on performing the differentiations,

$$A_1+C_1=0, \quad . \quad . \quad . \quad . \quad . \quad . \quad (3.51)$$

$$B_1+D_1=0, \quad . \quad . \quad . \quad . \quad . \quad . \quad (3.52)$$

$$A_1\cosh\lambda l'\mu_1+B_1\sinh\lambda l'\mu_1+C_1\cos\lambda l'\mu_1+D_1\sin\lambda l'\mu_1$$
$$=A_2\cosh\lambda l'\mu_2+B_2\sinh\lambda l'\mu_2+C_2\cos\lambda l'\mu_2+D_2\sin\lambda l'\mu_2$$
$$. \quad . \quad . \quad (3.53)$$

$$\lambda\mu_1(A_1\sinh\lambda l'\mu_1+B_1\cosh\lambda l'\mu_1+C_1\sin\lambda l'\mu_1+D_1\cos\lambda l'\mu_1)$$
$$=\lambda\mu_2(A_2\sinh\lambda l'\mu_2+B_2\cosh\lambda l'\mu_2$$
$$-C_2\sin\lambda l'\mu_2+D_2\cos\lambda l'\mu_2), \quad . \quad (3.54)$$

$$\lambda^2\mu_1^2(A_1\cosh\lambda l'\mu_1+B_1\sinh\lambda l'\mu_1-C_1\cos\lambda l'\mu_1-D_1\sin\lambda l'\mu_1)$$
$$=\lambda^2\mu_2^2\rho'(A_2\cosh\lambda l'\mu_2+B_2\sinh\lambda l'\mu_2$$
$$-C_2\cos\lambda l'\mu_2+D_2\sin\lambda l'\mu_2), \quad . \quad (3.55)$$

$$\lambda^3\mu_1^3(A_1\sinh\lambda l'\mu_1+B_1\cosh\lambda l'\mu_1+C_1\sin\lambda l'\mu_1-D_1\cos\lambda l'\mu_1),$$
$$=\lambda^3\mu_2^3\rho'(A_2\sinh\lambda l'\mu_2+B_2\cosh\lambda l'\mu_2$$
$$+C_2\sin\lambda l'\mu_2-D_2\cos\lambda l'\mu_2), \quad . \quad (3.56)$$

with similar equations when $\xi=l''$ and l''' (*i. e.* four equations at each junction) ; and finally,

$$A_4\cosh\lambda\mu_4+B_4\sinh\lambda\mu_4-C_4\cos\lambda\mu_4-D_4\sin\lambda\mu_4=0, \quad (3.57)$$

$$A_4\sinh\lambda\mu_4+B_4\cosh\lambda\mu_4+C_4\sin\lambda\mu_4-D_4\cos\lambda\mu_4=0, \quad (3.58)$$

The eliminant of these sixteen equations relating the sixteen constants $A_1, \ldots, D_4$ provides the determinantal equation.

If, for example, the ratios of the diameters of the sections of the rod are as 1 : 0·9 : 0·8 : 0·7, while

$$l'=0{\cdot}5, \qquad l''=0{\cdot}7, \qquad l'''=0{\cdot}8,$$
$$\rho'=0{\cdot}6560, \qquad \rho''=0{\cdot}6247, \qquad \rho'''=0{\cdot}5866,$$
$$\mu_1=1, \qquad \mu_2=1{\cdot}054, \qquad \mu_3=1{\cdot}118, \qquad \mu_4=1{\cdot}195,$$

and the resulting frequency determinant $\triangle$ is shown in Table I.

Comment on the enormous labour involved in locating and evaluating the lowest root is entirely unnecessary.

In order to use the new method, equation (3.1) may conveniently be written in the form

$$\frac{d^2}{dx^2}\left(r^4\frac{d^2y}{dx^2}\right)=4\frac{w}{Eg}\omega^2r^3y \quad . \quad . \quad . \quad . \quad (3.6)$$

(r being the radius of the rod at any cross-section, so that $I=\frac{\pi}{4}r^4$, $A=\pi r^2$), or, once again writing

$$x=l_4\xi,$$

$$\frac{d^2}{d\xi^2}\left\{\psi^4\frac{d^2y}{d\xi^2}\right\}=\frac{4wl_4{}^4\omega^2}{Egr_1{}^2}\psi^2y=\lambda^4\psi^2y=I_0, \quad . \quad (3.7)$$

where

$$\psi=\frac{r}{r_1}, \quad \text{and} \quad \lambda^4=\frac{4wl_4{}^4\omega^2}{Egr_1{}^2},$$

so that

$$\omega=\tfrac{1}{2}\left(\frac{\lambda}{l_4}\right)^2\sqrt{\frac{Egr_1{}^2}{w}}. \quad . \quad . \quad . \quad (3.701)$$

Integrating (3.7) successively, the following equations are obtained:

$$\frac{d}{d\xi}\left\{\psi^4\frac{d^2y}{d\xi^2}\right\}=\int_0^\xi I_0d\xi+A=I_1+A, \quad . \quad (3.71)$$

$$\psi^4\frac{d^2y}{d\xi^2}=\int_0^\xi I_1d\xi+A\xi+B=I_2+A\xi+B, \quad . \quad (3.72)$$

$$\frac{d^2y}{d\xi^2}=I_2/\psi^4+A\xi/\psi^4+B/\psi^4,$$

$$\frac{dy}{d\xi}=\int_0^\xi I_2/\psi^4d\xi+A\int_0^\xi\xi\psi^{-4}d\xi+B\int_0^\xi\psi^{-4}d\xi+C$$

$$=I_3+AK_3+BL_3+C, \quad . \quad . \quad . \quad (3.73)$$

$$y=\int_0^\xi I_3d\xi+A\int_0^\xi K_3d\xi+B\int_0^\xi L_3d\xi+C\xi+D$$

$$=I_4+AK_4+BL_4+C\xi+D, \quad . \quad (3.74)$$

where A, B, C, and D are constants of integration, and the meaning of the integrated terms I, K, and L will be apparent.

Since the integrated terms are definite integrals between 0 and ξ, they vanish when $\xi=0$, and the boundary conditions

$$\xi = 0, \qquad y = \frac{dy}{d\xi} = 0,$$

give

$$C=D=0, \quad . \quad . \quad . \quad . \quad . \quad . \quad (3.8)$$

while the conditions at $\xi=1$ become

$$\psi^4 \frac{d^2y}{d\xi^2} = 0, \qquad \frac{d}{d\xi}\left\{\psi \frac{d^2y}{d\xi^2}\right\} = 0,$$

whence

$$A=-I_1, \qquad B=I_1-I_2. \quad . \quad . \quad . \quad . \quad (3.9)$$

The detailed calculations are given in Tables II., III., and IV., in which the symbol μ' is used to indicate Shepherd's "averager"—so that the value on any line in the column headed $\mu' I_0$ is the mean of the value lying on the lines immediately above and immediately below in the preceding column—and δ indicates the "step" between successive ordinates as in fig. 2. Thus, for example, the column headed $\mu\delta' I_0$ contains the areas of each of the narrow strips which are to be summed to give the integral of I_0, and the column I_1 contains the cumulative sums of the $\delta\mu' I_0$, so the values in I_1 are the values of the required integral of I_0 up to each of the tabulated abscissæ.

The values of $\lambda^4 y$ originally assumed are given in the second column of Table II.: they were obtained by drawing a likely looking deflexion curve with a French curve. (It may be remarked that this example is given because it was the first case of its kind which was calculated by the method, so that there was no chance that any inherent difficulties of the method could have been masked by practice acquired during use.) The integrations were then performed, and the quantity I_4 obtained. Table III., giving K_3, K_4, L_3, and L_4 was next constructed by integrating $\xi\psi^{-4}$ and ψ^{-4} (whose values are known from the dimensions of the rod). A and B are then obtained from equations (3.9), and the value of y_1 found, whence the values of

$$\lambda^4 = y_0/y_1,$$

which are given in the last column of Table II.

It will be seen that the values of λ^4 vary considerably—from 3 to 33. The value of y_1 was accordingly used for the new assumed value of $\lambda^4 y$, and recalculated as shown in Table IV.,

whence a second approximation to y, *i. e.* y_2 is found, giving a closer approximation to

$$\lambda^4 = y_1/y_2.$$

The mean value of the last seven values of λ^4, from column 22 of Table IV. is 18.22—it will be found that greater accuracy is obtained by averaging over a length near the end of the rod, and not over the whole length of the rod, so that

$$\lambda^2 = 4{\cdot}270,$$

and ω can be found from (3.701). The total variation in λ^4 does not exceed 4 per cent., so that the error in λ^2 will not exceed 2 per cent. and will actually be substantially less than this, as is known from experience.

It may be said that the accuracy obtained is not very noteworthy in this case, and could readily be equalled by Rayleigh's method—this is true, though it may also be added that the present method has the advantage of showing a limit which the error will not exceed. An example will now be given of a case, the vibration of a plate, where it is very difficult to find an assumed form which is not liable to give considerable error when using Rayleigh's method—see, for example, a paper by Southwell [3], pp. 149–150, in which a very plausible assumption led to an error of 50 per cent. in frequency.

Consider the vibration of a flat plate in the form of a circular annulus clamped at the inner boundary and free at the outer, such as might be used as a vibrating piston for acoustical work.

The equation of vibration of a flat plate is, in polar co-ordinates, r and θ,

$$\Delta_1^4 w + \frac{3\rho(1-\sigma^2)}{gEh^2}\frac{\partial^2 w}{\partial t^2} = 0, \quad . \quad . \quad . \quad (3.10)$$

where

Δ_1^2 is the two dimensional Laplacian operator,
w = deflexion of plate normal to its own plane,
$2h$ = thickness of plate,
ρ = density of plate,
E = Young's modulus,
σ = Poisson's ratio,

and the boundary conditions are, if a' be the inner and a the outer radius of the annulus:

$$r = a', \qquad w = \frac{\partial w}{\partial r} = 0, \quad (3.11) \text{ and } (3.12)$$

$$r = a, \qquad \frac{\partial^2 w}{\partial r^2} + \sigma\left(\frac{1}{r}\frac{\partial w}{\partial r} + \frac{1}{r^2}\frac{\partial^2 w}{\partial \theta^2}\right) = 0, \qquad (3.13)$$

$$\frac{\partial}{\partial r}\left\{\frac{\partial^2 w}{\partial r^2} + \frac{1}{r}\frac{\partial w}{\partial r} + \frac{1}{r^2}\frac{\partial^2 w}{\partial \theta^2}\right\}$$

$$+ (1-\sigma)\frac{1}{r}\frac{\partial}{\partial \theta}\left\{\frac{\partial}{\partial r}\left(\frac{1}{r}\frac{\partial w}{\partial \theta}\right)\right\} = 0. \quad (3.14)$$

Now

$$\Delta^2 = \frac{\partial^2}{\partial r^2} + \frac{1}{r}\frac{\partial}{\partial r} + \frac{1}{r^2}\frac{\partial^2}{\partial \theta^2},$$

so that, assuming a solution of the form

$$w = z \sin n\theta \cos pt,$$

and introducing the new independent variable η, where

$$a\eta = r,$$

equation (3.10) becomes

$$\psi_1{}^4 z = \lambda^4 z, \qquad . \quad . \quad . \quad . \quad . \quad (3.15)$$

where

$$\psi_1{}^2 z = \left(\frac{d^2}{dr^2} + \frac{1}{r}\frac{d}{dr} - \frac{n^2}{r^2}\right)z$$

and

$$\lambda^4 = \frac{3\rho(1-\sigma^2)a^4}{g\mathrm{E}h^2}p^2, \qquad . \quad . \quad . \quad (3.151)$$

while the boundary conditions become

$$\eta = a'/a = s, \qquad z = \frac{dz}{d\eta} = 0, \quad (3.16 \text{ and } 3.17)$$

$$\eta = 1, \qquad \frac{d^2 z}{d\eta} + \sigma\frac{dz}{d\eta} - \sigma n^2 z = 0, \quad . \quad . \quad (3.18)$$

$$\frac{d^3 z}{d\eta^3} + \frac{d^2 z}{d\eta^2} - \{1 + (z-\sigma)n^2\}\frac{dz}{d\eta} + (z-\sigma)n^2 z = 0. \quad (3.19)$$

Now writing $\psi_1^2\chi$ in the well-known form,

$$\psi_1^2\chi = \frac{1}{\eta^{n+1}}\frac{d}{d\eta}\left\{\eta^{2n+1}\frac{d}{d\eta}(\chi\eta^{-n})\right\},$$

and substituting χ for $\psi_1^2 z$, (3.15) becomes

$$\frac{1}{\eta^{n+1}}\frac{d}{d\eta}\left\{\eta^{2n+1}\frac{d}{d\eta}(\chi\eta^{-n})\right\} = \lambda^4 z$$

or

$$\frac{d}{d\eta}\left\{\eta^{2n+1}\frac{d}{d\eta}(\chi\eta^{-n})\right\} = \lambda^4 z\eta^{n+1} = \mathrm{J}_0, \quad . \quad (3.20)$$

whence, integrating successively,

$$\eta^{2n+1}\frac{d}{d\eta}(\chi\eta^{-n}) = \int_s^\eta \mathrm{J}_0 d\eta + \mathrm{A} = \mathrm{I}_1 + \mathrm{A}, \quad . \quad (3.21)$$

$$\chi\eta^{-n} = \int_s^\eta \mathrm{J}_1\eta^{-(2n+1)}d\eta + \mathrm{A}\int_s^\eta \eta^{-(2n+1)}d\eta + \mathrm{B}$$

$$= \mathrm{J}_2 - \frac{\mathrm{A}}{2n}\eta^{-2n} + \mathrm{B}, \quad . \quad . \quad (3.22)$$

$$\chi = \frac{1}{\eta^{n+1}}\frac{d}{d\eta}\left\{\eta^{2n+1}\frac{d}{d\eta}(z\eta^{-n})\right\} = \eta^n\mathrm{J}_2 - \frac{\mathrm{A}}{2n}\eta^{-n} + \mathrm{B}\eta^n,$$

$$\eta^{2n+1}\frac{d}{d\eta}(z\eta^{-n}) = \int_s^\eta \mathrm{J}_2\eta^{2n+1}d\eta - \frac{\mathrm{A}}{2n}\int_s^\eta \eta d\eta + \mathrm{B}\int_s^\eta \eta^{2n+1}d\eta + \mathrm{C}$$

$$= \mathrm{J}_3 - \frac{\mathrm{A}}{2n}\mathrm{K}_3 + \mathrm{B}\mathrm{L}_3 + \mathrm{C}, \quad . \quad . \quad . \quad . \quad (3.23)$$

and finally,

$$z = \eta^n\left\{\int_s^\eta \mathrm{J}_3\eta^{-(2n+1)}d\eta - \frac{\mathrm{A}}{2n}\int_s^\eta \mathrm{K}_3\eta^{-(2n+1)}d\eta\right.$$

$$\left. + \mathrm{B}\int_s^\eta \mathrm{L}_3\eta^{-(2n+1)}d\eta + \mathrm{C}\int_0^\eta \eta^{-(2n+1)}d\eta + \mathrm{D}\right\}$$

$$= \eta^n\left(\mathrm{J}_4 - \frac{\mathrm{A}}{2n}\mathrm{K}_4 + \mathrm{B}\mathrm{L}_4\right). \quad . \quad . \quad . \quad . \quad . \quad . \quad . \quad (3.24)$$

Noting that all the integrated quantities vanish at $\eta = s$, the boundary conditions (3.16) to (3.19) give, on substituting from (3.24),

$$C=D=0$$

$$(1-\sigma)\{n(n-1)J_4'-J_3'\}+J_2'$$
$$-\frac{A}{2n}[(1-\sigma)\{n(n-1)K_4'-K_3'\}+1]$$
$$+B[(1-\sigma)\{n(n-1)L_0'-L_3'\}+1]=0, \quad (3.25)$$

and

$$n^2(1-\sigma)\{(1-n)J_4'-J_3'\}+nJ_2'+J_1'$$
$$-\frac{A}{2n}[n^2(1-\sigma)\{(1-n)K_4'-K_3'\}-n]$$
$$+B[n^2(1-\sigma)\{(1-n)L_4'-L_3'\}+n]=0 \quad (3.26)$$

(where the dashes indicate that the values are to be taken for $\eta=1$).

Moreover, on performing the integrations, it is seen that

$$\left.\begin{aligned} K_3&=\tfrac{1}{2}(\eta^2-s_2),\\ K_4&=\tfrac{1}{2}\left[\frac{1}{2n-2}(s^{-2n+2}-\eta^{-2n+2})+\frac{s^2}{2n}(s^{-2n}-\eta^{-2n})\right],\end{aligned}\right\} \quad (3.27)$$

$$\left.\begin{aligned} L_3&=\frac{1}{2n+2}(\eta^{2n+2}-s^{2n+2}),\\ L_4&=\frac{1}{2n+2}\left[\tfrac{1}{2}(\eta^2-s^2)-\frac{s^{2n+2}}{2n}(s^{-2n}-\eta^{-2n})\right]\end{aligned}\right\} \quad . \quad . \quad (3.28)$$

A sample calculation for a case in which $s=0.395$, evaluated for $n=4$, is given in Tables V. and VI. Table V. gives the step-by-step calculation on the J's, while Table VI. gives the values of K_4 and L_4 (calculated direct from (3.27) and (3.28) in this case), z and λ^4. Here again the first attempt at using the method is given, in order not to show it in an unduly favourable light. The stage given is actually the second approximation, and it will be seen that the initial estimate of z_0 was so bad that even after the second approximation λ^4 varies appreciably, and a third approximation would be desirable—it is, of course, unnecessary to recalculate the K's and L's each time, which results in a substantial saving of time in cases where the K's and L's have to be integrated step-by-step in the same way as the J's. With the values of the J's, K's, and L's in these tables it is found that

$$\frac{A}{2n}=-3.580\times10^{-5}, \qquad B=-3.405\times10^{-3},$$

whence the remaining values may be calculated.

4. *Conclusion.*

In concluding, two remarks may perhaps be made. Firstly, it may sometimes be convenient, having made one approximation, to employ Rayleigh's method, using the newly calculated deflexion form for this purpose. This will generally give good results, since the errors in y_1 are generally quite small, and the fluctuations in the value of

$$\lambda = y_0/y_1,$$

originate mainly from inaccuracies in y_0.

In the second place, it is useful to bear in mind the theorem contained in Temple's second paper[2], p. 270, that if

$$L(y) + \lambda\sigma(x)y = 0,$$

be the equation whose characteristic values λ in a range a_1 to a_2 are required, $-L(y)=0$ being a self-adjoint differential equation of even order $(2r)$, subject to linear homogeneous terminal conditions such as (2.5), and $\sigma(x)$ being a function that is not zero in the interval $a_1 \leq x \leq a^2$ and that, together with its differential coefficients up to the order $2r$, is continuous—the smallest characteristic value λ_0 satisfies the inequality

$$Q \leq \lambda_0 \leq P,$$

where P and Q are the upper and lower bounds of the function

$$F(x) = -L(\theta)/\{\theta(x)\sigma(z)\},$$

and $\theta(x)$ is a function which

(1) has continuous derivatives up to the rth order throughout the interval $a_1 \leq x < a_2$,

(2) satisfies the boundary conditions of the problem,

(3) is never negative in the interval $a_1 \leq x \leq a_2$.

Thus, in many cases, an approximate solution might be used as the function $\theta(x)$.

References.

(1) Temple, Proc. Roy. Soc. A, cxix. p. 276 (1928).
(2) Temple, Proc. London Math. Soc. (Ser. 2), xxix. p. 257.
(3) Southwell, Proc. Roy. Soc. A, ci. p. 133 (1922).

XCV. *The Temperature Variation of the Thermal Conductivity of Pyrex Glass. By* R. W. B. Stephens, *B.Sc., Imperial College of Science and Technology* *.

Introduction.

THE extensive application of pyrex glass in many branches of scientific work has emphasized the need for the determination of its physical constants. The existing data for the thermal conductivity of the glass is restricted to observations at room and steam temperatures, and the present work was undertaken at the suggestion of Dr. H. S. Gregory, with the object of investigating the variation of conductivity over an extended temperature range.

In the absolute measurement of thermal conductivity the method to be employed is dependent upon the nature of the substance under examination. When the material, especially in the case of poor conductors, can be formed into cylinders or hollow spheres, certain advantages are derived from the radial heat flow. In particular, the lateral heat loss may be totally or partially eliminated, though often this advantage has been lost by the manner of the temperature measurements. The cylindrical method has been more generally used in practice, by the reason of the fact that specimens can be more readily obtained in this shape than in the spherical form. In the scheme usually adopted, the solid cylinder is heated axially by the passage of an electric current along a wire, temperatures being measured at two or more points remote from the axis. In Niven's † experiments the specimen was in the form of two half-cylinders, and a similar procedure was used by Clement and Egy ‡, and by Poole §. The latter experimenter took great care to minimize the distortion of the lines of heat flow, when measuring the temperature of isothermal planes within the material, by a suitable disposition of the thermo-elements employed.

It is evident that the above-mentioned experimental difficulties will be considerably lessened if the heated wire were used to measure the temperature along the axis of the specimen, the temperature of the external surface being also observed directly. This latter measurement is rendered

* Communicated by Prof. H. S. Gregory, Ph.D.
† Proc. Roy. Soc. lxxvi. p. 34 (1905).
‡ Phys. Rev. xxviii. p. 71 (1909).
§ Phil. Mag. xxiv. p. 45 (1912); and xxvii. p. 58 (1914).

practicable if an external bath, preferably of a liquid in regular and efficient circulation, be employed to maintain the surface temperature constant; this latter quantity being measured by a platinum wire wound in close contact with the outer surface. The determination of the temperature of the internal surface of the specimen by the means indicated, will be dependent upon the degree of contact of the axial wire with the material. The required condition may be realized in practice if the substance under examination can be moulded around the wire. This process, however, is not without difficulty, as shown in experiments made by the author some years ago, on the embedding of thin wires in cylinders of resin. The experiments were unsuccessful owing to the breakage of the wires, consequent upon the strains set up in the material when solidifying. In the present work the problem is much simplified by the fact that thin platinum wire can be fused into intimate contact with the glass without great difficulty.

Description of Apparatus.

A platinum wire, 4 mm. in diameter, was threaded through a length (60 to 70 cm. of pyrex capillary tube of approximately 0·1 cm. internal and 1·0 cm. external diameter, and the glass was carefully melted around the wire working from the centre outwards over a length of about 30 cm. The finished specimen, which was remarkably free from observable air-bubbles, finally took the form of a U-tube, the ends of the capillary adjacent to the fused portion being "cupped" to act as mercury reservoirs. The general form of the apparatus is indicated in fig. 1, where R denotes the axial platinum wire which enters the enlarged portions of the capillary at B and C. The glass walls were thickened at these junctions in order to minimise the enhanced end effect, due to the presence of the mercury there. Electrical contact with the mercury at B and C was obtained by means of bare copper wires held firmly in the capillary tubes, so that their lower ends were in very close proximity to the ends of the embedded platinum wire, and their upper ends were connected to insulated terminals carried by the blocks T_1 and T_2. These ebonite blocks were rigidly attached to a wooden frame, W, which also served as a clamp for the U-tube. The platinum wire, *pp*, was tightly wound on the outer surface of the glass being anchored at the lower extremity, S, by a bead of glass. The free ends of the platinum wire were silvered-soldered to short lengths of fine

copper wire, which in turn were welded to thick copper leads, L_1 and L_2. These latter, held in position by a glass bridge, G, passed through holes in the frame, W, and were connected to insulated terminals on the blocks T_1 and T_2. For the readings between 50° C. and 250° C., an oil-bath,

Fig. 1.

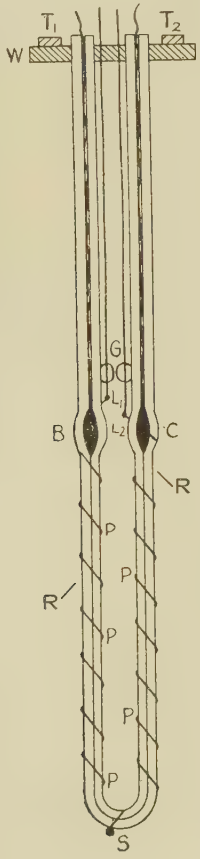

shown in fig. 2 was employed, the U-tube being mounted vertically in the upright limb of an L-shaped brass tube, L, and held in position by screws passing through W and the asbestos cover, A. This cover formed a close fitting lid to the iron vessel, V, which contained the oil and was centrally disposed within a galvanized iron bin, D. The interspace

between the vessels was filled with asbestos wool. A constant stream of oil was pumped over the surface of the specimen

Fig. 2.

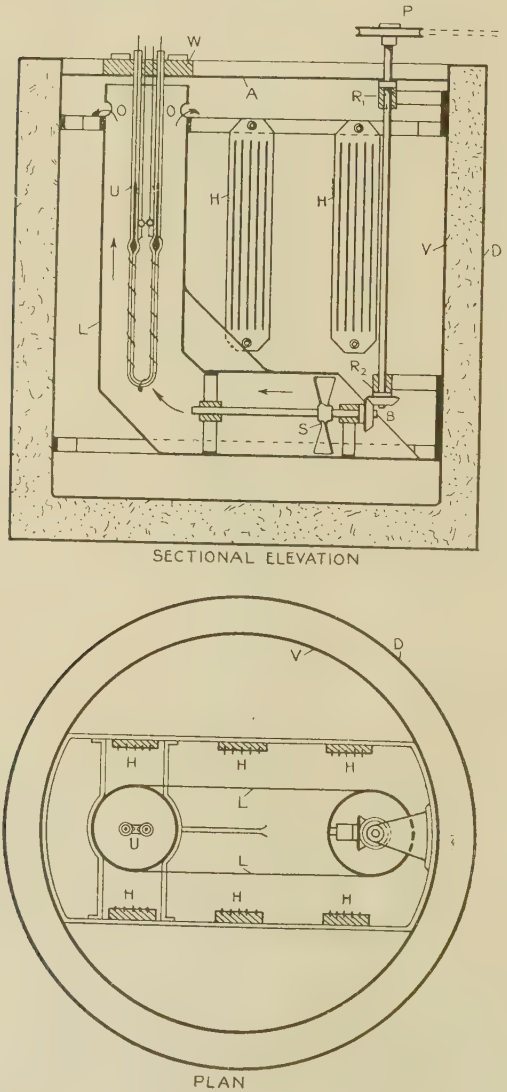

by means of the screw propeller, S, situated in the horizontal limb of the L-shaped tube. A pulley, P, fixed to a vertical

shaft which worked in ball-races, R_1 and R_2, at its upper and lower ends, was driven by an electric motor. The power was transmitted to the horizontal shaft carrying S by the bevel gearing situated at B. Six nichrome heating elements, H, were suitably disposed throughout the bath and arranged in two parallel sets of three to carry currents up to 12 amperes.

A bath containing crushed ice and water, and circulated in a similar manner to the oil-bath, was utilized for the observations in the neighbourhood of 0° C. Liquid air and a mixture of solid carbon dioxide and aviation spirit were the thermostatic substances employed to obtain the lower temperatures. These substances were contained in a vacuum vessel, and the U-tube was centrally disposed within the latter. A closely fitting ring of perforated brass, fixed to the end of a bakelite rod as handle, was found to be an efficient means of stirring the contents of the vessel.

The heating current for the central platinum wire was supplied by a battery of accumulators, the actual energy dissipated in the wire being found from a knowledge of the potential difference between its ends, and the current passing. The current was calculated from the measured potential difference between the terminals of a standard resistance connected in series with the platinum wire, the potential measurements being made with a Gambrell 4 dial potentiometer. The resistance of the wire was also evaluated from the same data, enabling the temperature to be calculated when the resistance at 0° C. and the fundamental interval of the wire were known. The resistance of the outside wire, *pp*, henceforth called the wall thermometer, was determined by means of a Callendar-Griffiths bridge. The standard resistance was a 1 ohm coil for readings below 0° C., but was substituted by a 10 ohm coil for the observations at the higher temperatures.

Theory of the Method.

Consider the ideal case of a uniform cylinder of material, of internal and external radii r_1 and r_2 respectively, in which heat is supplied axially by an electric current passing along a wire of radius r_1. Then in the steady state

$$\frac{Q}{4{\cdot}18} = \frac{2\pi K l.(\theta_1 - \theta_2)}{\log_e . r_2/r_1}, \quad . \quad . \quad . \quad . \quad (1)$$

where θ_1 and θ_2 are the temperatures ° C. of the inner and outer surfaces respectively, l cm. is the length of the

cylinder, K is the thermal conductivity (cal. cm.$^{-1}$ sec.$^{-1}$ deg.$^{-1}$) at a mean temperature $(\theta_1+\theta_2)/2^\circ$ C., and Q is the energy in watts dissipated by the wire. If C amperes be the current passing and R ohms the resistance of the wire,

$$Q=C^2R.$$

Alternatively (1) may be written

$$\frac{Q}{4{\cdot}18(\theta_1-\theta_2)}=\frac{2\pi l}{\log_e . r_2/r_1}.K=F.K, \quad . \quad . \quad (2)$$

where F is known as the form factor of the apparatus and is assumed to be independent of the temperature. From a knowledge of F and the value of $Q/(\theta_1-\theta_2)$, the conductivity K at the temperature $(\theta_1+\theta_2)/2^\circ$ C. may be calculated. In the present experiment the sinuous nature of the outer surface of the glass specimen, and also the somewhat wavy path of the platinum wire along its axis, rendered the calculation of F from dimensional measurements a matter of doubt. From the standpoint of studying the temperature variation of thermal conductivity, however, this uncertainty will not create any difficulty, and, furthermore, if the absolute value of the conductivity be known at a particular temperature, the form factor may be accurately determined.

In the above analysis the conduction problem has been treated as if the strictly radial heat flow persisted throughout the length of the body surrounding the wire. This interpretation of the problem is an approximation of the actual conditions existing, and more accurately equation (2) should be written

$$F.K=\frac{Q}{4{\cdot}18(\theta_1-\theta_2)}-\frac{2q}{(\theta_1-\theta_2)}, \quad . \quad . \quad . \quad (3)$$

where $2q$ represents the heat loss (cal./sec.) from the ends of the wire.

Let K_p be the thermal conductivity of platinum (cal. cm.$^{-1}$ sec.$^{-1}$ deg.$^{-1}$).

K be the thermal conductivity of pyrex (cal. cm.$^{-1}$ sec.$^{-1}$ deg.$^{-1}$),

S (sq. cm.) the cross-sectional area of the platinum wire,

l (cm.) the length of the platinum wire,

R// (ohm/cm.) the resistance per unit length of the wire, and

C the heating current in amperes.

Consider the thermal equilibrium of the elementary cylinder contained between the dotted lines in fig. 3. The equation representing this heat balance is as follows:

$$K_p.S.\frac{d^2\theta}{dx^2}.\delta x+\frac{C^2R}{4{\cdot}18l}.\delta x=\frac{2\pi K.\theta}{\log_e.r_2/r_1}.\delta x, \quad . \quad (4)$$

where θ° C. is the temperature excess at a point distant x cm. from one end.

Fig. 3.

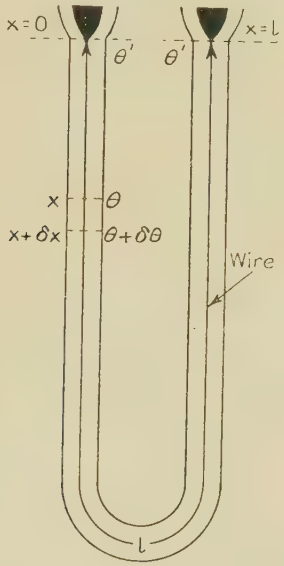

Again, equation (4) may be written

$$\frac{d^2\theta}{dx^2}-M\theta=-N, \quad . \quad . \quad . \quad . \quad . \quad (5)$$

where $M=\dfrac{2\pi.K}{K_pS.\log_e.r_2/r_1}$ and $N=\dfrac{C^2R/l}{4{\cdot}18.K_p.S}$.

The solution of this equation is

$$\theta=N/M+P.e^{\sqrt{M}.x}+Q.e^{-\sqrt{M}.x}, \quad . \quad . \quad . \quad (6)$$

P and Q are evaluated from the end conditions $\theta=\theta'$ at $x=0$ and at $x=l$.

On substitution

$$\theta = N/M + (\theta' - N/M).(e^{+(x-l).\sqrt{M}} + e^{-x\sqrt{M}}) \text{ approx.,} \quad (7)$$

since $e^{-l.\sqrt{M}}$ is extremely small.

Now the smallest value θ' can have is zero, therefore in this extreme but unlikely case

$$\theta = N/M.(1 - e^{\sqrt{M}.(x-l)} - e^{-\sqrt{M}.x}). \quad . \quad . \quad (8)$$

Furthermore, the heat conducted away per second from each end of the platinum wire will be given by

$$q = K_p.S.(d\theta/dx)_{x=0},$$

or

$$q = K_p.S.\frac{N}{M}.\sqrt{M}.(1 - e^{-\sqrt{M}.l}). \quad . \quad . \quad . \quad (9)$$

Hence

$$\frac{q}{Q/4{\cdot}18} = \frac{K_p.S.\dfrac{N}{M}\sqrt{M}.(1 - e^{-\sqrt{M}.l})}{C^2R/4{\cdot}18} = \frac{1}{l.\sqrt{M}}(1 - e^{-\sqrt{M}.l}).$$

$$= \frac{1}{l.\sqrt{M}} \cdot \text{approx.} \quad . \quad . \quad . \quad . \quad . \quad . \quad . \quad . \quad . \quad (10)$$

By substitution of (10) in equation (3),

$$F.K = \frac{Q}{4{\cdot}18.(\theta_1 - \theta_2)}.C. \quad . \quad . \quad . \quad (11)$$

where

$$C = \left(1 - \frac{2}{l.\sqrt{M}}\right),$$

and represents the correction factor to be applied to the experimental values of the ratio $Q/4{\cdot}18(\theta_1 - \theta_2)$. The calculated values of C. at -180° C. and 100° C. are 0·994 and 0·996 respectively, which are within the limits of experimental error. It is more important to note that the correction factor is almost independent of temperature, and so will not affect the variation of conductivity, which it is the purpose of the present experiment to investigate.

Method of Experiment.

By suitable adjustment of the current through the heaters, the temperature of the oil-bath could be set at various temperatures between room temperature and 250° C., and

actually observations were made approximately every 50° C. Assuming the temperature of the oil-bath to have become steady, as indicated by the wall thermometer, a current was passed through the inner platinum wire. The wall temperature was observed to increase almost immediately, but a new stationary value was soon attained. The advantage to be gained by using a thin cylinder of material was clearly indicated by the rapidity with which thermal equilibrium was established, and so enabled the following procedure to be adopted. Instead of waiting for the bath to reach a steady temperature, the current through the heaters was adjusted, so that the bath was slowly cooling and a series of potential and temperature readings obtained, at known time intervals. By interpolation of these observations it was possible to derive a set of readings connecting energy input with the temperature of the inner wire at a constant wall temperature. This method of working had a further advantage in expediting the experimental observations.

Evaluation of the Form Factor.

Using a method to be described in a subsequent paper, the thermal conductivity of pyrex was found to be 0·00235 cal. cm.$^{-1}$ sec.$^{-1}$ deg.$^{-1}$ at a mean temperature of 25° C. Now the value of $Q/(\theta_1-\theta_2)$ derived from the slope of the graph of Q against $(\theta_1-\theta_2)$ was 0·446 watts per degree C. at a temperature of 25° C., hence it follows that

$$F=\frac{0\cdot446}{4\cdot18\times0\cdot00255}=41\cdot9 \text{ cm.}$$

As a check on the above value, F was also determined from the dimensions of the apparatus, assuming that the U-tube could be regarded as a close approximation to a cylinder. The length l corresponded to that of the embedded platinum wire and was estimated from the observed resistance and the known value per cm. The value of l thus calculated was 29·5 cm., which was in excellent agreement with a measured trace of the wire. The average of sixty readings of the external diameter of the glass U-tube gave $r_2=0\cdot350$ cm. (the extreme values varying about 7 per cent. from the mean), so that

$$F=\frac{2\pi.l}{\log_e r_2/r_1}=\frac{2\pi\times29\cdot5}{\log_e\frac{0\cdot350}{0\cdot00508}}=43\cdot8 \text{ cm.}$$

Typical Experiment.

Liquid Air Bath.

Set.	Time. mins.	Potentiometer readings.	Resistance of axial platinum wire (R.). ohms.	Call. and Griff. bridge reading for wall thermometer cms. bridge wire.	Derived values for each set.
1.		S.C. 4969_0			
	0·2			130·54	
	1·0	S.R. 1928_2	$0{\cdot}9237_2$		$R=0{\cdot}9244_9$ ohm.
	2·5	W. 1781_0			
	3·0			130·55	$\theta=-182{\cdot}74°$ C.
	3·5	W. 1780_2	$0{\cdot}9245_4$		
	4·0	S.R. 1925_6			$\theta=-183{\cdot}44°$ C.
	5·0			130·50	
	5·5	W. 1925_5	$0{\cdot}9244_9$		$Q=0{\cdot}1438_2$ watts.
	6·0	S.R. 1780_0			
	6·5			130·50	
		S.C. 4969_0			
2.		S.C. 4969_0			
	0·0			130·53	$R=0{\cdot}9444_9$ ohm.
	0·5	W. 3138_9	$0{\cdot}9445_1$		
	1·5	S.R. 3322_2			$\theta=-181{\cdot}46°$ C.
	2·0			130·50	
	2·7	S.R. 3322_8	$0{\cdot}9444_6$		$\theta=-183{\cdot}44°$ C.
	3·2	W. 3138_3			
	3·7			130·50	$Q=0{\cdot}4375_1$ watts.
		S.C. 4969_2			

3.	0·0	S.C. 4969_2			
	0·7	W. 5027_5		130·58	$R=0{\cdot}9875_8$ ohm.
	1·7	S.R. 5089_5	$0{\cdot}9878_1$		$\theta=-178{\cdot}58°$ C.
	2·3			130·55	
	2·7	S.R. 5089_5			$\theta=-183{\cdot}46°$ C.
	3·5	W. 5026_2	$0{\cdot}9875_8$		
	4·0			130·54	$Q=1{\cdot}0734$ watts.
		S.C. 4969_3			
4.		S.C. 4969_2			
	0·5			130·64	
	1·2	W. 6340_2			
	2·0	S.R. 6185_0	·0251		$R=1{\cdot}0249$ ohms.
	2·5			130·54	
	3·5	S.R. 6184_8			$\theta=-176{\cdot}09°$ C.
	4·0	W. 6338_5	1·0249		
	4·5			130·56	$\theta=-183{\cdot}47°$ C.
	5·0	W. 6338_0			
	6·0	S.R. 6184_0	1·0249		$Q=1{\cdot}6447$ watts.
	6·5			130·56	
		S.C. 4969_0			

In the above table S.C., S.R., and W. refer to the Standard Cell, Standard Resistance (1 ohm), and Platinum Wire Readings respectively.

The E.M.F. of the Standard Cadmium Cell was $1{\cdot}018_8$ volts at 16° C.

Experimental Results.

The values of $Q/(\theta_1-\theta_2)$ set out in the table below are calculated from the slopes of the graphs obtained by plotting Q against $(\theta_1-\theta_2)$ at constant wall temperature (fig. 4).

$Q/(\theta_1-\theta_2)$. Watts per deg. C.	K. Cal. cm.$^{-1}$ sec.$^{-1}$ deg.$^{-1}$	Mean temperature. Deg. C.
0·548	0·00313	250
0·528	0·00302	209
0·508	0·00290	150
0·490	0·00280	112
0·484	0·00277	99
0·225	0·00129	−181

The following table contains the results calculated from random observations at various bath temperatures :—

$(\theta_1-\theta_2)$. Deg. C.	Q. Watts.	$Q/(\theta_1-\theta_2)$. Watts per deg. C.	K. Cal. cm.$^{-1}$ sec.$^{-1}$ deg.$^{-1}$	Mean temp. Deg. C.
3·41	1·458	0·429	0·00245	1·8
18·48	9·813	0·531	0·00303	215·4
14·26	6·951	0·487	0·00278	105·2
7·10	3·250	0·458	0·00262	55·0
13·46	6·215	0·462	0·00264	59·5
2·74	1·292	0·471	0·00269	65·6
10·21	4·792	0·469	0·00268	70·5
14·97	7·599	0·508	0·00290	155·0
0·97	0·356	0·367	0·00210	−77·7
5·31	1·979	0·373	0·00213	−74·9
11·34	4·920	0·433	0·00246	6·0

Fundamental interval of inner platinum wire = 138·24 cm.

Fundamental interval of wall thermometer = 181·16 cm.

The above readings are expressed in terms of the bridge wire.

The platinum temperatures of 0° C. were corrected to the gas scale by the use of Callendar's difference formula

$$t-t_{pt}=d.t.(t-100),$$

where d was taken as $1{\cdot}50\times10^{-4}$. The parabolic relation between resistance and temperature is not valid below −40° C. and was replaced by a formula involving the fourth power of the temperature, for the purposes of calculating the scale correction at the lower temperatures.

Stationary Liquid Layer on the Boundary Surface of the Heated Body.

During the course of the experiment it was noticed that an increase or decrease of the current through the inner platinum wire produced simultaneously a corresponding change in the wall temperature. Since this so-called skin effect is of considerable importance it was thought that some useful deductions might be derived from the data provided by the experiment. It has long been recognized that when

Fig. 4.

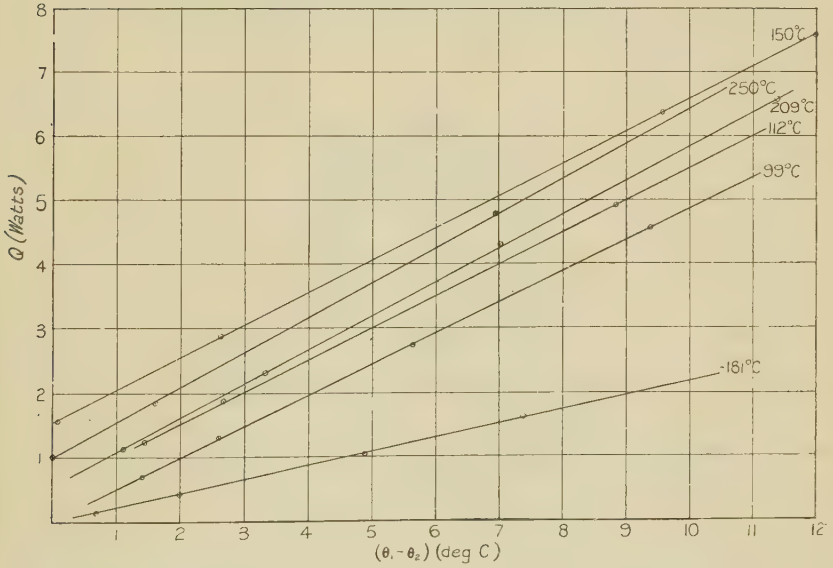

a heated body is placed in a cooling stream of liquid there exists a stationary layer of fluid in contact with the solid. The thickness of this layer will depend, amongst other quantities, upon the velocity of flow and the viscosity of the fluid; furthermore, the temperature drop across the stratum will vary inversely as the thermal conductivity of the liquid. The present experiment enables an approximate estimate to be made of the effective thickness of this layer. For, consider fig. 5, where r_1, r_2, and r_3 represent the radius of the platinum wire, the radius of the outer glass surface and the outer radius of the liquid layer respectively. θ_1, θ_2, and θ_3 denote the corresponding temperatures.

Then if Q be the energy (in watts) dissipated by the wire in the steady state,

$$\frac{Q}{4{\cdot}18} = \frac{2\pi K l.(\theta_1-\theta_2)}{\log_e r_2/r_1} = \frac{2\pi k l.(\theta_2-\theta_3)}{\log_e r_3/r_2}, \quad . \quad (12)$$

where K = thermal conductivity of glass in cal. cm.$^{-1}$ sec.$^{-1}$ deg.$^{-1}$ at a mean temperature $(\theta_1+\theta_2)/2°$ C.,

k = thermal conductivity of the liquid in cal. cm.$^{-1}$ sec.$^{-1}$ deg.$^{-1}$ at a mean temperature $(\theta_2+\theta_3)/2°$ C.,

and l = effective length of the specimen.

Suppose the current through the wire to be increased, and let dQ be the corresponding increment of energy dissipated per second.

Fig. 5.

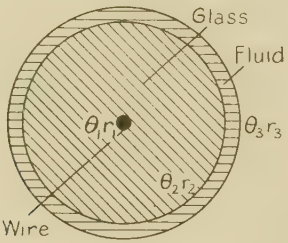

Cross-section of U-tube and inner platinum wire.

Then, assuming θ_3 and k to remain constant, if $d\theta_2$ be the increase in the wall temperature,

$$\frac{dQ}{4{\cdot}18} = \frac{2\pi k l.d\theta_2}{\log_e r_3/r_2}. \quad . \quad . \quad . \quad . \quad . \quad (13)$$

From this expression r_3 can be calculated, the other quantities being known.

The following observations were made with the oil-bath :—

Bath temp. Deg. C.	$\frac{d\theta_2}{dQ}$. Deg. C./watts.	r_3. cm.	r_3-r_2. cm.
249	0·094	0·360	0·010
206	0·111	0·362	0·012
147	0·182	0·371	0·021
112	0·396	0·398	0·048
97	0·411	0·400	0·050
50	0·662	0·438	0·088

The physical constants of the thermostat oil were as follows :—

Density = 0·91 gm. per c.c. at 60° F.

Viscosity (in Redwood seconds) 1250 at 140° F., 310 at 200° F., and 128 at 250° F.

Thermal conductivity at 20° C. = 0·00044 cal. cm.$^{-1}$ sec.$^{-1}$ deg.$^{-1}$

The relation between the effective thickness of the oil layer and the temperature of the bath is indicated in fig. 6.

Fig. 6.

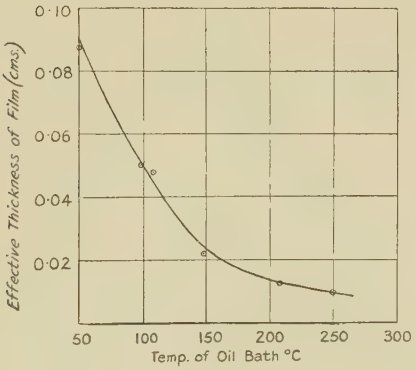

It would appear from the limited number of values of viscosity available that the thickness is proportional to the logarithm of the viscosity. Hence since liquid air has a very small viscosity, no appreciable wall effect should have been noticed with the corresponding bath, and this conclusion was verified by experiment. It is noteworthy that even with the ice-bath experiments a small but definite increase in the wall temperature was produced by an increase in the heating current through the wire. The typical observations set out below indicate this rise of temperature, and an estimate of the thickness of the water layer has been made, assuming the thermal conductivity of water to be 0·00145 cal. cm.$^{-1}$ sec.$^{-1}$ deg.$^{-1}$ at 0° C.

Ice-Bath.

dQ. Watts.	$d\theta_2$. Deg. C.	$\frac{d\theta_2}{dQ}$. Deg. C./watts.	Effective thickness of water layer ($r_3 - r_2$) cm.
0·93	$0{\cdot}04_7$	$0{\cdot}050_6$	0·020
3·46	$0{\cdot}21_3$	$0{\cdot}058_3$	0·025

Fig. 7.

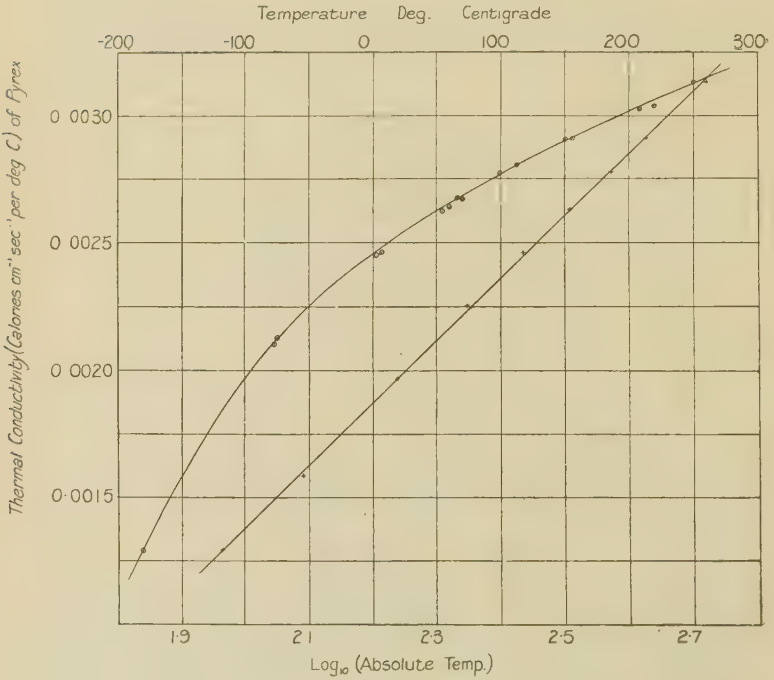

Summary.

The thermal conductivity of pyrex glass has been investigated over the temperature range from $-180°$ C. to 250°C. The variation of conductivity may be satisfactorily represented by the relation $K = A + b.\log_{10} T.$, where A and b are constants having the values $-0{\cdot}00352_3$ and $0{\cdot}00245_4$ respectively. K is expressed in cal. cm.$^{-1}$ sec.$^{-1}$ deg.$^{-1}$, and T is the absolute temperature. The following table

indicates how closely this relation satisfies the experimental observations :—

T deg....	92	198	275	372	423	482	523
K (calc.).	0·00129	0·00211	0·00246	0·00278	0·00292	0·00306	0·00315
K (obs.).	0·00129	0·00213	0·00245	0·00277	0·00290	0·00302	0·00313

A length of capillary tube, identical with that used in the experiment, was carefully fused into a spherical shape free of observable air-bubbles. The density of the glass, found from this specimen, was $2{\cdot}23_3$ gm. per c.c. at 21° C. The composition of the glass, as quoted by the manufacturers,

Fig. 8.

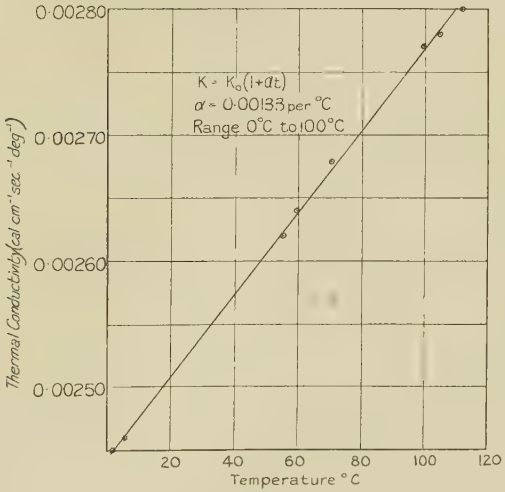

was as follows :—80·5 per cent. silica, 2 per cent. alumina, 12·5 per cent. boric oxide, and 4 per cent. sodium oxide.

The above results show good agreement with those of previous observers *. P. W. Bridgeman, using a cylindrical method, found no variation of the conductivity over the temperature range 30° C. to 75° C., and obtained the value 0·00261 cal. cm.$^{-1}$ sec.$^{-1}$ deg.$^{-1}$ The composition of the glass was given as 81·35 per cent. silica, 11·50 per cent. boric oxide, 4·0 per cent. sodium oxide, 2·1 per cent. alumina, 0·2 per cent. calcium oxide, and 0·28 per cent. magnesium oxide, and the density was 2·234 gm. per c.c. at room

* Am. Journ. Sci. ser. 5, vii. Jan.–June 1924.

temperature*. M. Rene Reulos adopted the plate method, and found the thermal conductivity of a disk of pyrex in terms of that of water. The final value obtained was 0·0023 cal. cm.$^{-1}$ sec.$^{-1}$ deg.$^{-1}$ at a mean temperature of about 75° C., but no figures are quoted for the density and composition of the glass. The conductivity as determined from the present experiments was 0·00256 and 0·00270 cal. cm.$^{-1}$ sec.$^{-1}$ deg.$^{-1}$ at 30° C. and 75° C. respectively. Assuming a linear relation between conductivity and temperature over the range 0° C. and 100° C., viz., $K = K_0(1 + \alpha t)$, $\alpha = +0{\cdot}00133$ per deg. C. It is interesting to note that this value is intermediate between the corresponding figures for plate glass † (density 2·55 gm. per c.c.) +0·00168 and fused silica ‡ +0·00063. It may also be mentioned that some preliminary experiments with the moulding of sulphur around platinum wires were so promising as to merit further continuance of the work.

In conclusion the author derives great pleasure in recording his thanks to Dr. H. S. Gregory for the kind interest he has shown in the progress of the research.

XCVI. *Studies in Coordination.*—Part IV. *Some Fluorides and Chlorides and their Complex Ions.* *By* F. J. Garrick, *B.A.* §

1. *Introduction.*

THE previous papers of this series [1] dealt with coordination compounds in which a central ion combines with neutral molecules ; and it was shown that a simple electrostatic model (ion-dipole linkage) reproduces the observed phenomena satisfactorily. It is now of interest to investigate how far the electrostatic model is satisfactory in cases where the coordination sphere contains acido groups (negative ions, in the electrostatic theory), and in this paper cases of the type

$$MX_n + n'X^- = MX^{n'-}_{(m=n+n')},$$

where X is F or Cl, will be considered.

A discussion of this problem was given in 1922 by Magnus [2]. His analysis, while it was as complete as was

* *Revue d'Optique.* nos. 6–7, June-July 1931.
† Ensor, Proc. Phys. Soc. xliii. p. 590 (1931).
‡ Kaye and Higgins, Proc. Roy. Soc. ser. A, cxiii. no. 764 (1926).
§ Communicated by the Author.

possible at the time, can only be regarded as semi-quantitative, since it was necessary to make estimates of the ionic radii based largely on the Bohr atom-model, and to neglect polarization effects, which have a pronounced influence on the coordination-number and its variation with the size of the central ion (see paper I.); moreover, the results could only apply to the formation of complexes in the (ionized) gas phase, since at the time no information was available as to the energy changes occurring on the introduction of the ions into solution or crystal-lattice (see secs. 5 and 6 of the present paper). Nevertheless, the results fall well enough into line with observation to indicate that a more precise treatment, such as is now possible, should be worth while.

The method of treatment here used is, in outline, as follows: The molecule MX_n and the complex ion $MX_m^{n'-}$ will both be regarded as hetero-polar; that is, as consisting of the n-times positive M ion surrounded by a sheath of n or m singly negative X ions. It must not be supposed that this picture is regarded as valid for all purposes, but merely as giving an approximately correct value for the energy necessary to split up the molecule or complex ion into atom-ions at infinity; that is to say, the energy terms corresponding to other effects are assumed to be negligible within the limit of error of the calculation. The validity of this assumption is checked wherever possible by thermochemical considerations.

The energy liberated when the molecule or complex ion is formed from its constituent ions in the state of infinitely dilute gas may be termed the Energy of Coordination; it will be calculated in terms of the sizes, charges, and polarizabilities of the ions, the calculation being supposed to refer to absolute zero.

The term "size" of the ions merits further consideration. Strictly, the equilibrium distances should be determined by their "intrinsic" repulsive fields, using, *e.g.*, the force-constants given by Lennard-Jones[3]. On the other hand, the force-laws for some of the ions can only be roughly estimated, and there remains a doubt as to how accurately they hold under conditions of intense force and polarization such as would obtain in a heteropolar $SiCl_4$ or other such molecule. For these reasons, and since the models are so crude in other respects, it seems more reasonable to dispense with this refinement. The ions are therefore considered as spheres of fixed radii, namely, the empirical crystal radii given by Goldschmidt[4], and the contributions of the "intrinsic" repulsions to the potential energy are neglected.

That the error so introduced can only be small is shown by the following considerations: The crystal radii are based on interionic distances in crystals, where the forces operative are much smaller than those to be discussed here. For the compounds under consideration, then, the ionic distances used must be rather too great, and therefore the electrostatic part of the energy of coordination based on them will be too small. On the other hand, this must be very nearly counterbalanced by the neglect of the repulsion terms, for at distances corresponding to the crystal radii this quantity (which may be denoted ϕ_R) is of the order of 10 per cent. of a crystal lattice energy, which in its turn is of the order of 10 per cent. of the energy of coordination. Then, remembering that in the neighbourhood of the equilibrium distance $d/dr(\phi_E + \phi_R) \sim 0$ where r is the distance and ϕ_E the electrostatic potential energy, it follows that the use of ϕ_E alone at the distance given by the crystal radii instead of $\phi_E + \phi_R$ at the true equilibrium distance cannot lead to an error of greater than about 1 per cent.

The polarizabilities of the anions will be taken from Born and Heisenberg [5], and assumed constant. This assumption is crude and presumably leads to high results for the energy; indeed the work of Fajans and Joos [6] indicates that the polarizability does fall off as the polarization increases; but it is impossible to take account of this effect at present, and the error due to neglecting it is probably not serious; thus in an extreme case (CCl_4) a change of 10 per cent. in the polarizability affects ϕ_E by only about 2 per cent.

Thus, granting the correctness of the general picture and of the other numerical data, the results for the energy of coordination should not be in error by more than a few per cent. (the error of the crystal radii) and should, if anything, be high, while the *relative* values of ϕ_E for different complexes formed by a given pair of ions should be considerably more reliable, probably to within 1 per cent.

2. *The Calculation of the Energy of Coordination.*

(a) "*Regular*" *coordination numbers.* As the theory is chiefly concerned with complex ions stable in solution such cases as $NaCl + Cl^- \rightarrow NaCl_2^-$ need not be considered; the calculation is therefore limited to ions of valency (z) from three to six, and to coordination numbers (n) from three to eight where $n \leqslant z$.

It is assumed that where possible the symmetrical arrangement is the most stable, so that for $n = 4$, 6, or 8, the anions

are at the corners of a regular tetrahedron, regular octohedron, or cube, while for $n = 3$ the arrangement is an equilateral triangle.

Let r be the distance between the centres of the central and one of the outer ions, $+ze$ the charge of the central ion and $-e$ the charge of the outer ion, while α and p are the polarizability and induced moment of the latter. It follows from symmetry that the r's and p's are all equal, and that p is directed along r.

Let $s_{kk'}$ be the distance between the centres of the kth and k'th outer ion, while $\theta_{kk'}$ is the angle between r and $s_{kk'}$. Again, from symmetry, $\theta_{kk'} = \theta_{k'k}$.

Then we have

$$-\phi_E = \frac{nze^2}{r} - \frac{1}{2}\sum_k \sum_{k'}' \frac{e^2}{s_{kk'}} + \frac{nzpe}{r^2} - \sum_k \sum_{k'}' \frac{pe}{s_{kk'}^2} \cdot \cos\theta_{kk'}$$
$$- \frac{1}{2}\sum_k \sum_{k'}' \frac{p^2}{s_{kk'}^3}(1 + \cos^2\theta_{kk'}) - \frac{np^2}{2\alpha},$$

while the field strength (directed along r, by symmetry) at the centre of the kth outer ion is

$$E = \frac{ze^2}{r^2} - \sum_{k'}' \frac{e}{s_{kk'}^2} \cdot \cos\theta_{kk'} - \sum_{k'}' \frac{p}{s_{kk'}^3} \cdot (1 + \cos^2\theta_{kk'}),$$

and therefore

$$p = \alpha E = \frac{\alpha e\left\{zr^{-2} - \sum_{k'}' s_{kk'}^{-2}\right\}}{1 + \alpha \sum_{k'}' (1 + \cos^2\theta_{kk'}) s_{kk'}^{-3}}.$$

(The dashed summations refer to the condition $k \neq k'$.)

The values of $\theta_{kk'}$ and of the ratio $\frac{s_{kk'}}{r}$ depend on the geometry of the system and thus vary with n as follows:

$n=3$; $s_{kk'}=r\sqrt{3}$, $\cos\theta_{kk'}=\frac{1}{2}\sqrt{3}$.

$n=4$; $s_{kk'}=\frac{2}{3}r\sqrt{6}$, $\cos\theta_{kk'}=\frac{1}{3}\sqrt{6}$.

$n=6$, $k=1$, $k'=2\ldots5$; $s^{kk'}=r\sqrt{2}$, $\cos\theta_{kk'}=1/\sqrt{2}$.

$k=1$, $k'=6$; $s_{kk'}=2r$, $\cos\theta_{kk'}=1$.

$n=8$, $k=1$, $k'=2, 3, 4$; $s_{kk'}=\frac{2}{3}r\sqrt{3}$, $\cos\theta_{kk'}=1/\sqrt{3}$.

$k'=5, 6, 7$; $s_{kk'}=\frac{2}{3}r\sqrt{6}$, $\cos\theta_{kk'}=\frac{1}{3}\sqrt{6}$.

$k'=8$; $s_{kk'}=2r$, $\cos\theta_{kk'}=1$.

In the equations, if the central ion is sufficiently large r is simply the sum of the ionic radii, namely, $r_M + r_X$.

When, however, r_M is less than a certain value depending on n and X the outer ions touch, and the value of r is then a lower limit defined by $s_{12}=2r_X$.

(b) "*Irregular*" *coordination numbers.* For $n=5$ or 7, the spatially symmetrical arrangement is no longer possible. The latter case occurs only rarely and need not be considered, but the former is important. It is assumed that the stablest arrangement is that in which three anions occupy the corners of an equilateral triangle, with the central ion at its centroid, while the other two are in a straight line with the central ion, and equidistant from it, in a direction at right angles to the plane of the triangle. When r_M is sufficiently great the r's (but not necessarily the p's) are equal. When r_M becomes small this will no longer hold.

Using subscripts 1 and 2 to refer to the ions in the straight line and in the triangle respectively, when r_M is less than a certain limiting value the ions of the two kinds touch and $r_1^2+r_2^2=4r_X^2$. When this holds ϕ_E is a minimum for minimum r_2, r_1 increasing as r_M decreases. This may be simply illustrated by neglecting the polarization terms, for

$$-\phi_E=\frac{3ze^2}{r_2}+\frac{2ze^2}{r_1}-\frac{3e^2}{s_{22}}-\frac{e^2}{s_{11}}-\frac{6\theta^2}{s_{12}};$$

or noting that $s_{12}=2r_X$, $s_{22}=r_2\sqrt{3}$, $s_{11}=2r_1$,

$$-\frac{1}{e^2}\phi_E=\frac{1}{r_2}(3z-\sqrt{3})+\frac{1}{r_1}(2z-\tfrac{1}{2})-\frac{3}{r_X},$$

and

$$-\frac{1}{e^2}\cdot\frac{d}{dr_2}\cdot\phi_E=-\frac{1}{r_2^2}(3z-\sqrt{3})+\frac{r_2}{r_1^3}(2z-\tfrac{1}{2}),$$

for $\dfrac{dr_1}{dr_2}=-\dfrac{r_2}{r_1}$, since $r_1^2+r_2^2=$ constant. That is $\dfrac{d}{dr_2}\cdot\phi_E$ has the same sign as

$$\frac{1}{r_2^3}(3z-\sqrt{3})-\frac{1}{r_1^3}(2z-\tfrac{1}{2}).$$

For $z>1$ this is always +ve if $r_2\leqq r_1$. It may be pointed out in passing that this result implies that where the central ion is small a pentahalide will have two of its halogen atoms much less firmly bound than the other three—a phenomenon which may be observed with PCl_5 and related compounds.

There are then three cases to be distinguished :

Case I., when $r_M + r_X \nleq r_X \cdot \sqrt{2}$; $r_1 = r_2 = r_M + r_X (= r)$.

Case II., when $r_M + r_X \leq r_X\sqrt{2} > \frac{2}{\sqrt{3}} r_X$;

$$r_1 = \sqrt{4r_X^2 - r_2^2} \text{ ; } r_2 = r_M + r_X.$$

Case III., when $r_M + r_X \leqq \frac{2}{\sqrt{3}} r_X$;

$$r_1 = \tfrac{2}{3}\sqrt{6} \cdot r_X, \; r_2 = \tfrac{2}{3}\sqrt{3} \cdot r_X.$$

Case III. is the limiting case when the central ion is small and the outer ions are close-packed.

Now using the subscripts 1 and 2 as above, and denoting the angles as follows : θ_{12} between r_1 and s_{12}, θ_{21} between r_2 and s_{12}, θ_{22} between r_2 and s_{22} ; so that $\theta_{12} + \theta_{21} = \pi/2$; $\theta_{22} = \pi/3$,

$$-\phi_E = \frac{2ze^2}{r_1} + \frac{3ze^2}{r_2} - \frac{6e^2}{s_{12}} - \frac{3e^2}{s_{22}} - \frac{e^2}{s_{11}}$$
$$+ \frac{2p_1ze}{r_1^2} + \frac{3p_2ze}{r_2^2} - \frac{6p_2e}{s_{22}^2}\cos\theta_{22}$$
$$- \frac{6e}{s_{12}^2}(p_1\cos\theta_{12} + p_2\cos\theta_{21}) - \frac{2p_1e}{s_{11}^2}$$
$$- \frac{3p_2^2}{s_{22}^3}(1 + \cos^2\theta_{22}) - \frac{18p_1p_2}{s_{12}^3}\sin\theta_{12}\cos\theta_{12} - \frac{2p_1^2}{s_{11}^3}$$
$$- \frac{1}{2\alpha}(2p_1^2 + 3p_2^2).$$

While for the p's we have the simultaneous equations

$$\left.\begin{aligned} \frac{p_1}{\alpha} &= \frac{ze}{r_1^2} - \frac{3e}{s_{12}^2}\cos\theta_{12} - \frac{e}{s_{11}^2} - \frac{9p_2}{s_{12}^3}\sin\theta_{12}\cos\theta_{12} - \frac{2p_1}{s_{11}^3}, \\ \frac{p_2}{\alpha} &= \frac{ze}{r_2^2} - \frac{2e}{s_{22}^2}\cos\theta_{22} - \frac{2e}{s_{12}^2}\cos\theta_{21} - \frac{2p_2}{s_{22}^3}(1 + \cos^2\theta_{22}) \\ &\qquad - \frac{6p_1}{s_{12}^3}\sin\theta_{12}\cos\theta_{12} \end{aligned}\right\}.$$

The values of the s's and θ's are as follows :

Case I. :

$$r_1 = r_2 = r_M + r_X (= r) \text{ ; } s_{12} = r\sqrt{2}, \; s_{22} = r\sqrt{3}, \; s_{11} = 2r \text{ ;}$$
$$\cos\theta_{12} = \cos\theta_{21} = r_1/s_{12} = 1/\sqrt{2} \text{ ; } \cos\theta_{22} = \tfrac{1}{2}.$$

Case II. :

$$r_1 = \sqrt{4r_X^2 - r_2^2},\ r_2 = r_M + r_X\ ;\ s_{12} = 2r_X,\ s_{22} = r_2\sqrt{3},\ s_{11} = 2r_1\ ;$$

$$\sin\theta_{21} = \cos\theta_{12} = \frac{1}{2r_X}\sqrt{4r_X^2 - r_2^2}\ ;\ \cos\theta_{22} = \tfrac{1}{2}.$$

Case III. :

$$r_1 = r_X \cdot \tfrac{2}{3}\sqrt{6}\ ;\ r_2 = \tfrac{2}{3}r_X\sqrt{3}\ ;\ s_{12} = s_{21} = 2r_X\ ;$$

$$\cos\theta_{12} = \sin\theta_{21} = \tfrac{1}{3}\sqrt{6}\ ;\ \cos\theta_{22} = \tfrac{1}{2}.$$

3. *Numerical Data and Results for* $-\phi_E$.

In applying the equations the following numerical data are used :

Ionic radii. (B^{3+} 0·25) ; Al^{3+} 0·57 ; Cr^{3+} 0·65; C^{4+} 0·2 ; Si^{4+} 0·39 ; Ti^{4+} 0·64 ; Sn^{4+} 0·74 ; (P^{5+} 0·35) : V^{5+} 0·4 ; (As^{5+} 0·47) ; (Sb^{5+} 0·62) ; S^{6+} 0·34 ; (Cr^{6+} 0·35) ; F^- 1·33 ; Cl^- 1.81.

These are in Å.U. and are taken direct from Goldschmidt (*loc. cit.*) except for the five entries which are bracketed ; these are obtained as follows : For B^{3+} Goldschmidt gives no value ; 0 25 is obtained by interpolation between his values for Be^{2+} and C^{4+}. (Pauling's [7] calculated value of 0·2 seems rather low for consistency with the empirical radii of the neighbouring ions.) For P^{5+} Goldschmidt gives 0·3 to 0·4 and the mean between these limits is here used. Similar remarks apply to Cr^{6+}. For As^{5+} and Sb^{5+} Goldschmidt gives no data, and there are no empirical data for neighbouring elements on which an interpolation might be based ; the calculated values of Pauling are therefore used.

Other data. The polarizabilities are taken as $0{\cdot}99 \times 10^{-24}$ E.S.U. and $3{\cdot}06 \times 10^{-24}$ E.S.U. for F^- and Cl^- respectively (Born and Heisenberg, *loc. cit.*). e is the electronic charge and is taken as $4{\cdot}774 \times 10^{-10}$, and the results are expressed in k. cal./mol. using Avogadro's number ($6{\cdot}06 \times 10^{23}$) and the erg-k. cal. equivalent ($4{\cdot}185 \times 10^{10}$).

The results are shown in Table I. Where $n = 5$ a Roman numeral placed after the symbol of the ion indicates which of the three cases applies. In other cases (r_0) or (Σ) is placed after the figure for r to indicate whether this is the lower limit or not. The values of p are in E.S.U. $\times 10^{18}$, of r in Å.U., and of $-\phi_E$ in k. cal./mol. to the nearest 10.

A comparison of p_1 and p_2 where $n = 5$ brings out clearly the effect of the geometry of the system on the relative

strengths of binding of halide ions in the first and second positions. It is to be noted that the effect depends on the *relative* sizes of the central and outer ions, and is thus more pronounced with chlorides than with fluorides, while for a given anion the difference very rapidly diminishes as the size of the central ion increases. On the other hand, decreasing the size of the central, or increasing that of the halide ion, does not indefinitely increase the divergence of p_1 and p_2, owing to the attainment of the limiting condition (Case III.). The behaviour of the pentahalides of phosphorus illustrates the point: the dissociation increases markedly from fluoride to chloride, but only slightly if at all from chloride to bromide.

Values are given in the table for one or two hypothetical molecules, *e.g.*, $AsCl_5$ and CrF_6, for the sake of comparison. Concerning the possibility of the existence of these, more will be said in the next section.

4. *Thermochemical Values for the Energy of Coordination.*

The values of $-\phi_E$ calculated in the previous section can, of course, only represent the true energy difference between the actual molecule and the (gaseous) ions if the former approximates fairly closely to the heteropolar model. On the other hand, a value can in many cases be obtained for this energy difference by thermochemical methods, and this value is quite independent of any hypothesis whatsoever as to the structure of the molecule. By comparing the calculated and thermochemical values, an indication may then be obtained as to whether or no the molecule may justly be regarded as hetero-polar. A discrepancy larger than the probable error, and in the direction of $-\phi_E$ being too small, may be considered to imply that homo-polar influences are of importance. On the other hand, a discrepancy in the opposite direction cannot be explained in this way, as it would imply that the hypothetical, purely hetero-polar molecule is more stable than the actually existing form. In such a case the discrepancy must be regarded as due to incorrectness of some of the data employed.

It is very unfortunate that in some cases, where conclusions as to the possibility of the hetero-polar molecule would be of particular interest (*e.g.*, $AsCl_5$), sufficient data are not available for even a plausible estimate of the thermochemical energy of coordination. Estimates will, however, be attempted in all cases, the basis of the estimation and its probable degree of uncertainty being taken into account.

TABLE I.—Calculated Energies of Coordination.

Central ion.	Fluorides. r.	p.	$-\phi_E$.	Chlorides. r.	p.	$-\phi_E$.
($n = 3$.)						
B^{3+}	1·58 (Σ)	3·91	1910	2·09 (r_0)	6·61	1530
Al^{3+}	1·90 (Σ)	2·89	1460	2·38 (Σ)	5·42	1250
Cr^{3+}	1·98 (Σ)	2·69	1380	2·46 (Σ)	5·14	1200
($n = 4$.)						
B^{3+}	1·63 (r_0)	2·93	2000	2·22 (r_0)	4·68	1510
Al^{3+}	1·90 (Σ)	2·34	1630	2·38 (Σ)	4·27	1370
Cr^{3+}	1·98 (Σ)	2·20	1550	2·46 (Σ)	4·08	1310
C^{4+}	1·63 (r_0)	4·35	3190			
Si^{4+}	1·72 (Σ)	4·02	2940	2·22 (r_0)	6·95	2440
Ti^{4+}	1·97 (Σ)	3·26	2420	2·45 (Σ)	6·07	2090
Sn^{4+}	2·07 (Σ)	3·01	2260	2·55 (Σ)	5·73	1970
($n = 6$.)						
B^{3+}	1·88 (r_0)	1·32	1510			
Al^{3+}	1·90 (Σ)	1·30	1490	2·56 (r_0)	2·08	1120
Cr^{3+}	1·98 (Σ)	1·24	1420			
C^{4+}	1·88 (r_0)	2·30	2770			
Si^{4+}	1·97 (Σ)	2·17	2620	2·56 (r_0)	3·64	2080
Ti^{4+}	2·07 (Σ)	2·04	2460			
Sn^{4+}						
P^{5+}, V^{5+}, As^{5+}	1·88 (r_0)	3·30	4390	2·56 (r_0)	5·20	3310
Sb^{5+}	1·95 (Σ)	3·15	4220			
S^{6+}, Cr^{6+}	1·88 (r_0)	4·28	5660	2·56 (r_0)	6·75	4280

($n = 8$.)

B^{3+}, Al^{3+}, Cr^{3+}	2·30 (r_0)	0·36	880	3·13 (r_0)	0·57	460
C^{4+}, Si^{4+} ..... / Ti^{4+}, Sn^{4+}	2·30 (r_0)	1·03	1840	3·13 (r_0)	1·63	1360
P^{5+}, V^{6+} .... / As^{5+}, Sb^{5+}	2·30 (r_0)	1·70	3130	3·13 (r_0)	2·69	2320
S^{6+}, Cr^{6+}	2·30 (r_0)	2·38	4490	3·13 (r_0)	3·76	3350

($n = 5$.)

Central ion.	r_1.	r_2	p_1.	p_2.	$-\phi_E$.		r_1.	r_2.	p_1.	p_2.	$-\phi_E$.
B^{3+} (II.)	2·14	1·58	0·49	3·18	1890	(III.) ...	2·95	2·09	0·44	5·09	1470
Al^{3+} (I.)	1·90		1·87	1·81	1620	(II.).....	2·73	2·38	1·70	3·84	1270
Cr^{3+} (I.)	1·98		1·75	1·71	1530	(II.).....	2·66	2·46	2·17	2·19	1210
C^{4+} (III.)	2·18	1·54	0·96	4·98	3300	(III.) ...	2·95	2·09	1·26	8·07	2480
Si^{4+} (II.).....	2·03	1·72	1·83	3·82	2890	(II.).....	2·88	2·20	1·89	7·19	2380
Ti^{4+} (I.)	1·97		2·71	2·75	2650	(II.)... ..	2·67	2·45	3·58	5·33	2100
Sn^{4+} (I.)	2·07		2·53	2·55	2430	(II.).....	2·57	2·55	4·38	4·65	2060
P^{5+} (II.)	2·07	1·67	2·34	5·26	4320	(II.)	2·91	2·15	2·62	10·00	3530
V^{5+} (II.).....	2·02	1·73	2·71	5·04	4240	(II.).....	2·87	2·21	3·04	9·45	3400
As^{5+} (II.)	1·96	1·80	3·20	4·53	4130	(II.).....	2·81	2·28	3·56	8·79	3270
Sb^{6+} (I.)	1·95		3·78	3·77	3760	(II.).....	2·68	2·43	4·83	7·40	3080

The cycle used is as follows (taking BF_3 as example) :

(1) Decompose gaseous BF_3 into its elements

$$BF_{3\,gas} \rightarrow B_{cryst} + \tfrac{3}{2}F_{2\,gas} - Q,$$

where Q is the heat of formation.

(2) Convert solid boron and gaseous fluorine into their gaseous ions

$$B_{cryst} + \tfrac{3}{2}F_{2\,gas} = B^{3+}{}_{gas} + 3F^{-}{}_{gas} - S_B - \Sigma J_B - \tfrac{3}{2}D_{F_2} + 3E_F,$$

where S_B is the heat of sublimation of boron, ΣJ_B the sum of the works of ionization, D_{F_2} the heat of dissociation of fluorine, and E_F the electron affinity of the fluorine atom.

(3) Let the gaseous ions reform gaseous BF_3 :

$$B^{3+}{}_{gas} + 3F^{-}{}_{gas} = BF_{3\,gas} + \phi_{th},$$

where ϕ_{th} is the thermochemical energy of coordination.

Then $\phi_{th} = Q + S + \Sigma J - 3(E - \frac{1}{2}D)$, and in general, for a molecule MX_n, $\phi_{th} = Q_{MX_n} + S_M + \Sigma J_M - n(E - \frac{1}{2}D)_X$.

Where the element is not a solid giving a monatomic vapour, "S_M" must be replaced by the appropriate terms ; thus for phosphorus "S_P" includes not only the heat of sublimation, but also the heat of dissociation of P_4 to single atoms.

The Q and D terms are taken, where possible, from the International Critical Tables ; in other cases estimates are made. The S values are not in general available as such ; they are either calculated from the vapour pressures, or where these also are not available, estimated from the boiling-points by the von Wartenburg formula ($7{\cdot}4T_S \log T_S$). The electron affinities of the halogens are taken from Mayer and Helmholz[8], while the works of ionization are computed from the ionizing potentials spectroscopically determined wherever possible *. In other cases estimates are made for the sake of comparison, though, of course, they can only be rough. All quantities which are estimated are enclosed in parentheses, and the basis of the estimation explained in footnotes. Where an estimate introduces an uncertainty which is of importance in the final value of ϕ_{th} this also is bracketed. The numbers are shown in Table II., in which all quantities are in k. cal./mol., and the values of ϕ_{th} are given to the nearest 10 k. cal., or to the nearest 100, according to their probable inaccuracy.

* Detailed references to the individual determinations would occupy too much space. The papers of Bowen, Millikan, and White, and their collaborators in the 'Physical Review,' and the summary given by Braunbek[9] have been used.

Table II.

Thermochemical Energies of Coordination.

	Elements.		Fluorides.			Chlorides.		
M.	S_M.	ΣJ_M.	Q_{MF_n}.	$n(E-\frac{1}{2}D)_F$.	ϕ_{th}.	Q_{MCl_n}.	$n(E-\frac{1}{2}D)_{Cl}$.	ϕ_{th}.
B	(70)	1660	256		1800	88		1640
Al	(65)	1250	(300)[1]	189	1430	(150)[2]	174	1290
Cr^{iii}	(63)	(1250)[3]	(250)[4]		(1370)	(120)[5]		(1260)
C	(170)	3460	(350)[6]		(3700)	25		3420
Si	(40)	2420	360	252	2570	142	232	2370
Ti	(50)	2150	(350)[6]		(2300)	170		2140
Sn	(66)	2180	(360)[6]		(2300)	118		2130
P	(50)	4150	(200)[7]		(4100)	(150)[8]		4060
V	(50)	(4080)[9]	(200)[10]	315	? (4000)	—	290	(> 3800)
As	(50)	(3890)[11]	(250)[12]		? (3900)	—		? (> 3650)
Sb	(38)	(3560)[13]	(250)[14]		? (3500)	94		? (3400)
S	(60)	6360	?	378	> 6000	—	348	> 6000
Cr^{vi}	(63)	(c. 6000)	—		> c. 5700			> c. 5700

[1] $Q_{solid} = 330$. [2] $Q_{solid} = 166$. [3] Put J. Cr III. ~ 30 v.; cp. J. V III = 29·6 v. [4] $Q_{soln} = 292$. [5] $Q_{soln} = 180$. [6] Analogy with Si. [7] $> Q_{PF_3}$ (~ 108, Berthelot), and probably $> Q_{PCl_5, g.v.}$ [8] $Q_{solid} = 163$. [9] Put J V. V. ~ 73 v., cp. J. Cr V = 72·8 v. [10] Analogy with P. [11] Put J. As II. ~ 18 v., J. As IV. 45 v., interpolation P—Sb. [12] Analogy with Sb. [13] Put J. Sb V. ~ 57 v., extrapolation from P and As. [14] Presumably $> Q_{SbF_3}$, which = 217.

In comparing ϕ_{th} with $-\phi_E$, allowance must be made for the uncertainties of the two quantities. (The terms arising from the difference between heats at ordinary temperature and energies at absolute zero are always negligible.) Now the errors in ϕ_{th} depend on the data used, and vary from probably not more than some 10 k. cal. in the best cases (boron and silicon fluorides and most of the chlorides) to possibly more than 100 k. cal. in such cases as the halides of V, As, and especially Sb, where large terms (ionizing potentials, and for Sb the highest of these), rest only on interpolations or extrapolations from analogous elements.

The uncertainty of ϕ_E depends chiefly on that of r. This is least where r depends chiefly on the radius of the halide ion; as a general average r may be assumed correct to some 5 per cent., which would mean a margin of error of some 7 per cent. in ϕ_E; where $n=5$, however, ϕ_E is especially sensitive to the radius of the central ion, and it happens that the radii of the pentavalent ions are the least reliable (see sec. 3), so that in these cases the margin of error of ϕ_E must be extended to about 10 per cent.

On comparing ϕ_{th} with $-\phi_E$, five cases appear in which the latter is low by an amount definitely greater than the probable error:

Molecule.	CF_4.	CCl_4.	SCl_6.	$CrCl_6$.	PCl_5.
ϕ_{th}	(3700)	3420	>6000	>c. 5700	4060
$-\phi_E$	3190	2440	4280	4280	3530

It must be concluded that these molecules can only exist (if at all) in the homopolar form*. In the subsequent applications, therefore, ϕ_{th} and not $-\phi_E$ will be used for the energy of coordination for these molecules.

For the penta-halides of V, As, and Sb, ϕ_{th} and $-\phi_E$ differ by about 200 k. cal. (about 5 per cent.) for the fluorides and about 400 k. cal. (about 10 per cent.) for the chlorides. The discrepancy is in such a direction ($-\phi_E$ low) as to indicate that the chlorides are homopolar where they exist, but the values of ϕ_{th}, depending on unreliable estimates of large ionizing potential terms, are too rough for any definite conclusions to be drawn. For these compounds $-\phi_E$ will accordingly be used.

The comparison in the remaining cases is shown in Table III.

Except for SiF_4, which needs further discussion, the agreement is satisfactory. The tendency for $-\phi_E$ to be low

* See, however, de Boer and Arkel (10).

for chlorides and high for fluorides may be attributed to some systematic error in either the polarizabilities or the radii of these ions.

The discrepancy with SiF_4 can hardly be explained by supposing the hetero-polar model to be inapplicable, since it is in such a direction as to give the actual molecule a higher energy than the hypothetical one. The other possibilities are that $-\phi_E$ is high due to the value used for the radius of the Si ion being too low, or else that ϕ_{th} is incorrect due to

TABLE III.

Comparison of ϕ_{th} and $-\phi_E$.

Molecule.	$-\phi_E$.	ϕ_{th}.	$-\phi_E/\phi_{th}$.
BF_3	1910	1800	1·06
AlF_3	1460	1430	1·02
CrF_3	1380	(1370)	1·01
SiF_4	(2940)	2570	1·14
TiF_4	2420	(2300)	1·05
SnF_4	2260	(2300)	0·98
PF_5	4320	(4100)	1·05
SF_6	5660	6000	1·06
BCl_3	1530	1640	0·93
$AlCl_3$	1250	1290	0·97
$CrCl_3$	1200	(1260)	0·95
$SiCl_4$	2440	2370	1·03
$TiCl_4$	2090	2140	0·98
$SnCl_4$	1970	2130	0·97

erroneous data. Neither seems very probable, since an error of about 0·1 Å.U. in the radius, or of (say) some 10 volts in an ionizing potential, would be necessary to account for the discrepancy ; but of the two, the former assumption seems least unlikely, and ϕ_{th} will be used. In that case the calculated energy of coordination for any silicon compound must be regarded as suspect, except where the value of r is independent of the radius of the central ion as a result of close-packing of the outer ions.

5. *The Formation of Complex Ions in Solution.*

The quantity $-\phi_C-(-\phi_M)$ may be taken to represent the Energy Decrease when, at absolute zero and in the state

of infinitely dilute gas, the reaction $MX_n + n'X^- \longrightarrow MX_{n+n'}^{n'-}$ takes place. But this cannot be used as criterion for the stability of complex ions under more ordinary conditions. For such a reaction as $KF_{cryst} + BF_{3\,gas} \longrightarrow KBF_{4\,cryst}$ the energy change is $-\phi_C - (-\phi_M) + U_{KBF_4} - U_{KF}$, where U_{KBF_4} and U_{KF} are the respective lattice energies. Again, for $KF_{aq} + BF_{3\,gas} \longrightarrow KBF_{4\,aq}$ the energy change is given by $-\phi_C - (-\phi_M) + W_{BF_4^-} - W_{F^-}$, where the W terms are the (free) energies of hydration. Finally, these quantities, which are calculated for absolute zero, must be used to compare with actual equilibria at room temperature. This is tantamount to neglecting the temperature variation of the quantities and is plausible in view of their large magnitude.

Thus it becomes necessary to obtain numerical values for the lattice energies of hypothetical complex salts, and for the free energies of hydration of hypothetical complex ions. The former is a difficult problem, and the most that can be done is to derive rough estimates in a few special cases; the latter is easier, so in the first instance the discussion will be confined to the formation of complex ions in solution.

The free energy of hydration of an ion may be calculated by a formula due to Born [11], according to which $W = 164z^2/r_i$ k. cal. per mol., where z and r_i are the valency and radius of the ion. The numbers so obtained appear to be too great, especially for small ions. This would be expected from the simplifying assumptions employed, and a more elaborate treatment by Webb [12] leads to better results. (In the same paper Webb points out that the quantities so calculated are, in fact, free and not total energies.) Webb's method is inapplicable for the complex ions for lack of data, but as r_i increases his values and those obtained by the Born formula approach one another, so that the error obtained by using the simpler method should not be serious for complex ions, especially as any residual tendency of the numbers to be high will be partially compensated by the use of a *maximum* value for the radius of the complex ion. This value, denoted by r_C, is $r + r_X$ (r having the same significance as in secs. 2 and 3) for cases where $n = 4$, 6, or 8, while where $n = 5$ the complex ion is regarded as a prolate spheroid and r_C is taken as $\frac{1}{3}(2r_2 + r_1 + 3r_X)$, an "average radius."

The procedure is crude, of course, but in any case too great accuracy is superfluous in view of the errors in the much greater ϕ terms, on account of which a margin of some 20 k. cal./mol. is allowed.

For the halide ions the numbers obtained by Webb (*loc. cit.*) are used, namely, $W_{F^-} = 87$, $W_{Cl^-} = 70$.

Table IV. shows the calculation of $W_C - n'W_{X^-}$ for the various complex ions.

The quantity which is to be compared with the energy of coordination of the molecule, namely, $(-\phi_E)_c + W_C - n'W_{X^-}$, may be denoted ψ_C, and values of this quantity are collected, and the comparison made, in Table V.

Strictly speaking the energy of coordination of the molecule should refer to the state in which the substance actually exists at room temperature, rather than to the gaseous state for which it is calculated. This point, however, is unimportant, as all the substances are quite volatile, so that the correction is less than the margin of error. The value actually used in the comparison is $-\phi_E$, as calculated in sect. 3, except in a few cases, namely, the five for which the hetero-polar model seems to be inapplicable, and the case of SiF_4; for these substances ϕ_{th} is used, for the reasons given in sect. 4. Actually in four of the five cases, although the use of $-\phi_E$ is clearly incorrect, it leads to the same conclusions as with ϕ_{th}.

As regards the values of ψ_C, these are in all cases the sums of the energies of coordination $(-\phi_{E_C})$ calculated in sect. 3 and the quantities $(W_C - n'W_{X^-})$ given in Table IV. The value for SiF_5^- is marked suspect. This is due to the assumption that the discrepancy between $-\phi_E$ and ϕ_{th} for SiF_4 is due to an incorrect radius for the Si^{4+} ion; the other complexes are not affected by this since, in them the outer ions are close-packed.

That complex for which ψ_C is a maximum will be regarded as the stablest, provided that $\psi_C > -\phi_{E_M}$; but other complexes might also exist under certain circumstances. Denoting various complexes formed by the addition of 1, 2, ... etc., halide ions to a molecule by subscripts C_1, C_2, etc., we may distinguish four degrees of stability.

(1) ψ_{C_n} maximum and greater than $-\phi_{E_M}$ ... "stablest."

(2) A complex having a lower coordination number than that of the stablest complex may exist in presence of a limited supply of halide ion, provided that it cannot break up into neutral molecule and the higher complex. There are thus two criteria: (say)

$$\psi_{C_1} > -\phi_{E_M} < \psi_{C_2},$$

$$2\psi_{C_1} > -\phi_{E_M} + \psi_{C_2}.$$

This might be called "also stable."

TABLE IV.

Central ion.	Fluorides. ($W_{F^-} = 87.$) r.	r_C.	$W_C = 164z^2/r_C$.	$W_C - n'W_{F^-}$.	Chlorides. ($W_{Cl^-} = 70.$) r.	r_C.	$W_C = 164z^2/r_C$.	$W_C - n'W_{Cl^-}$.
				($n = 4.$)				
B^{3+}	1·63	2·96	55	−32	2·22	4·03	41	−29
Al^{3+}	1·90	3·22	51	−36	2·38	4·19	39	−31
Cr^{3+}	1·98	3·31	49	−38	2·46	4·27	38	−32
				($n = 6.$)				
B^{3+}	1·88	3·21	450	189				
Al^{3+}	1·90	3·23	447	186	2·56	4·37	331	111
Cr^{3+}	1·98	3·31	436	175				
C^{4+}, Si^{4+}	1·88	3·21	205	31				
Ti^{4+}	1·97	3·30	200	26	2·56	4·37	147	7
Sn^{4+}	2·07	3·40	195	21				
P^{5+}, V^{5+}, As^{5+}	1·88	3·21	51	−36				
Sb^{5+}	1·95	3·28	50	−37	2·56	4·37	37	−33

$(n = 8.)$

B^{3}, Al^{3+}, Cr^{3+}	2·30	3·63	1130	695	3·13	4·94	830	480
C^{4+}, Si^{4+} ..... / Ti^{4+}, Sn^{4+}	2·30	3·63	720	370	3·13	4·94	530	290
P^{5+}, V^{5+} ..... / As^{5+}, Sb^{5+}	2·30	3·63	405	145	3·13	4·94	300	90
S^{6+}, Cr^{6+}	2·30	3·63	180	6	3·13	4·94	132	−8

$(n = 5.)$

	(r_1)	(r_2)				(r_1)	(r_2)			
B^{3+}.....	2·18	1·54	3·08	213	39	2·95	2·09	4·19	156	16
Al^{3+}	1·90		3·22	202	28	2·73	2·38	4·30	153	13
Cr^{3+}	1·98		3·31	198	24	2·66	2·46	4·33	151	11
C^{4+}.....	2·18	1·54	3·08	54	−33	2·95	2·09	4·19	39	−31
Si^{4+}	2·03	1·72	3·16	51	−36	2·88	2·20	4·23	39	−31
Ti^{4+}	1·97		3·30	50	−37	2·67	2·45	4·33	38	−32
Sn^{4+}	2·07		3·40	49	−38	2·57	2·55	4·37	37	−33

Table V.

Fluorides.

Molecule.	ϕ_E*.	ψc for complex ions of coordination number n.				Calculated.		Observed.	
		$n=4$.	$n=5$.	$n=6$.	$n=8$.	"Stablest."	"Also Stable."	"Stablest."	"Also stable."
BF_3	1910	1970	1930	1700	1500	BF_4^-	—	BF_4^-	—
AlF_3	1460	1590	1650	1680	1500	AlF_6^{3-}	AlF_5^{2-}, AlF_4^-	AlF_6^{3-}	AlF_5^{2-}
CrF_3	1380	1510	1550	1600	1500	CrF_6^{3-}	CrF_5^{2-}, CrF_4^-	CrF_6^{3-}	
CF_4	(3480)		3270	2800	2210	none		none	
SiF_4	(2570)		2850†	2800	2210	? SiF_5^- or Si_6^{2-}		SiF_6^{2-}	
TiF_4	2420		2610	2650	2210	TiF_6^{2-}	TiF_5^-	TiF_6^{2-}	
SnF_4	2260		2390	2480	2210	SnF_6^{2-}	? SnF_5^-	SnF_6^{2-}	
PF_5	4320			4350	3280	PF_6^-		PF_6^-	
VF_5	4240			4350	3280	VF_6^-		VF_6^-	
AsF_5	4130			4350	3280	AsF_6^-		AsF_6^-	
SbF_5	3760			4220	3280	SbF_6^-		SbF_6^-	
SF_6	5660				4500	none		none	
CrF_6	5660				4500	none		unknown	

Chlorides.

BCl_3	1530	1480	1490	1230	1940	none	none
$AlCl_3$	1250	1340	1280	1230	940	$AlCl_4^-$	$AlCl_4^-$
$CrCl_3$	1200	1280	1220	1230	940	$CrCl_4^-$	
CCl_4	(3400)		2150	2090	1610	none	none
$SiCl_4$	2440		2350	2090	1610	none	none
$TiCl_4$	2080		2070	2090	1610	? $TiCl_6^{2-}$	$TiCl_5^{2-}$ unstable
$SnCl_4$	1970		2030	2090	1610	$SnCl_6^{2-}$? $SnCl_5^-$	$SnCl_6^{2-}$
PCl_5	(4060)			3280	2410	none	none
VCl_5	3400			3280	2410	none	none
$AsCl_5$	3270			3280	2410	? $AsCl_6^-$, but molecule unknown	
$SbCl_5$	3080			3280	2410	$SbCl_6^-$	$SbCl_6^-$
SCl_6	(6000)				3350	none	unknown
$CrCl_6$	(5700)				3350	none	unknown

* Where ϕ_{th} is used instead of $-\phi_E$ the number is bracketed.
† Suspect: see above and sect. 4.

(3) Of the two criteria above, the first but not the second might be fulfilled. In this case the complex is "unstable."

(4) Any complex for which $\psi_C < -\phi_{E_M}$, or which has a higher coordination number than the stablest, must be regarded as incapable of existence.

It appears at present unnecessary to distinguish between the last two cases. In the table complexes coming under the first two heads are indicated, and a comparison with observation is given. It is to be observed that a certain element of doubt comes in here: it is difficult to say with certainty just what complex ions are actually present in solution, and the complexes listed as observed are those corresponding to complex salts which crystallize unchanged. That other complex ions might be present in the solution cannot be denied, and thus it is only to be expected that some of the complexes given by the theory as stable in solution should not yet have been observed. In a few cases the consideration of the next section is of interest with regard to this point.

6. *Crystallized Complex Salts.*

In some cases it is possible to investigate the formation of a crystal lattice by the complex ion and a simple kation, for example that of potassium. The procedure is to estimate on the basis of plausible assumptions the lattice energy of the complex salt, and then to substitute for ψ_C the quantity $-\phi_{E_C} + U_{K_{n'}C} - n'U_{KX}$.

It is necessary for the complex ion to be uni- or di-valent, and to be symmetrical, otherwise it is impossible to fit it into a regular lattice. Thus only ions of the type MX_4^-, MX_6^-, and MX_6^{2-} come under consideration. For the last of these we have a CaF_2 type lattice with the complex ion replacing Ca^{2+} and K^+ replacing F^-, while for the univalent ions both the NaCl and the CsCl types are considered.

The orientation of the complex ion in the lattice will be decided by the symmetry of the latter; thus in the NaCl lattice, with coordination number six, the tetrahedral MX_4^- ion must arrange itself so that the K^+ ions occupy the mid-points of the edges of the tetrahedron, while in the CsCl lattice with coordination number eight, each K^+ ion must be at a vertex of one tetrahedron and opposite the centre of a face of another; or in other words, an edge of the tetrahedron lies on a face diagonal of the unit cube.

Again, in a CsCl lattice the octohedral MX_6^- ion must have a K^+ ion at the centre of each face, so that two neighbouring octohedra have their axes in a straight line, while in a NaCl lattice the octohedron has a K^+ ion at each vertex.

Finally, in a CaF_2 lattice the octohedron has a K^+ ion in the centre of each face, as in the CsCl lattice.

a, the unit-cube-side of the lattice, can now be given in terms of known quantities.

KMX_4 (NaCl type) : $a = 2d_{KC}$, where d_{KC} is the distance between the centres of the K^+ and the complex ion.

Here $d_{KC} = \frac{r}{\sqrt{3}} + \sqrt{(r_K + r_X)^2 - \frac{2}{3}r^2}$, where r has the same significance as in sect. 2.

KMX_4 (CsCl type) : $a = \frac{2}{\sqrt{3}} . d_{KC} = \frac{2}{\sqrt{3}}(r_K + r_C)$.

r_C is as given in Table IV.

KMX_6 (NaCl type) : $a = 2d_{KC} = 2(r_K + r_C)$,

(CsCl type) : $a = 2r_C$.

K_2MX_6 : $a = \frac{4}{\sqrt{3}} . d_{KC}$;

$$d_{KC} = \sqrt{r^2 - \frac{4}{3}r_X^2} + \sqrt{(r_K + r_X)^2 - \frac{4}{3}r_X^2}.$$

Then the lattice energies of the salts are inversely proportional to the values of a for the particular lattice-type in question. Thus a hypothetical KBF_4 crystallizing in the CsCl type would have a lattice energy $= U_{CsCl} \times \frac{a_{CsCl}}{a_{KBF_4}}$. For consistency the unit-cube-sides of the type-salts are taken as calculated from the Goldschmidt radii, *e.g.*, for KCl, $a = 2(r_K + r_{Cl}) = 6{\cdot}20$ Å.U., and their lattice energies from Born[13], namely, $U_{KCl} = 162$, $U_{CsCl} = 156$, $U_{CaF_2} = 609$. The lattice energies so obtained are shown in Table VI.

These numbers (selecting for univalent salts the value for the NaCl type, which is always the greater) may now be combined with $U_{KF} = 210$, $U_{KCl} = 162$ (Born, *loc. cit.*) to give the quantity $U_{KC} - n'U_{KX}$ which is to be substituted for

$W_C - W_{X-}$ in obtaining ψ_C. We find, to the nearest 10 k. cal.:

Salt.	KMF_4.	$KMCl_4$.	KMF_6.	$KMCl_6$.	K_2SiF_6.	K_2TiF_6.	K_2SnF_6.	K_2MCl_6.
$U_{KC} - n'U_{KX}$	−50	−30	−100	−70	+20	+10	−10	+60

Comparing these with the values of $W_C - n'W_{X-}$ in Table IV., and with Table V., we find the same conclusions as before with regard to the stabilities of the various com-

TABLE VI.

Type.	CsCl.	NaCl.	CaF_2.
KBF_4	128	157	—
$KAlF_4$	120	157	—
$KCrF_4$	118	157	—
KPF_6, KVF_6, $KAsF_6$	98	112	—
$KSbF_6$	94	107	—
K_2SiF	—	—	445
K_2TiF_6	—	—	427
K_2SnF_6	—	—	407
$KBCl_4$	101	133	—
$KAlCl_4$	98	133	—
$KCrCl_4$	97	133	—
$KPCl_6$, $KVCl_6$, $KAsCl_6$, $KSbCl_6$	72	89	—
K_2SiCl_6	—	—	382
K_2TiCl_6	—	—	
K_2SnCl_6	—	—	

plexes, with two important exceptions, namely, that while the ion $TiCl_6^{2-}$ is of doubtful stability in solution the salt K_2TiCl_6 is definitely stable, and that the ion PF_6^-, which was found to be stable in solution, cannot exist in a regular space-lattice.

7. *Discussion.*

Bearing in mind that a complex ion may exist in solution even though the corresponding crystalline complex salt is

unknown, the agreement of comparison and observation in Table V. is remarkably close, the only definite discrepancy being the case of the fluoride complexes of Si, and here the data are suspect. The modifications introduced in the last section are peculiarly interesting, since while the salts of the type K_2TiCl_6 are well known and stable, the complex ion in solution is apparently unstable, only existing if, at all, in highly concentrated solution. Again, the PF_6^- ion appears to exist in solution, but although crystalline salts of the empirical formula KPF_6 certainly exist, they appear not to contain the ion PF_6^- as a structural unit[14]. That these two peculiarities should be reproduced by the theory is a very striking result.

8. *Summary.*

The energies of coordination for fluoride and chloride molecules and complex ions are calculated in terms of a hetero-polar model. For molecules the same quantity is estimated thermochemically. The energies of hydration of complex ions, and the lattice energies of complex salts are considered, and from these and the energies of coordination conclusions as to the stabilities of various known and hypothetical complex ions and salts are obtained.

References.

(1) Garrick, Phil. Mag. ix. p. 131; x. p. 77 (1930); xi. p. 741 (1931). Subsequently referred to as I., II., and III.
(2) Magnus, *Z. Anorg. Chem.* cxxiv. p. 289 (1922).
(3) Lennard-Jones, Proc. Roy. Soc. A, cix. p. 584 (1925).
(4) Goldschmidt, *Ber. d. D. Chem. Ges.* lx. p. 1273 (1927).
(5) Born and Heisenberg, *Z. Physik.* xxiii. p. 388 (1924).
(6) Fajans and Joos, *Z. Physik.* xxiii. p. 1 (1924).
(7) Pauling, J. Amer. Chem. Soc. xlix. p. 765 (1927).
(8) Mayer and Helmholz, *Z. Physik.* lxxv. p. 19 (1932).
(9) Braunbek, *Z. Physik.* lxiii. p. 20 (1930).
(10) de Boer and van Arkel, *Z. Physik.* xii. p. 27 (1927).
(11) Born, *Z. Physik.* l. p. 45 (1920).
(12) Webb, J. Amer. Chem. Soc. xlviii. p. 2587 (1926).
(13) Born, *Verh. d. D. Phys. Ges.* xxi. p. 13 (1919).
(14) Lange, *Ber. d. D. Chem. Ges.* lxi. p. 799 (1928); lxiii. p. 1058 (1930). Seifert, *Z. Kryst.* lxxvi. p. 455 (1930).

Inorganic Chemistry Dept.,
The University, Leeds.

XCVII. *A Note on Huygens' Principle.* *By* Joseph S. Mitchell, *B.A.**

THE well-known theorem of Kirchhoff (*Ann. d. Phys. u. Chem.* xviii. p. 663 (1883)), generally accepted as a rigorous formulation of Huygens' principle, can be derived shortly by an application of Fourier's integral theorem, somewhat similar to Schott's treatment of the electromagnetic potentials in his book 'Electromagnetic Radiation.'

By Green's theorem

$$\iint\left(\phi\frac{\partial\psi}{\partial\nu}-\psi\frac{\partial\phi}{\partial\nu}\right)d\mathrm{S}=\iiint_{\mathrm{V}}(\phi\nabla^2\psi-\psi\nabla^2\phi)\,dv=0,$$

where ϕ and ψ are solutions of the wave equation of form $\phi(r,t)=\Phi(r)e^{int}$, and ν is the outward normal to the enclosing surface of volume V. Introducing

$$\psi=\frac{e^{in\left(t-\frac{r}{c}\right)}}{r},$$

$$\iint\left\{\phi\frac{\partial}{\partial\nu}\left(\frac{e^{in\left(t-\frac{r}{c}\right)}}{r}\right)-\frac{e^{in\left(t-\frac{r}{c}\right)}}{r}\frac{\partial\phi}{\partial\nu}\right\}d\mathrm{S}=0.$$

$$\therefore\ \iint\left\{\phi\frac{\partial}{\partial\nu}\left(\frac{1}{r}\right)-\frac{1}{cr}\frac{\partial r}{\partial\nu}\frac{\partial\phi}{\partial t}-\frac{1}{r}\frac{\partial\phi}{\partial\nu}\right\}e^{in\left(t-\frac{r}{c}\right)}d\mathrm{S}=0.$$

In the usual way, let S_1, the stationary bounding surface of the isotropic region over which the integration is extended, include the origin, at which the disturbance is to be determined; then exclude the origin by a small spherical surface, having the origin as centre. S_1 must neither coincide with nor include any obstacle. r and r_1 are respectively the distances from the surface element $d\mathrm{S}$ to the origin and source. The disturbance at the origin is given by

$$4\pi\phi_0(t)=\iint_{\mathrm{S}_1}\left\{\frac{1}{r}\frac{\partial\phi}{\partial\nu}+\frac{1}{cr}\frac{\partial r}{\partial\nu}\frac{\partial\phi}{\partial t}-\phi\frac{\partial}{\partial\nu}\left(\frac{1}{r}\right)\right\}e^{-\frac{inr}{c}}d\mathrm{S},$$

and applying Fourier's integral theorem

$$4\pi\phi_0(t)=\iint_{\mathrm{S}_1}\frac{d\mathrm{S}}{2\pi}\int_{-\infty}^{+\infty}dn\int_{-\infty}^{+\infty}\left\{\frac{1}{r}\frac{\partial\phi}{\partial\nu}+\frac{1}{cr}\frac{\partial r}{\partial\nu}\frac{\partial\phi}{\partial\theta}-\phi\frac{\partial}{\partial\nu}\left(\frac{1}{r}\right)\right\}_{\theta}e^{in\left(t-\frac{r}{c}-\theta\right)}d\theta$$

* Communicated by the Author.

$$= \iint_{S_1} \left[\frac{1}{r} \frac{\partial \phi}{\partial \nu} + \frac{1}{cr} \frac{\partial r}{\partial \nu} \frac{\partial \phi}{\partial \theta} - \phi \frac{\partial}{\partial \nu} \left(\frac{1}{r} \right) \right]_{\theta = t - \frac{r}{c}} dS.$$

The more explicit classical formulation of Huygens' principle is obtained immediately by introducing

$$\phi(r_1, t) = \frac{A}{r_1} \cos 2\pi \left(\frac{t}{T} - \frac{r_1}{\lambda} \right)$$

and neglecting terms $O\left(\frac{1}{rr_1^2}\right)$ and $O\left(\frac{1}{r_1 r^2}\right)$; thus

$$\phi_0(t) = \frac{A}{2\lambda} \iint_{S'} \frac{\cos(\nu r) + \cos(\nu r_1)}{r r_1} \sin 2\pi \left(\frac{t}{T} - \frac{r + r_1}{\lambda} \right) dS$$

(*cf.* Drude's 'Optics,' English edition, 1922, p. 181), which is often further simplified to Stokes' form and the elementary form.

XCVIII. *An X-ray Analysis of Iron Pyrites by the Method of Fourier Series.* *By* H. M. Parker, *M.Sc.*, *and* W. J. Whitehouse, *B.Sc.*, *Manchester University* *.

Introduction.

Following the account of the determination of parameters in crystal structures by means of a double Fourier Series, given by W. L. Bragg [1], he and J. West published a paper [2] dealing with the imperfections involved in a Fourier representation of a crystal structure. For their purpose an ideal crystal of sodium chloride, composed of Na and Cl atoms derived from the Hartree atom-models, was considered. The projection on the plane (110) was discussed, and the Fourier Series evaluated for F-values appropriate to absolute zero and to room temperature, respectively. In each case the series was artificially terminated at a glancing angle θ_0, equal to $\pi/6$ for Rh K$_\alpha$ radiation (*i.e.* $\frac{\sin \theta_0}{\lambda} = 0{\cdot}8$).

The "diffraction effects" introduced by terminating the series at finite values of h, k, and l were investigated and found to be closely analogous to optical diffraction.

* Communicated by Prof. W. L. Bragg, M.A., F.R.S.

The influence of spurious diffraction rings, which have no real counterpart in the crystal structure, on the apparent distribution of electrons in the projection was pointed out. The application of a " false temperature factor " to make the series converge more rapidly, and thus to obtain a more reliable electron count was recommended.

In the present paper an account is given of an analysis of Iron Pyrites by a double Fourier Series, which verifies in an experimental case the deductions of Bragg and West from their ideal crystal. The results yield an accurate value of the parameter which defines the position of the sulphur atoms, and give some corroborative evidence for the view that the pyrites structure is based on homopolar binding. Since the structure involved only one unknown parameter, an opportunity was afforded of studying the diffraction effects more closely than would be possible with a complex crystal in which the overlapping diffraction rings due to the various atoms could not be sorted out.

Crystallographic Details.

The structure of iron pyrites was one of the first to be investigated by W. L. Bragg [3], when X-ray crystallography was developed. It was further examined by P. P. Ewald [4] and others. The iron atoms lie on a face-centred cubic lattice, and the sulphur atoms lie on the trigonal axes of this cubic framework, associated in pairs with the unoccupied cube corners. The space group is T_h^6, the symmetry being represented in fig. 1.

If the point O be chosen as the origin of coordinates, and OA and OC as the axes of x and y, respectively, the coordinates (u, u, u) may be ascribed to the sulphur atom S_1, and the positions of all the sulphur atoms are then determined by the single parameter u. There are four molecules in the unit cell, and the following coordinates may be assigned to the typical atoms :—

$$\text{Fe} : (\tfrac{1}{2}, 0, 0)\,; \quad (0, \tfrac{1}{2}, 0)\,; \quad (0, 0, \tfrac{1}{2})\,; \quad (\tfrac{1}{2}, \tfrac{1}{2}, \tfrac{1}{2})\,:$$
$$\text{S} : \pm(u, u, u)\,; \quad \pm(\tfrac{1}{2}-u, \tfrac{1}{2}-u, u)\,;$$
$$\pm(u, \tfrac{1}{2}-u, \tfrac{1}{2}+u)\,; \quad \pm(\tfrac{1}{2}+u, u, \tfrac{1}{2}+u).$$

The positions of the sulphur atoms may be visualized by placing one at the head and tail of every arrow in fig. 1.

Experimental Details.

Several natural crystals were available for the analysis. The intensities of the corresponding ($h00$) reflexions from the natural cube faces were the same for all the crystals, and were not greatly increased by grinding the faces. A set of measurements of the integrated

Fig. 1.

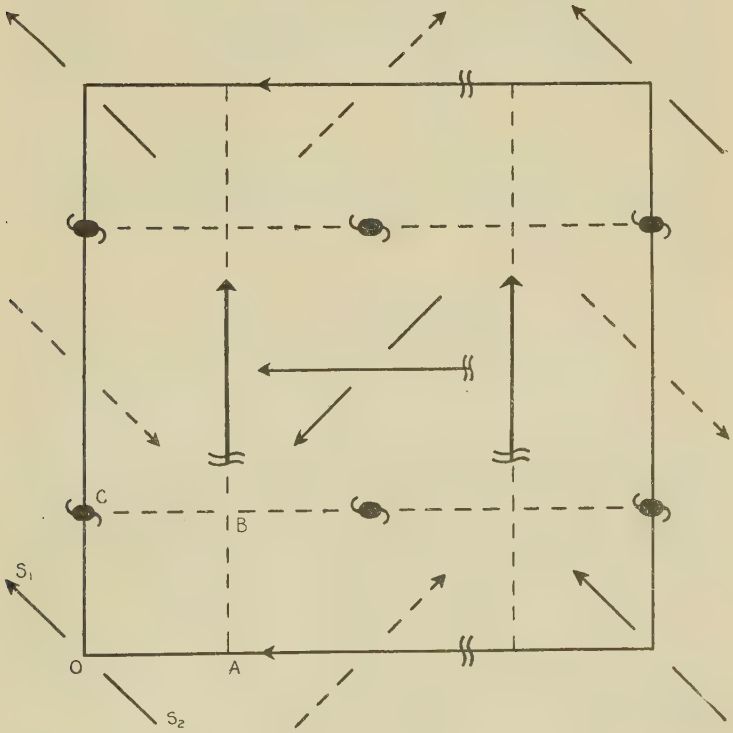

The symmetry of the space-group T_h^6.

reflexion from the ($h00$) planes was obtained, using a rock-salt standard with Mo K_α radiation. Two crystal slips were cut, one parallel to (001) and the other parallel to (110). The transmission method was used to determine the intensities of reflexion from the ($hk0$) planes with the first slip, and from the (hhl) planes with the second. It is well known that for this purpose the optimum thickness of the slip is the reciprocal of the linear absorption

coefficient of the crystal for the radiation used. In the present case the calculated absorption coefficient μ_0 was 114 (from Jönsson's tables [5]), so that the optimum thickness t_0 was 0·009 cm. It was found to be impracticable to grind the slips to the optimum thickness, and the slips used were respectively 0·015 cm. and 0·013 cm. thick. These values of the thickness were derived indirectly from the measured absorption by the slips of a monochromatic beam of Mo K_α radiation obtained by reflexion from a (111) face of fluorspar.

The spacing, $a = 5{\cdot}405$ Å, was derived from a powder photograph kindly taken by Dr. A. J. Bradley *.

Reduction of the Observations.

The integrated intensity of reflexion ρ of a beam of X-rays of wave-length λ from an extended face of a mosaic crystal is

$$\rho = \frac{N^2\lambda^3}{4\mu} \cdot \left(\frac{e^2}{mc^2}\right)^2 . F^2 . \frac{1+\cos^2 2\theta}{\sin 2\theta} \quad . \quad . \quad . \quad (1)$$

$$= \frac{Q}{2\mu} \quad . \quad . \quad . \quad . \quad . \quad . \quad . \quad . \quad . \quad . \quad . \quad (2)$$

N is the number of unit cells per unit volume ; e, m, the charge and mass of the electron ; c, the velocity of light ; F, the structure-amplitude factor for the reflexion considered ; θ, the glancing angle of reflexion, and μ the linear absorption coefficient. The integrated reflexion by the transmission method is

$$\rho_s = Q \, . \, te^{-\mu t} . \quad . \quad . \quad . \quad . \quad . \quad . \quad . \quad (3)$$

where $t = t_0 \sec\theta$, the effective thickness of the slip at a glancing angle θ.
Hence

$$\rho = \frac{e^{\mu t}}{2\mu t} \cdot \rho_s \, . \quad . \quad . \quad . \quad . \quad . \quad . \quad . \quad (4)$$

where ρ and ρ_s refer to the same spectrum measured from a face and through the slip. This relation gives the values of ρ in terms of the experimental measurements of ρ_s. If the values of ρ_s are known only on an arbitrary scale, absolute values of ρ may be obtained by the

* W. F. de Jong obtained the result $5{\cdot}403 \pm {\cdot}003$ Å. for the spacing (Physica, vii. p. 23, 1927).

application of a constant multiplying factor, provided that the absolute value of ρ is accurately known for one reflexion from a face. Thus in the present experiments the factor was deduced from the strong (200) reflexion, and the intensities of the series ($h00$), derived from the measurements of ρ_s agreed exactly with the preliminary measurements of those intensities from an extended face.

The intensities have still to be corrected for the effects of extinction. Assuming this to be entirely due to secondary extinction, a correction can be made by replacing the true absorption coefficient μ_0 by μ where

$$\mu=\mu_0+g\mathrm{Q} \quad . \quad . \quad . \quad . \quad . \quad . \quad . \quad (5)$$

in which g is a constant for the crystal.

If the observed intensity of reflexion be denoted by ρ' the corrected intensity ρ to be used in equation (1) is given by the relation

$$\rho=\frac{\rho'}{1-2g\rho'} \quad . \quad . \quad . \quad . \quad . \quad . \quad . \quad (6)$$

To evaluate g, an approximate value of the parameter u of the sulphur atoms was obtained by trial from a comparison of the calculated and experimental values of F($h00$). With a knowledge of u, ρ was calculated for the ($h00$) reflexions, and g followed from equation (6). The revised values of the intensities may lead to a new value of the parameter, and so upset the previous calculation of g. If the extinction is small as it is in pyrites the extinction correction has very little effect on the estimated parameter and it is not necessary to recalculate g.

Data.

Linear absorption coefficient=114.
Spacing of pyrites=5·405 Å.
Extinction coefficient, $g=1{\cdot}63\times10^3$.

The Fourier Analysis.

The application of a double Fourier Series to the analysis of crystal structures has been fully discussed by W. L. Bragg [1]. The expression for the electron density at any point in the projection of the unit cell on a plane is greatly simplified if a centre of symmetry

be chosen as origin. In this case ρ_{xy} the electron density at the point (x, y) projected on (001) reduces to

$$\rho_{xy} = \frac{1}{A} \sum_{-\infty}^{\infty} \sum_{-\infty}^{\infty} F(hk0) \cdot \cos 2\pi(hx/a + ky/b), \quad . \quad . \quad . \quad (7)$$

where A is the area of the projection, and a and b are the lengths of the edges of the unit cell in the directions x and y. $F(000) = Z$, the total number of electrons in the unit cell.

The ($hk0$) Reflexions.

The X-ray spectra given by pyrites may conveniently be divided into two classes:—Type I., including the spectra corresponding to a cubic symmetry of the rock-salt type; and Type II., including any other spectra permitted by the special symmetry of pyrites. For the ($hk0$) reflexions Type I. is specified by h and k both even, and the structure factor becomes

$$F(hk0) = 4f_{Fe} + 8f_S \cos 2\pi hu \cdot \cos 2\pi ku \quad . \quad . \quad (8)$$

Both iron and sulphur atoms contribute to the spectra of this type.

With the axes defined as in fig. 1, Type II. has h odd and k even. The appropriate structure factor is

$$F(hk0) = 8f_S \cdot \sin 2\pi hu \cdot \sin 2\pi ku. \quad . \quad . \quad . \quad (9)$$

The iron atoms make no contribution to the reflexions of this type.

The signs of the Fourier coefficients were determined by using the approximate value of the parameter to calculate theoretical F-values, the atomic scattering factors f, being obtained from the Thomas fields. The experimental F-values agreed closely in magnitude with the calculated structure factors and were therefore given the same sign. With only one unimportant exception, the coefficients of the first type were positive on account of the positive contribution of the iron atoms. The experimental results and the calculated F-values are given in Table I. For convenience in presentation the analysis was performed in two sections, including the coefficients of Types I. and II. respectively.

Fig. 2 *a* represents the projection of the electron density on (001) over 1/16th of the cell face, using the

terms of Type I. The omission of all except the rock-salt terms leads to the imposition of the rock-salt symmetry on the picture. Instead, therefore, of finding two sulphur atoms (S_1 and S_2 of fig. 1) on a single diagonal through O, we find four peaks at S′ (fig. 2 *a*) and in corresponding positions in the other three quadrants. These peaks

Fig. 2 *a*.

Fourier diagram of projection of a portion (1/16th) of the unit cell on (001) using terms of Type I. only. The contours represent the density in "electrons per square Ångstrom."

represent halves of sulphur atoms modified by the background.

The analysis involving only the terms of Type II. is shown in fig. 2 *b*. In the first quadrant about O a negative peak round S″ is obtained and is repeated in the third quadrant. The figure repeats with change

Table I.

The ($hk0$) reflexions.

Type I.					Type II.				
Reflexion.	$\sin\theta/\lambda$.	$\rho\times10^6$.	$F_{obs.}$	$F_{calc.}$	Reflexion.	$\sin\theta/\lambda$.	$\rho\times10^6$.	$F_{obs.}$	Calc.
(200)	0·184	99·7	22·4	22·4	(120)	0·206	27·7	10·8	13·9
(220)	·260	51·8	17·5	17·1	(320)	·333	23·3	12·8	14·1
(400)	·370	0·21	1·3	−1·8	(140)	·380	1·14	2·9	2·6
(240)	·413	14·0	11·0	11·4	(340)	·461	1·05	3·2	3·0
(440)	·522	35·7	21·5	23·7	(520)	·497	2·59	5·3	−6·2
(600)	·554	2·74	5·8	6·3	(160)	·561	4·77	7·9	−7·6
(260)	·583	5·67	8·8	9·8	(540)	·591	0·97	2·0	−1·3
(640)	·666	7·93	11·4	13·2	(360)	·619	5·03	8·6	−8·9
(800)	·736	11·5	16·0	17·0	(720)	·672	6·80	10·7	−9·9
(280)	·760	3·40	8·2	9·1	(560)	·720	0·64	3·4	4·2
(660)	·784	3·78	8·7	9·1	(740)	·744	0·29	2·3	−2·2
(480)	·826	0·18	2·0	0·3	(180)	·744	0·48	3·0	−3·1
(10, 0, 0)	·922	3·52	9·3	11·4	(380)	·788	0·60	3·5	−3·6

(680)	·922	0·41	3·2	4·5
(2, 10, 0)	·942	1·41	5·9	7·3
(4, 10, 0)	·990	0·19	2·2	2·5
(880)	1·044	3·33	9·1	11·0
(6, 10, 0)	1·077	0·46	3·3	4·7
(12, 0, 0)	1·109	—	—	1·8
(2, 12, 0)	1·123	0·99	4·7	5·4
(920)	·850	—	—	1·8
(760)	·850	1·70	6·2	6·9
(580)	·870	0·13	1·7	1·8
(940)	·908	—	—	0·4
(1, 10, 0)	·927	0·51	3·6	4·2
(3, 10, 0)	·963	0·54	3·7	4·8
(780)	·980	0·24	2·5	3·2
(960)	·998	0·20	2·3	−1·4
(11, 2, 0)	1·031	0·90	4·7	6·3
(5, 10, 0)	1·031	0·21	2·3	−2·3
(11, 4, 0)	1·080	—	—	1·5
(980)	1·111	—	—	−0·6
(1, 12, 0)	1·111	—	—	2·6
(7, 10, 0)	1·126	—	—	−4·4

N.B.—These structure factors were calculated on the assumption that $u = 0{\cdot}115$, and also refer to atoms at absolute zero. The observed values refer to atoms at room temperature. The numerical agreement between $F_{obs.}$ and $F_{alc.}$ is improved if this difference is allowed for, but this is not necessary in determining the signs.

of sign in the second and fourth quadrants. The distance OS″ is the same as OS′, which indicates that the two sets of terms give consistent results for the parameter. The complete analysis over $\frac{1}{8}$th of the cell face is shown in fig. 3. On adding the distributions of figs. 2 *a* and 2 *b* the fractional sulphur peaks cancel out in the first

Fig. 2*b*.

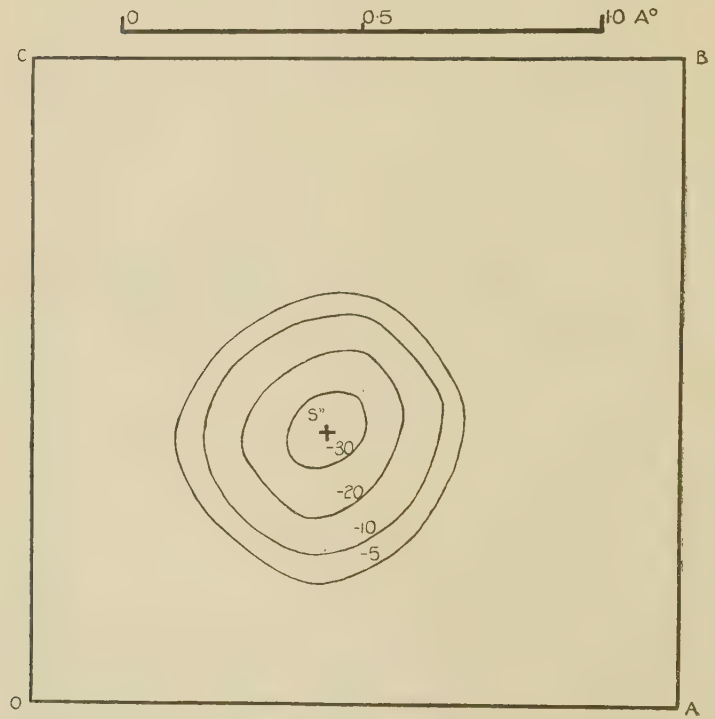

Fourier diagram of 1/16th of cell face using terms of Type II. only.

and third quadrants and produce the complete atoms (S_1 and S_2 of fig. 1) in the second and fourth quadrants. The contours for a full cell face are shown in fig. 4 which is derived from fig. 3 by the operation of the symmetry elements. The corresponding areas are lettered in the same way.

Fig. 3.

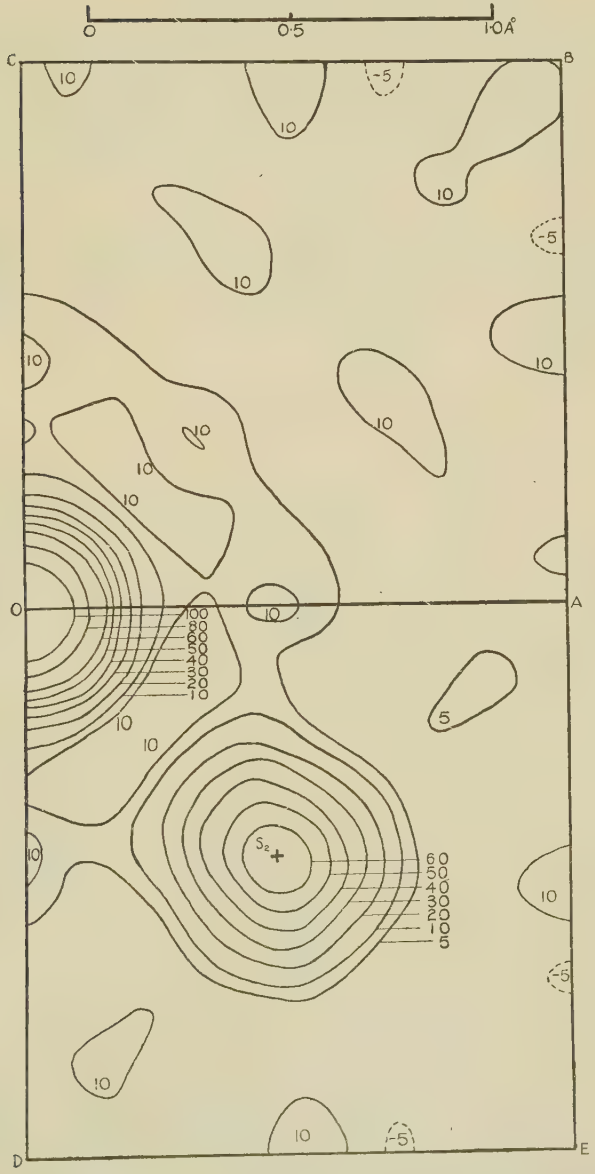

Fourier diagram of projection of $\frac{1}{8}$th of unit cell on (001) using all terms of the series.

Diffraction Effects.

Outside the regions of figs. 2 *a*, 2 *b*, and 3, which define the iron and sulphur atoms, there are many small regions in which the electron density is appreciable. It is obvious that these do not represent any real distribution of scattering matter at the corresponding

Fig. 4.

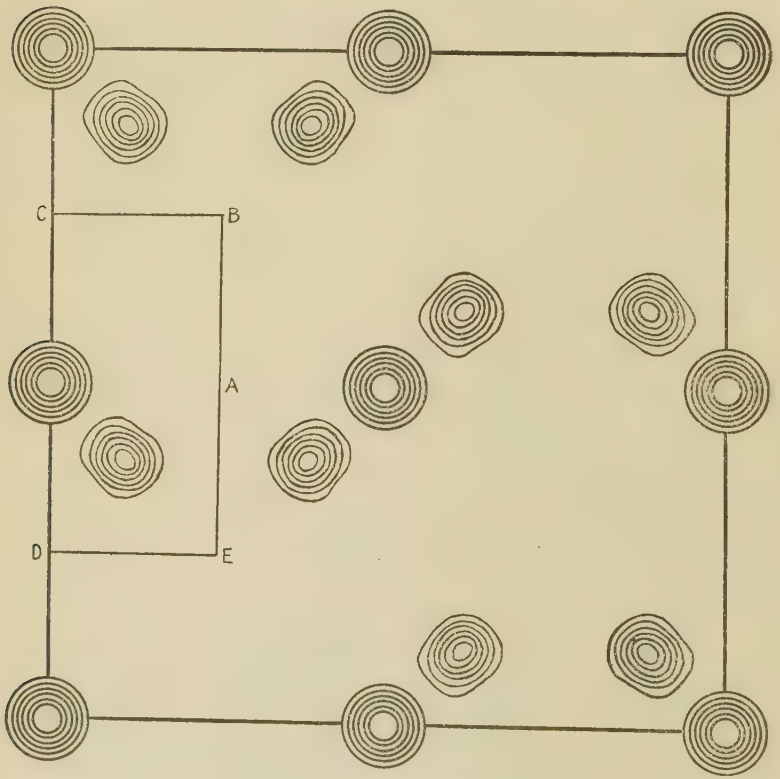

Complete Fourier diagram of the cell projected on (001).

points of the cell. They are merely diffraction effects introduced by the omission of the higher terms from the Fourier Series. Such effects have been fully discussed in the paper by Bragg and West [2] to which previous reference has been made. Equation (7) involves a double summation of F($hk0$) over all values of h and k from

$-\infty$ to ∞. The limitations of the ionization spectrometer prevent the observations from being extended beyond a certain maximum value of $(h^2+k^2+l^2)$, which defines a minimum spacing d_0 $\left(=\frac{a}{\sqrt{h^2+k^2+l^2}}\right)$ for the sets of planes considered. This produces an effect analogous to that of a limiting circular aperture in optics. Hence circular diffraction rings are produced in the projections, and the electron density at a point distant r from a centre of scattering, assumed to be a point source, is given approximately by the Bessel Function :

$$\rho(r)=\frac{\pi}{d_0^2}\frac{J_1(2m)}{m} \quad . \quad . \quad . \quad . \quad . \quad (10)$$

where $\frac{m}{\pi}=\frac{r}{d_0}$.

The overlapping of the diffraction rings from the iron and sulphur atoms produces the complicated system of " optical ghosts " in the Fourier diagrams. To discuss the diffraction in detail it is convenient to consider the section along some definite direction, in particular along the diagonal $x=-y$. The curves A and B in fig. 5 represent the electron density along $x=\pm y$ and $x=0$, respectively, in fig. 2 *a*, which corresponds to terms of Type I. The maximum of curve B at $r=0{\cdot}590$ Å is obviously the second diffraction ring * of the iron atom. Assuming the diffraction pattern of the iron atom to be circular, the distribution of curve B will persist in the direction $x=-y$. In that direction curve A represents the distribution of $(\mathrm{Fe}+\frac{1}{2}\mathrm{S})$. The curve C, which is obtained by subtracting curve B from A, therefore represents the distribution of $\frac{1}{2}$S along the diagonal, derived solely from the terms of Type I. Curve E represents the electron density along the direction $x=-y$ in fig. 2 *b*, *i. e.* the distribution of $\frac{1}{2}$S obtained independently from the terms of Type II. Curves C and E are practically identical. Actually C has been over-corrected for the diffraction effect of the iron.

* The first *minimum* of the Bessel function corresponds to the first observed diffraction ring in optics, since the Bessel function gives the amplitude and the intensity is actually observed.

B is not the true diffraction curve for iron as the first minimum is not negative; an analysis of the two-dimensional diagrams (figs. 2 and 3) shows that the rings due to the iron and sulphur atoms overlap additively in the

Fig. 5.

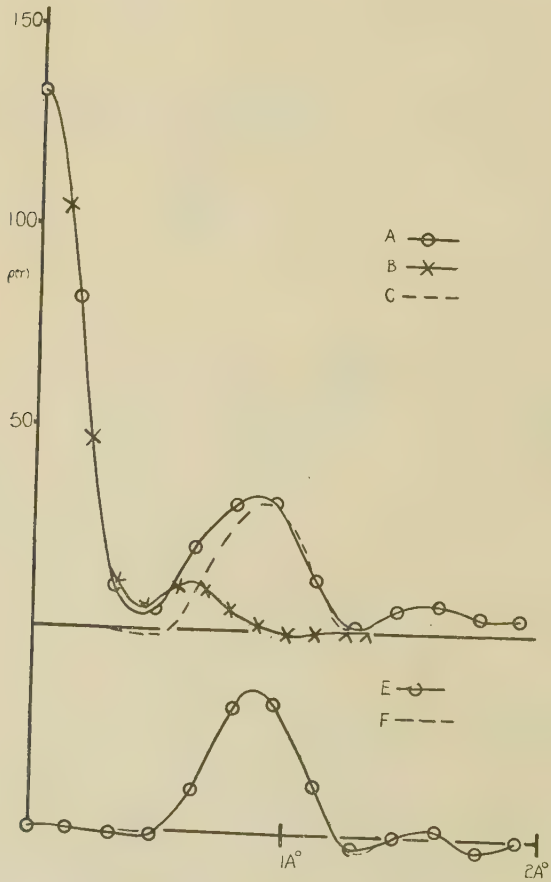

Electron density along $x=-y$ and $x=0$ in figs. 2 *a* and 2 *b*.

region between the first and second rings of the iron atom along $x=0$.

It was found possible to extend the observations to a maximum value of $(h^2+k^2+l^2)$ of 150, which makes $d_0=0{\cdot}430$ Å. for Mo K_α radiation. On substituting this

value in equation (10) the radius of the second diffraction ring becomes 0·590 Å., which is exactly the measured radius of the second rings of the iron and the sulphur atoms, from the Fourier diagrams. The radius of the first ring is also in good agreement with the calculated value. Curve F of fig. 5 is the Bessel function curve for the appropriate value of d_0 adjusted to fit E at the central maximum. Curves E and F then coincide over the first three rings on the side remote from the associated sulphur atom. The mathematics of the rings put forward by Bragg and West is therefore verified by experiment.

The Parameter of the Sulphur Atom.

Curve D of fig. 6 represents the section along the diagonal $x = -y$ of fig. 3. The complete sulphur peak is only slightly distorted by the diffraction rings of the iron atom. This distortion can be removed by applying a false temperature factor, but the peaks are flattened in the process so that their positions become more indefinite. The estimated parameter proved to be the same in either case and had the value $u=0{\cdot}114$. Thus the distance between the sulphur atoms in the associated pairs is 2·14 Å. A false temperature factor of the form $e^{-B \cdot \sin^2\theta}$ with the particular value $B=4{\cdot}6$ was applied. This reduced the structure factors of the outermost spectra to about one-eighteenth of their original values. An approximate calculation of the temperature factor for pyrites between absolute zero and room temperature gives $B=0{\cdot}2$, and is negligibly small compared with the artificial factor applied to make the Fourier series converge. The small heat motion in pyrites accounts for the well-marked diffraction effects in the projections, as the atoms approximate sufficiently to point sources of diffraction. Curve D_1 in fig. 6 is the modified form of D after the application of the false temperature factor. For comparison the curve D_2 has been drawn from a calculation on the assumption that the atoms behave as true point sources. When the false temperature factor is applied the atoms in the projection overlap to a considerable extent, and it is impossible to count the number of electrons in the atoms. For this reason the projection on (110) in which the sulphur

atoms are clearly separated from the iron atoms was also carried out.

Fig. 6.

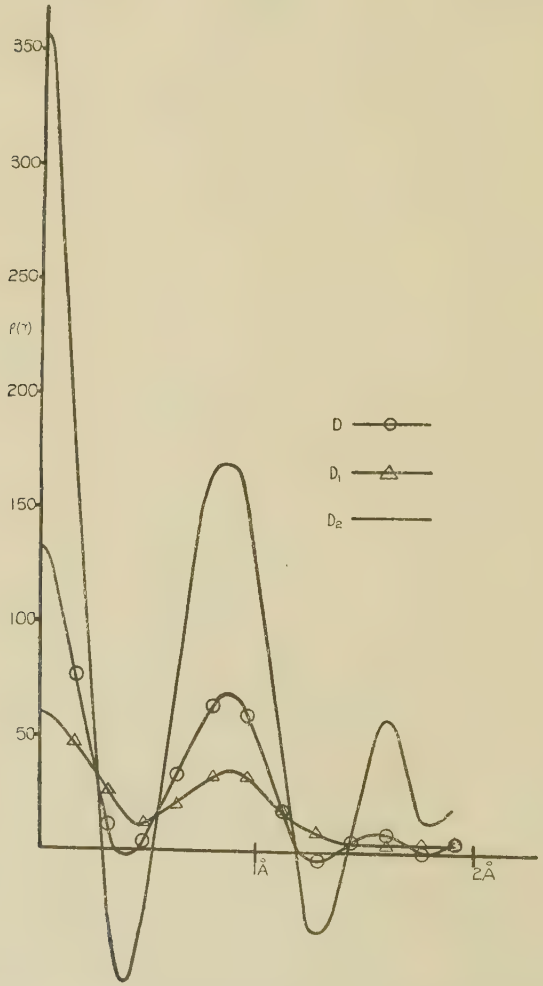

Section through the sulphur atom in fig. 3 with modifications introduced (1) by the imposition of a false temperature factor, and (2) by regarding the atoms as point sources.

The (*hhl*) Reflections.

Table II. shows the observed intensities and the corresponding F-values for the (*hhl*) reflexions, together with

the F-values calculated on the assumption that $u=0{\cdot}114$. The structure factors become :—

Type I.

—h and l both even : $F(hhl)= 8 f_S \cdot \cos^2 2\pi hu \cos 2\pi lu + 4f_{Fe}$.

—h and l both odd : $F(hhl)= 8f_S \cdot \cos^2 2\pi hu \cos 2\pi lu - 4f_{Fe}$.

Type II. $F(hhl)= 8f_S \cdot \sin 4\pi hu \cdot \sin 2\pi lu$.

Fig 7.

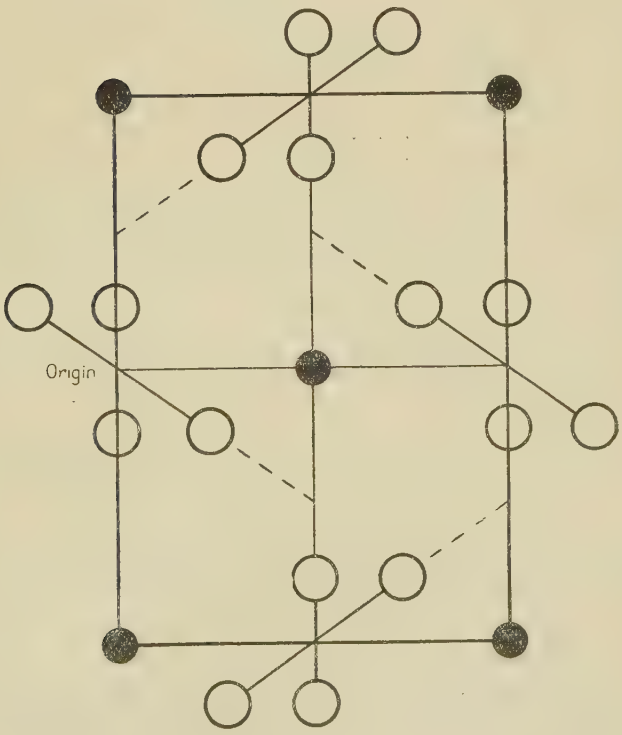

Projection of the structure on (110). The bounding lines of the diagram define the projection of the new unit cell.

The coefficients were set into a form suitable for the Fourier calculation by a transformation of axes such that (hhl) becomes (HOL), where $H=h$ and $L=l$. The new projection is indicated in fig. 7. By trial, the false

Table II.

The (*hhl*) reflexions.

Type I.					Type II.				
Reflexion.	sin θ/λ.	$\rho \times 10^6$.	$F_{obs.}$	$F_{calc.}$	Reflexion.	sin θ/λ.	$\rho \times 10^6$.	$F_{obs.}$	$F_{calc.}$
(111)	0·160	44·0	12·4	−13·1	(112)	0·226	24·2	10·5	9·9
(002)	·184	99·7	22·9	22·9	(221)	·276	0·57	1·7	1·9
(220)	·261	54·4	18·2	17·2	(223)	·380	0·30	1·5	2·1
(113)	·305	61·0	21·3	−21·0	(114)	·390	0·69	2·3	2·4
(222)	·322	36·4	16·1	15·0	(332)	·432	4·93	6·5	−6·6
(004)	·370	0·32	1·5	−1·4	(225)	·529	—	—	−0·8
(331)	·403	14·25	11·0	−9·9	(441)	·529	0·51	2·4	−2·5
(224)	·453	17·3	13·1	12·3	(334)	·536	0·59	2·7	−1·8
(115)	·480	29·9	18·5	−19·3	(116)	·567	2·96	6·2	−5·5
(333)	·480	19·7	14·6	−14·4	(443)	·590	0·35	2·2	−2·9
(440)	·522	37·6	21·9	23·5	(336)	·679	1·86	5·5	4·2
(442)	·554	9·56	11·1	12·5	(552)	·679	0·96	4·0	3·7
(006)	·554	3·12	6·2	5·8	(227)	·695	0·18	1·7	−1·6
(335)	·606	12·8	13·8	−13·3	(445)	·695	0·04	0·9	1·2
(226)	·612	6·60	9·3	9·9	(554)	·748	—	—	1·0
(444)	·640	0·14	1·4	−0·5	(118)	·748	0·43	2·9	−2·6
(117)	·660	3·06	7·0	−7·7	(661)	·785	0·20	2·0	2·4
(551)	·661	·55	2·9	−2·6	(663)	·829	0·25	2·3	2·9
(553)	·709	10·4	4·4	−4·1	(447)	·829	0·13	1·7	2·4
(008)	·738	14·2	16·7	16·7	(338)	·834	0·10	1·5	2·2
(337)	·756	2·42	6·9	−7·4	(556)	·854	0·30	2·6	−2·7

(446)	·762	1·19	4·8	4·6
(660)	·782	3·38	8·4	9·4
(228)	·782	3·20	8·1	8·0
(555)	·800	9·29	15·5	−14·5
(662)	·805	3·54	8·6	7·9
(119)	·842	0·07	1·4	−2·7
(664)	·868	1·86	6·6	5·9
(448)	·906	6·41	12·8	13·1
(771)	·920	1·38	5·9	−6·4
(557)	·920	1·17	5·3	−5·0
(339)	·920	0·94	4·8	−4·6
(0, 0, 10)	·924	3·92	10·1	11·7
(773)	·957	1·68	6·5	−7·0
(666)	·960	1·51	6·1	6·1
(2, 2, 10)	·960	1·64	6·4	6·7
(1, 1, 11)	1·022	1·66	6·5	−6·5
(775)	1·022	1·79	6·7	−6·9
(880)	1·044	3·60	9·5	10·7
(559)	1·058	—	—	−1·1
(882)	1·062	1·45	6·0	6·7
(4, 4, 10)	1·062	2·96	8·6	9·7
(668)	1·077	1·84	6·7	6·8
(3, 3, 11)	1·090	1·22	5·4	−6·0
(0, 0, 12)	1·106	—	—	2·1
(884)	1·106	0·42	3·1	2·1
(777)	1·117	1·15	5·2	−5·7
(229)	·870	—	—	0·1
(665)	·905	—	—	−1·2
(1, 1, 10)	·929	0·30	2·7	2·7
(772)	·929	—	—	−1·8
(449)	·978	—	—	0·2
(774)	·984	—	—	−0·5
(558)	·984	—	—	−1·4
(3, 3, 10)	1·000	—	—	−2·1
(667)	1·011	—	—	−2·5
(881)	1·045	0·20	2·2	−2·0
(2, 2, 11)	1·045	—	—	1·0
(776)	1·058	—	—	1·3
(883)	1·078	0·30	2·7	−2·4
(1, 1, 12)	1·111	—	—	2·3
(5, 5, 10)	1·127	—	—	1·4

The parameter used in calculating these F-values is $u = 0{\cdot}114$.
The theoretical F-values refer to Thomas atoms at absolute zero.

temperature factor corresponding to B=3·5 was found to be just sufficient to remove the diffraction rings. The contours with this factor are sketched in fig. 8. The iron atoms project in pairs, one above the other, and the

Fig. 8.

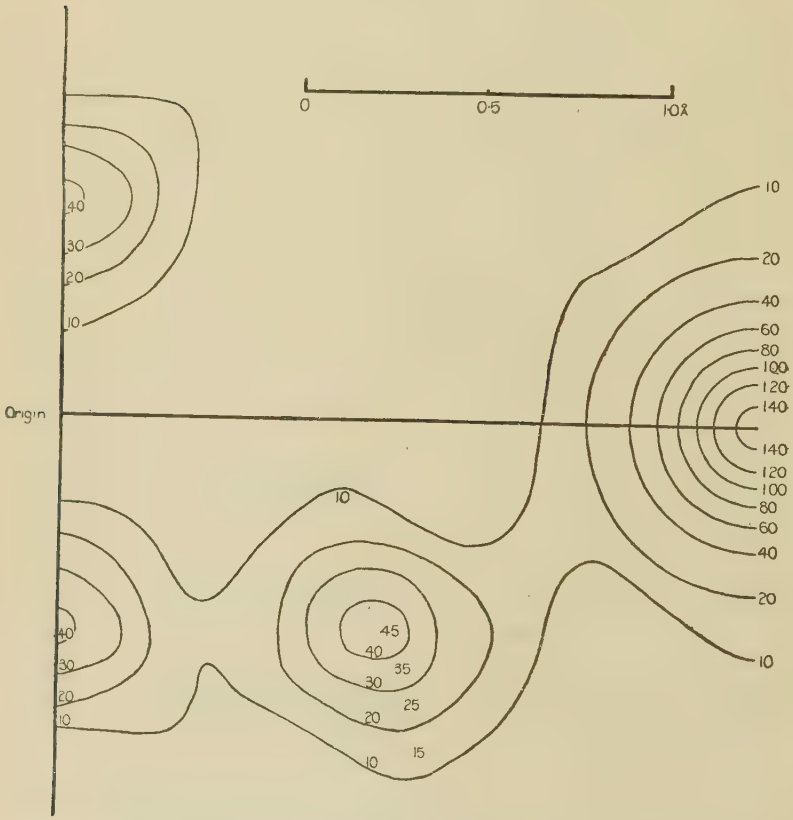

Contour diagram of the (110) projection. The relation to the complete cell face will be seen by reference to fig. 7.

sulphur groups become crossed pairs, as shown in the figures. The parameter derived from this projection agreed exactly with that previously obtained.

Electron Counting.

The iron atom.

The pairs of iron atoms are well separated from the sulphur groups and are accurately symmetrical up to a radius of 0·5 Å. Outside this radius the electron density sinks to zero along the axes of x and y, but remains just appreciable in other directions. This is due to a very slight influence from the sulphur atoms, which have no effect along the axes. The distribution along the axes was therefore taken to be the true one, and it was integrated to obtain the total number of electrons in the iron atoms. The result is 51·7 electrons for the two iron atoms, making 25·9 for each. The atomic number of iron is 26, and thus the result indicates that the iron atom is not ionized.

The sulphur atoms.

One of the main points of interest in this investigation is the information it may give about the form of the homopolar bond between the sulphur atoms. Two electrons are supposed to be shared between each pair of sulphur atoms. We might therefore expect to find an appreciable electron density at the centre of the crossed pairs of sulphur atoms in fig. 8. The effect, if it exists, is masked by diffraction, and when the diffraction has been removed by a false temperature factor the expected effect is smeared out too much to be recognized with certainty.

There is, moreover, a more serious difficulty in that the theory of scattering for electrons in a homopolar link has never been worked out. In any case the effects would probably depend upon the intensities of quite a few spectra, for in the theoretical f-curve of the sulphur atom the contribution of the electrons of the M-shell becomes extremely small at values of $\frac{\sin\theta}{\lambda}$ greater than 0·3 to 0·4. We can only conclude, therefore, that if the four electrons do gather together to form a sudsidiary peak at the centre of the crossed pair, the magnitude of this peak is of the same order as the diffraction effects.

Conclusion and Summary.

A Fourier analysis of iron pyrites projected on (001) and (110) has been carried out. All spectra of the types $(hk0)$ and (hhl) up to $\frac{\sin\theta}{\lambda} = 1{\cdot}1$ were measured by the method of transmission through thin crystal slips, with Mo K_α radiation, and reduced to absolute values by comparison with the reflexions from an extended face. An extinction correction was made on the basis of a comparison between the observed value of the (200) reflexion and that calculated from an approximate parameter for the sulphur atom. The signs of the coefficients were taken to be those of the calculated structure factors derived from the Thomas f-curves, using the approximate value of the sulphur parameter.

The results of the investigation may be divided into two groups. The first is of purely crystallographic interest and consists of precise measurements of the spacing of the crystal and the parameter of the sulphur atom. These lead to accurate values of the sulphur-sulphur distance and the sulphur-iron distance in the compound.

Spacing of iron pyrites= 5·405 Å.

Parameter of the sulphur atom= 0·114.

Distance between centres of adjacent sulphur atoms = 2·14 Å.

Distance between centres of adjacent sulphur and iron atoms= 2·26 Å.

The second group of results is of more general physical interest in that it provides a confirmation of the predictions of Bragg and West concerning the diffraction effects in a Fourier analysis, and the possibility of counting electrons.

(*a*) The diffraction rings surrounding each peak were found to have the predicted radii.

(*b*) A false temperature factor was applied and the number of electrons in the iron atom was counted. The iron atom was found to have its full complement of 26 electrons. This indicates definitely that the compound is not ionic, and is in agreement with chemical and other evidence. No direct evidence of the electrons

of the homopolar bonds could be obtained with the present sensitivity.

In conclusion, the authors wish to express their sincere thanks to Professor W. L. Bragg, F.R.S., and Mr. R. W. James, M.A., for their continued interest and advice throughout the work.

References.

(1) W. L. Bragg, Proc. Roy. Soc. A, cxxiii. p. 537 (1929).
(2) W. L. Bragg and J. West, Phil. Mag. x. p. 823 (1930).
(3) W. L. Bragg, Proc. Roy. Soc. A, lxxxviii. p. 428 (1913); A, lxxxix. p. 468 (1914).
(4) P. P. Ewald, *Ann. d. Phys.* xliv. p. 1183 (1914); *Phys. Zeit.* xv. p. 399 (1914).
(5) A. Jönsson, Dissertation, Upsala (1928).

XCIX. *Generalizations of Maxwell's Theory.* *By* Dr. Irene E. Viney *.

1. *Introduction.*

ATTEMPTS to modify Maxwell's Theory, defined by the well-known system of field equations, have in the past almost invariably ended in hopeless inconsistencies, and few writers nowadays will admit the possibility of making any serious modification of the theory without disturbing the whole foundations of the scheme. As, however, these equations are seemingly inconsistent with the results of nearly all recent investigations into the microscopic behaviour of matter and its electrical constituents, which apparently require much more elaborate ideas for their explanation, attempts are still being made to obtain some modification of the theory which will extend it to cover some of these more complex details. One of the most recent, and at the same time most ingenious, suggestions to this end was made by R. Ferrier in 1925, in a paper entitled "Les nouveaux Axiomes de l'Electronique" †, but it is not difficult to see that his suggestion is inconsistent with a dynamical formulation. An attempt to derive such a formulation, however, soon led me to a simple generalization of the theory, which,

* Communicated by Prof. G. H. Livens.

† *Revue Générale de l'Electricite*, Paris (1925). *Cf.* Also a pamphlet published in 1927 "Quelques idées sur l'Electrodynamique."

although dynamically consistent, proved to be ultimately incompatible with certain other physical criteria for the theory. Since, quite recently, another writer, M. Al Proca *, has derived certain results of this work by an alternative and quite independent method and has used them to offer an explanation of certain complex atomic phenomena, it seemed to me to be desirable to give an exposition of the whole theory and to point out the serious disadvantages attaching to its use, disadvantages not apparent in the limited number of results derived and used by Al Proca. This discussion may also serve the purpose of showing the steps leading towards the still more general theory dealt with in a previous paper in which none of these difficulties are present.

2. *Ferrier's Theory.*

The essential point of this theory is the introduction of an additional arbitrary scalar function which Ferrier calls the Ampèrean. This function which we shall denote by E_0 †, is defined by the system of equations

$$\text{(i.)} \quad \text{curl } \mathbf{B} = \frac{4\pi}{c}\mathbf{C} + \text{grad } E_0,$$

$$\text{(ii.)} \quad \text{div } \mathbf{E} = 4\pi\rho - \frac{1}{c}\frac{\partial E_0}{\partial t},$$

wherein $\mathbf{C}$ denotes the total current vector of Maxwell's theory ; it is equal to $\frac{1}{4\pi}\frac{\partial \mathbf{E}}{\partial t} + c\mathrm{j}$, where j is the true conduction current in the field. These equations are the fundamental equations of the theory and replace the usual equations of Ampère and Gauss of the classical theory to which they reduce when $E_0 = 0$; they are derived by Ferrier from more or less elementary ideas.

We may well stop at this point to notice that the vector $\mathbf{C}$ in this theory has lost its circuital property—a feature so characteristic of Maxwell's original scheme. We have here

$$\text{div. } \mathbf{C} = -\frac{c}{4\pi}\nabla^2 E_0,$$

which means that, to the displacement current $\frac{1}{4\pi}\partial \mathrm{E}/\partial t$ of

* "Sur une explication possible de la difference de masse entre le proton et l'electron," *Journ. de Phys.* vii. Feb. (1932), p. 83.

† In keeping with the notation adopted by Al Proca in his exposition which will be dealt with later.

Maxwell's theory an additional aethereal current $\frac{c}{4\pi}\operatorname{grad} E_0$ has to be added in order to complete the closure of the field currents. It is this difference in character of the current vector **C** which marks the real point of departure of Ferrier's theory from that of Maxwell. Ferrier maintains that Maxwell's supposition, that the general laws of induction are those which avail themselves in the case of closed conductors, is a mere assumption and that generally its hypothetical nature has escaped notice. His theory attempts to reveal the uselessness of this restrictive hypothesis relating to closed currents and at the same time conforms to all the requirements of the general energy and other physical relations contained in the Maxwell-Lorentz theory and its later development.

3.

The other relation for defining E_0, viz.,

$$\operatorname{div} \mathbf{E} = 4\pi\rho - \frac{1}{c}\frac{\partial E_0}{\partial t},$$

is a modified form of the Gaussian equation of the classical theory. It constitutes the fourth symmetric equation of the four-dimensional set, of which the modified Ampèrean equations comprise the remaining members.

The other field equations of the classical theory, viz., Faraday's equation,

$$\operatorname{curl} \mathbf{E} = -\frac{1}{c}\frac{\partial \mathbf{B}}{\partial t}$$

and the corresponding characteristic equation

$$\operatorname{div} \mathbf{B} = 0$$

are shown by Ferrier by elementary reasoning to retain their original forms and are not in any way modified to include terms in the new function E_0.

Ferrier also gives the appropriate expressions for the total energy density and for the energy flux vector in the field of an electrodynamical system containing only electric charges. These are given by

$$W' = \frac{1}{8\pi}(\mathbf{E}^2 + \mathbf{B}^2 + E_0^2),$$

$$S' = \frac{c}{4\pi}([\mathbf{EB}] + E_0\mathbf{E}),$$

respectively.

This, roughly speaking, completes the scheme of modification of the classical theory suggested by Ferrier.

4. *The Dynamical Formulation of Ferrier's Theory.*

If we try to formulate the above theory, proposed by Ferrier, on more general lines by applying the Principle of Least Action, we shall of course derive results which are wholly consistent with a general dynamical formulation of the relations of the field, but then we find that this procedure leads naturally to a slightly more general form of the theory reducing to the original one only in conditions appropriate to statical or quasi-statical fields. For this analysis, as before, we restrict the discussion to fields containing electric charges only.

The variational method follows the lines of the usual application of the calculus of variations to dynamical problems of this type. We start from the total energy density of the system, viz.,

$$\mathrm{T}+\mathrm{V}=\mathrm{W}'=\frac{1}{8\pi}(\mathbf{E}^2+\mathbf{B}^2+E_0^2),$$

and assume tentatively *,

$$\mathrm{T}=\frac{1}{8\pi}(\mathbf{B}^2+E_0^2), \qquad \mathrm{V}=\frac{1}{8\pi}\mathbf{E}^2$$

for the expressions of the kinetic and potential energy densities of the system respectively. The action-integral of the system then assumes the form

$$\int dt\left[\frac{1}{8\pi}\int(\mathbf{B}^2+E_0^2-\mathbf{E}^2)\,dv+\mathrm{L}_0\right],$$

wherein L_0 as usual relates to the intrinsic inertia of the electrons of the system.

As equations of condition governing the variation of the integral we take the two fundamental field equations

$$\operatorname{curl}\mathbf{B}=\frac{1}{c}\frac{\partial\mathbf{E}}{\partial t}+4\pi\mathbf{j}+\operatorname{grad}E_0$$

$$\operatorname{div}\mathbf{E}=4\pi\rho-\frac{1}{c}\frac{\partial E_0}{\partial t}$$

of the complete set. The modified action integral of the system is then formed by the introduction of arbitrary scalar

* Actually with $\mathrm{T}=\frac{1}{8\pi}\mathbf{B}^2$, $\mathrm{V}=\frac{1}{8\pi}(\mathbf{E}^2+E_0^2)$ we obtain exactly similar results.

and vector functions **A** and ϕ and then its variation, showing no novel features, gives finally the equations,

$$\mathbf{B} = \text{curl } \mathbf{A}, \qquad \mathbf{E} = -\nabla\phi - \frac{1}{c}\frac{\partial \mathbf{A}}{\partial t}$$

familiar in electric theory as the equivalent of the Faraday equations, together with

$$E_0 = \text{div } \mathbf{A} + \frac{1}{c}\frac{\partial \phi}{\partial t}$$

and the expression for the forcive per unit volume on the moving charges, which takes the form

$$\mathbf{F} = \rho\Big(-\nabla\phi - \frac{1}{c}\frac{\partial \mathbf{A}}{\partial t} + \frac{1}{c}[\dot{\mathbf{r}}.\text{curl } \mathbf{A}]\Big)$$

$$= \rho\Big(\mathbf{E} + \frac{1}{c}[\dot{\mathbf{r}}.\mathbf{B}]\Big).$$

5.

These relations show that, while the forms of the fundamental force vectors **E**, **B**, and **F** in terms of the potential functions **A** and ϕ remain as in the classical theory and also in Ferrier's original modification of it, we have here a new relation introduced between the potential functions, viz.,

$$E_0 = \text{div } \mathbf{A} + \frac{1}{c}\frac{\partial \phi}{\partial t}.$$

Ferrier's original discussion actually suggested the relation

$$E_0 = \text{div } \mathbf{A},$$

and it is to this extent that our theory is a generalization of his. Our form is obviously the only one consistent with a dynamical foundation and has, of course, other reasons to commend it.

The importance of this relation is that it is precisely the relation required to make the potential functions ϕ and **A** satisfy the usual equations *,

$$\nabla^2\phi - \frac{1}{c^2}\frac{\partial^2\phi}{\partial t^2} = -4\pi\rho,$$

$$\nabla^2\mathbf{A} - \frac{1}{c^2}\frac{\partial^2\mathbf{A}}{\partial t^2} = -4\pi\mathbf{j},$$

* It is interesting to note that, starting from these equations of propagation of the potential functions, de Broglie also arrived at the complete set of equations of our theory and he was the first to regard them together as constituting a modified and generalized form of the Maxwell-Lorentz theory. *Cf.* "Ondes et Mouvements," 'Collection de Physique et Mathématique,' ch. viii. p. 69.

as is easily verified by the usual procedure of the classical theory ; and now it is easy to see the futility in the whole argument. In fact, by differentiation of the above equations, we obtain at once

$$\left(\nabla^2-\frac{1}{c^2}\frac{\partial^2}{\partial t^2}\right)\left(\operatorname{div}\mathbf{A}+\frac{1}{c}\frac{\partial\phi}{\partial t}\right)=-4\pi\left(\frac{\partial\rho}{\partial t}+\operatorname{div}\mathbf{j}\right),$$

or

$$\nabla^2\mathrm{E}_0-\frac{1}{c^2}\frac{\partial^2 E_0}{\partial t^2}=-4\pi\left(\frac{\partial\rho}{\partial t}+\operatorname{div}\mathbf{j}\right).$$

If now electric charge is everywhere conserved, the right-hand side of this equation is zero, and E_0 is then a wave-function without poles and therefore essentially a constant. Thus the existence of E_0 definitely implies non-conservation of charge, a hypothesis we are not as yet inclined to envisage.

6.

In spite of this very fundamental difficulty we decided to pursue the development of the theory still further towards obtaining the general stress-energy relations of the field defined by the new equations.

The energy relations of the field may be expected to satisfy the principle of the conservation of energy, and the equation of energy, viz.,

$$\frac{\partial \mathrm{W}}{\partial t}+\operatorname{div}\mathbf{S}=-c(\mathbf{Ej}),$$

wherein W denotes the total energy density and **S** the corresponding energy flux vector, will then be satisfied at all points of the field *.

For present considerations W has the value

$$\frac{1}{8\pi}(\mathbf{E}^2+\mathbf{B}^2+E_0^2),$$

and thus we have

$$\operatorname{div}\mathbf{S}=\frac{1}{8\pi}\frac{\partial}{\partial t}(\mathbf{E}^2+\mathbf{B}^2+E_0^2)-c(\mathbf{Ej})$$

$$=\frac{c}{4\pi}\operatorname{div}[\mathbf{EB}]+\frac{c}{4\pi}\operatorname{div}(E_0\mathbf{E})-cE_0\rho.$$

* Larmor, Phil. Trans. A, cxc. p. 285 (1897).

We might then suppose, with Ferrier, that the energy flux of the system is equal to

$$\mathbf{S} = \frac{c}{4\pi}[\mathbf{EB}] + E_0\mathbf{E},$$

but then the unspecified term

$$cE_0\rho$$

would have to represent latent energy of some kind or other in the electric charge. According to modern investigations electrons seem to be capable of losing and gaining energy almost spontaneously, and it is difficult theoretically to explain precisely how and why these changes occur, unless we assume such energy of this kind. The theory, with E_0, is thus proposed by Ferrier to bring the electrodynamic formulations into line with modern thought. But since it also introduces the idea of the spontaneous generation or annihilation of charge, it will probably create more difficulties than Ferrier imagines it resolves.

7.

Corresponding to this discussion of the energy relation of the theory there is, of course, a similar discussion for the stress and momentum equations. If we can express the electromagnetic forcive per unit volume, F_k, in the form

$$F_k = \sum_{i=1}^{3} \frac{\partial O_{ik}}{\partial x_i} - \frac{\partial G_k}{\partial t} \quad (k = 1, 2, 3),$$

then we may take G_k to denote the momentum vector and O_{ik} the stress tensor with nine components $(i, k = 1, 2, 3)$.

Taking the hint from the energy equation we might try for G the vector

$$\frac{1}{4\pi c}([\mathbf{EB}] - E_0\mathbf{E})$$

and then we should obtain a relation of the form

$$\sum_{i=1}^{3} \frac{\partial O_{ik}}{\partial x} = -\frac{1}{8\pi}\frac{\partial}{\partial x_k}(\mathbf{E}^2 + \mathbf{B}^2 - E_0^2) + \frac{1}{4\pi}\{\mathbf{E}_k \operatorname{div} \mathbf{E} + \mathbf{B}_k \operatorname{div} \mathbf{B}\} - \frac{1}{4\pi}\operatorname{curl}_k (E_0\mathbf{B}) + E_0 \mathrm{j}k.$$

If then we take for the stress tensor the expression

$$O_{ik} = \frac{1}{4\pi}(\mathbf{E}_i\mathbf{E}_k - \tfrac{1}{2}\mathbf{E}^2\delta_{ik}) + \frac{1}{8\pi}E_0^2\delta_{ik}$$
$$+ \frac{1}{4\pi}(\mathbf{B}_i\mathbf{B}_k - \tfrac{1}{2}\mathbf{B}^2\delta_{ik}) - \frac{1}{4\pi}\mathrm{E}_0(\mathbf{B}_m\delta_{il} - \mathbf{B}_l\delta_{lm}),$$

where (k, l, m) denote the components (x, y, z) taken in rotary order and δ_{ik} is the usual tensor which is such that

$$\delta_{ik} = 1, \qquad i = k,$$
and $$\delta_{ik} = 0, \qquad i \neq k,$$

then we are left with the unspecified term

$$E_0\mathfrak{j}$$

to be identified somehow. If we take this term over to the right-hand side and include it in the expression for the total force, then we may endeavour to interpret its significance in a measure much the same as that in which the significance of the term $cE_0\rho$ in the energy equation was explained. If we do this then for the total force per unit volume acting on the charge we should have the expression

$$\rho(\mathbf{E} + \frac{1}{c}[\mathbf{v}\mathbf{B}]) - E_0\mathfrak{j},$$

or its equivalent

$$\rho(\mathbf{E} + \frac{1}{c}[\mathbf{v}\mathbf{B}] - \frac{1}{c}E_0\mathbf{v}).$$

This result now implies that

$$(\mathbf{F}\mathbf{v}) = c(\mathbf{E}\mathfrak{j}) - \frac{1}{c}\rho E_0\mathbf{v}^2$$

is the total amount of energy dissipated per unit time into heat and other forms of energy of a non-electric nature. Comparing this expression with the right-hand side of the energy equation, to which it should be equal, we see that they agree only if

$$\frac{1}{c}.\mathrm{E}_0\mathbf{v}^2 = cE_0, \qquad \mathfrak{j} = \rho\mathbf{v},$$

or, if $$|\,\mathbf{v}\,| = c,$$

which implies that the velocity of the charges through space is identical with the velocity of radiation. Thus on all counts the theory breaks down as a suitable account of the

physical behaviour of electric charge as we know it at present. Let us now therefore proceed to the next generalization, recently formulated by Al Proca.

8. *Al Proca's Theory.*

The theory put forward by Al Proca is derived by him by an application of quaternion methods. It is a similar but generalised form of our modified form of Ferrier's theory. The essence of the theory is the introduction of two new functions E_0, B_0 instead of one, as in Ferrier's theory. The method of approach at once suggests that the theory is of ideal mathematical symmetry, but since, as we shall see later, there is no corresponding symmetry in the physical world, the theory is wholly untenable as a physical theory.

We need not enter into any details of the derivation, which we do not propose to criticise. It will be sufficient therefore if we quote the final form of his fundamental equations and the main conclusions he tries to draw from them. The fundamental field equations are the set

$$\frac{1}{c}\frac{\partial B_0}{\partial t} + \operatorname{div}\mathbf{B} = 0,$$

$$\frac{1}{c}\frac{\partial E_0}{\partial t} + \operatorname{div}\mathbf{E} = 4\pi\rho,$$

$$\operatorname{curl}\mathbf{E} + \frac{1}{c}\frac{\partial \mathbf{B}}{\partial t} + \operatorname{grad} B_0 = 0,$$

$$\operatorname{curl}\mathbf{B} - \frac{1}{c}\frac{\partial \mathbf{E}}{\partial t} - \operatorname{grad} E_0 = 4\pi\mathbf{j},$$

where E_0 and B_0 are the new scalar functions introduced into the theory and the other vectors have their usual significance.

The field equations in terms of the potential functions are shown to have the forms

$$\mathbf{E} = -\nabla\phi - \frac{1}{c}\frac{\partial \mathbf{A}}{\partial t} - \operatorname{curl}\mathbf{L},$$

$$\mathbf{B} = -\nabla L_0 - \frac{1}{c}\frac{\partial \mathbf{L}}{\partial t} + \operatorname{curl}\mathbf{A},$$

$$E_0 = \frac{1}{c}\frac{\partial \phi}{\partial t} + \operatorname{div}\mathbf{A},$$

$$B_0 = \frac{1}{c}\frac{\partial \mathrm{L}_0}{\partial t} + \operatorname{div}\mathbf{L},$$

where ϕ and $\mathbf{A}$ are the old potential functions and L_0 and $\mathbf{L}$ are newly introduced ones.

In addition to these the expression for the force per unit volume on the charge is shown to be

$$\mathbf{F}=\rho(\mathbf{E}+\frac{1}{c}[\mathbf{vB}])-E_0\mathbf{j},$$

exactly as in the theories expounded above.

This theory obviously reduces to the modified forms of Ferrier's theory if, in it, the functions $\mathbf{L}$, L_0, B_0 are all given zero values.

9.

Al Proca makes use of the modified form of the Lorentz force as a possible means of explaining the difference in mass between the electron and the proton. If m_0 denotes the rest-mass of an electron then Al Proca says that the fundamental law of motion of the electron is given by the equation

$$\frac{d}{dt}(m_0\mathbf{v})=\text{force},$$

so that

$$\mathbf{v}\frac{dm_0}{dt}+m_0\frac{d\mathbf{v}}{dt}=e\left(\mathbf{E}+\frac{1}{c}[\mathbf{vB}]-E_0\frac{\mathbf{v}}{c}\right),$$

where e is the charge of an electron.

As in the Lorentz theory, when $m_0=\text{const.}$ and $E_0=0$, we have

$$m_0\frac{d\mathbf{v}}{dt}=e\left(\mathbf{E}+\frac{1}{c}[\mathbf{vB}]\right),$$

and so it follows that we must have also

$$\mathbf{v}\frac{dm_0}{dt}=-eE_0\frac{\mathbf{v}}{c}$$

or

$$m_0=\text{const.}-\frac{e}{c}\int E_0\,dt$$

$$=\mu_0-\frac{e}{c}\int E_0\,dt,$$

say, where μ_0 denotes the inertial mass of the electron. And now, supposing that a proton and an electron have the same inertial mass μ_0, then, since their signs of charge

are opposite, we see that their rest masses would then be equal to

$$\mu_0 - \frac{e}{c}\int E_0\,dt \quad \text{and} \quad \mu_0 + \frac{e}{c}\int E_0\,dt$$

respectively. This result, so Proca maintains, might easily explain the difference in mass between a proton and an electron.

The weak point in this argument seems to be the insufficient explanation of the significance of the functions E_0 and B_0. It is obvious that, whatever their real significance, if they are to be at all measurable experimentally, they must be associated with some physical entity or other. If they arise from the charge then it is very unlikely that they are anything but proportional to the charge. But if this is the case and we write $E_0 = eE_0'$, then the formula for the mass becomes

$$m_0 = \mu_0 - \frac{e^2}{c}\int E_0'\,dt,$$

and does not alter with the sign of e. Of course E_0 may be an extraneous effect not depending on the charge or particle itself, but then the formula makes the mass depend on the whole past history of the field of E_0, so that this assumption seems even more unlikely.

10.

Further criticism of this theory follows, as in the case of Ferrier's theory, from an attempt to formulate its Least Action foundation. If we carry out the variation of the Action-integral

$$\frac{1}{8\pi}\int (\mathbf{B}^2 - \mathbf{E}^2 + B_0^2 - E_0^2)\,dv\,dt$$

subject to the conditions *

$$\operatorname{div}\mathbf{B} = -\frac{1}{c}\frac{\partial B_0}{\partial t}, \qquad \operatorname{div}\mathbf{E} = 4\pi\rho - \frac{1}{c}\frac{\partial E_0}{\partial t},$$

$$\operatorname{curl}\mathbf{E} = -\frac{1}{c}\frac{\partial \mathbf{B}}{\partial t} - \operatorname{grad} B_0, \quad \operatorname{curl}\mathbf{B} = \frac{1}{c}\frac{\partial \mathbf{E}}{\partial t} + \operatorname{grad} E_0 + 4\pi\mathbf{j},$$

* Notice that here the whole system of fundamental equations is required as equations of condition, that is, twice as many as in the classical theory. The extra equations are necessary to define the new functions E_0 and B_0. It thus appears that the introduction of new functions into the old equations of the theory in this way requires *a priori* a greater knowledge of the field equations, and hence is not likely to be of any real aid in our researches.

then we derive immediately the field relations of Proca's theory in terms of the potentials ϕ, $\mathbf{A}$, L_0, $\mathbf{L}$ exactly as they appear above together with an expression for the electromotive forcive $\mathbf{F}$, viz. :—

$$\mathbf{F} = \rho\Big(-\operatorname{grad}\phi - \frac{1}{c}\frac{\partial \mathbf{A}}{\partial t} - \operatorname{curl}\mathbf{L} + \Big[\mathbf{v}\operatorname{curl}\mathbf{A} - \operatorname{grad} L_0 - \frac{1}{c}\frac{\partial \mathbf{L}}{\partial t}\Big]\Big),$$

which, using the other relations, again reduces to the ordinary Lorentz expression of the classical theory, viz. :—

$$\mathbf{F} = \rho\Big(\mathbf{E} + \frac{1}{c}[\mathbf{vB}]\Big).$$

The expression

$$\mathbf{F} = \rho\Big(\mathbf{E} + \frac{1}{c}[\mathbf{vB}] - E_0\mathbf{j}\Big)$$

which forms part of both Ferrier's and Proca's theories, and in the latter plays the most important part of the whole theory, is really a consequence of an attempt to fit up the terms in the stress momentum equation for the field when there is a distribution of charge present. The extra term appears only in the stress momentum analysis and indicates in reality a failure to effect the determination of the stress-energy tensor. Al Proca assumes that this extra term is equal to a rate of change of momentum, that is, that it is somehow or other a perfect differential with respect to the time, but there is no justification for this, and it might with equal justification be included in the stress specification.

11.

Again, the set of fundamental equations of this new theory

$$\operatorname{div}\mathbf{B} = -\frac{1}{c}\frac{\partial B_0}{\partial t} \quad . \quad . \quad . \quad . \quad . \quad . \quad . \quad (1)$$

$$\operatorname{div}\mathbf{E} = 4\pi\rho - \frac{1}{c}\frac{\partial E_0}{\partial t} \quad . \quad . \quad . \quad . \quad . \quad . \quad . \quad (2)$$

$$\operatorname{curl}\mathbf{E} = -\frac{1}{c}\frac{\partial \mathbf{B}}{\partial t} - \operatorname{grad} B_0 \quad . \quad . \quad . \quad . \quad (3)$$

$$\operatorname{curl}\mathbf{B} = +\frac{1}{c}\frac{\partial \mathbf{E}}{\partial t} + 4\pi\mathbf{j} + \operatorname{grad} E_0 \quad . \quad . \quad . \quad (4)$$

gives, immediately on combining equations (1) and (3),

$$\text{div curl } \mathbf{E} = -\frac{1}{c^2}\frac{\partial^2 B_0}{\partial t^2} - \nabla^2 B_0 = 0,$$

so that B_0, being thus a wave function with no poles, is essentially a constant. And, exactly as in Ferrier's theory, the equations (2) and (4) of the set give immediately

$$\text{div curl } \mathbf{B} = \frac{4\pi}{c}\left(\frac{\partial \rho}{\partial t} + \text{div } \mathbf{j}\right) - \frac{1}{c^2}\frac{\partial^2 E_0}{\partial t^2} + \nabla^2 E_0 = 0,$$

so that, if the equation for continuity of charge is to be satisfied, E_0 is similarly essentially a constant.

We thus see that unless E_0 and B_0 are mere constants the theories of Ferrier and Al Proca imply a flat denial of the fundamental principle of the conservations of charge energy and momentum. It is, of course, not out of the question that such revolutionary changes may not provide the ultimate solution to all our difficulties, but if they are to be made, we must make them with our eyes open, and not in the haphazard manner suggested by these writers.

The beautiful symmetry of Al Proca's theory and its means of derivation thus seem to be its only redeeming features: these might even have been made more perfect if in addition one assumed the existence (hypothetical) of isolated magnetic charge and magnetic currents due to its flux. That is, if we assumed that

$$\text{div } \mathbf{B} = \frac{1}{c}\frac{\partial B_0}{\partial t} + 4\pi\mu,$$

where μ denotes the density of magnetic charge and is analogous to the ρ for the electric charge, then the functions E_0 and B_0 of the analysis would be entirely symmetrical, and an almost perfect symmetrical theory in 4-dimensional analysis will have been obtained. But at the same time the theory would entirely lose its claim to be a true and exact representation of physical facts, and would be in addition quite unnecessarily complicated.

12. *A more general form of theory.*

In spite of the many difficulties inherent in these generalizations it still seems possible to develop them far enough to obtain apparently complete consistency in all the relations of the field. The generalization was in the first place suggested by the fact that the field defined by the set of fundamental

equations in terms of E_0 and B_0 is capable of complete decomposition into two distinct fields. If we write

$$\mathbf{E} = \mathbf{E}_1 + \mathbf{E}_2, \qquad \mathbf{B} = \mathbf{B}_1 + \mathbf{B}_2,$$

then the original set of equations may be replaced by the two sets

$$\text{I.} \quad \begin{cases} \operatorname{curl} \mathbf{E}_1 = -\dfrac{1}{c}\dfrac{\partial \mathbf{B}_1}{\partial t}, \\ \operatorname{div} \mathbf{E}_1 = 4\pi\rho, \\ \operatorname{curl} \mathbf{B}_1 = \dfrac{1}{c}\dfrac{\partial \mathbf{E}_1}{\partial t} + 4\pi\mathbf{j}, \\ \operatorname{div} \mathbf{B}_1 = 0, \end{cases}$$

and

$$\text{II.} \quad \begin{cases} \operatorname{curl} \mathbf{E}_2 = -\dfrac{1}{c}\dfrac{\partial \mathbf{B}_2}{\partial t} + \operatorname{grad} B_0, \\ \operatorname{div} \mathbf{E}_2 = -\dfrac{1}{c}\dfrac{\partial E_0}{\partial t}, \\ \operatorname{curl} \mathbf{B}_2 = \dfrac{1}{c}\dfrac{\partial \mathbf{E}_2}{\partial t} + \operatorname{grad} E_0, \\ \operatorname{div} \mathbf{B}_2 = -\dfrac{1}{c}\dfrac{\partial B_0}{\partial t}. \end{cases}$$

The equations in set I. are identical with those of the original Maxwellian scheme, and on Larmor's model * are the equations of a rotationally elastic medium without compressibility. The second set of equations refer to a compressible elastic medium of the ordinary type †.

13.

This separation of the fields is not, however, as complete as this analysis suggests. In fact, as soon as we begin to consider the energy relations we get into difficulties, because the total energy of the field does not divide up into two separate and distinct parts relating each to a separate field. The condition for complete decomposition is

$$\int \{(\mathbf{E}_1\mathbf{E}_2) + (\mathbf{B}_1\mathbf{B}_2)\}\, dv,$$

* Larmor, 'Aether and Matter,' App. E (1900).

† Ferrier himself divides the vector **E** only so that in his analysis $\mathbf{B}_2 = 0$, and then the set II. refers to an irrotational compressible medium.

the integral being taken over the whole extent of the system, and this is not satisfied except under very special conditions which cannot possibly hold over the whole of space in any real system.

It might, of course, be rather surprising and, perhaps too, not really very helpful if the complete separation of the original field did actually take place. It would mean that the phenomena in the two fields were absolutely and entirely independent, whereas it is a requisite of modern theories that intrinsic energy, once it leaves a charge and becomes located in the surrounding field, is capable of interaction with other charges, and it might be difficult to see how the energy in one type of field could be transformed into effective energy in the other field.

14.

However, it is only necessary to go two steps further to obtain a perfectly consistent scheme for a generalized theory. The first step is to realize that the field defined by the second set of equations in the above separation cannot possibly have any physical significance * unless it has its origin in some fundamental property—charge, in the general sense—of matter, which must be independent of that which gives rise to the electromagnetic field ; and, further, the equations must be generalized to show their origin in this charge. The realization of this fact has lead to the suggestion put forward by Prof. Livens, and dealt with in a recent paper, that we have here the possibility of explaining the gravitational phenomena by means of the concept of a gravitational charge associated with matter and distinct from its ordinary inertial mass.

It is not, however, possible to generalize the equations as they stand, but it is not difficult to see that they form the special case of a much more general set which are suggested at once by attempting to obtain a general invariantive tensor form of the theory. According to this method, if the action integral is expressed in its most general invariantive tensor form and then the space to which it is referred is subjected to a certain type of infinitesimal transformation, then the equations of the theory and the stress energy relations are obtained directly as the conditions of invariance. The first thing to be done therefore is to specify the Lagrangian function of the system in its most general invariantive form.

* The equations define a field without poles anywhere, and this is a physical impossibility.

In Maxwell's theory the Lagrangian function in its simplest form is expressed as the integral of

$$\frac{1}{16\pi}\sqrt{-g}\mathrm{F}^{rs}\mathrm{F}_{rs},$$

where g is the discriminant of the fundamental quadratic form *.

The actual form for the integrand in the action integral suggested by Ferrier's discussion is

$$\frac{1}{16\pi}\sqrt{-g}\{F_{rs}F^{rs}+E_0{}^2g^{rs}g_{rs}\},$$

which at once suggests that the theory is but a particular case of a much more general theory, obtained by replacing the tensor E_0g^{rs} by a general symmetric second order tensor G^{rs}. In such a generalized theory the Lagrangian function of the field would then be

$$\frac{1}{16\pi}\sqrt{-g}\{\mathrm{F}^{rs}\mathrm{F}_{rs}+\mathrm{G}^{rs}\mathrm{G}_{rs}\},$$

or in its rectangular form for use in ordinary Euclidean space

$$\frac{1}{16\pi}\{F_{rs}F_{rs}+G_{rs}G_{rs}\}.$$

This form of function has actually been suggested by Eddington † but with a negative sign to the second term, which, in fact, it is convenient for other purposes to adopt ; but he makes no attempt to derive any field theory from it. It suggests, however, that the generalized field is obtained by the superposition of a Maxwellian field and a somewhat similar field interpreted, however, in terms of a general second order symmetrical force-tensor. As indicated above, of course, this second field would have no significance unless it had its origin in some fundamental charge, and the only step then is to find a suitable relation defining the way in which the force tensor depends on this charge. The way in which this is done and its ultimate consequences are, however, fully elaborated elsewhere ‡, so that we can close the present note without more ado, but in the hope that it has proved that generalizations of Maxwell's theory still seem to be fruitless unless we are prepared to admit the possibility of a new field entity akin to, but distinct from, electric charge.

* $g=|g_{ik}|$, where $ds^2=g_{ik}\,dx^i\,dx^k$ $(i, k=1, 2, 3, 4)$, and the summation convention for repeated indices is employed throughout.

† 'Math. Theory of Relativity,' p. 230 (1923).

‡ Phil. Mag. [7] xiv. p. 243 (August 1932).

C. *Hyperfine-structure of Arc Lines in Vacuum of Bismuth in the Visible and the Ultra-Violet Regions.* *By* Wali Mohammad, *M.A.(Punjab), B.A.(Cantab.), Ph.D. (Göttingen), Professor of Physics, Lucknow University, and* Prem Nath Sharma, *M.Sc., Research Fellow, Lucknow University* *.

Part I.

In earlier papers, fine-structure of arc lines of cadmium [1], thallium [2], lead [5], zinc [3, 4], and silver [6], have been investigated. This paper is an extension of the same work to bismuth.

Hyperfine-structure of bismuth lines have been investigated by many workers. Gehrcke and Von Baeyer [7], O. V. Baeyer [9], Lunelund [8], Wali Mohammad [10], Takamine [11], Aronberg [12], and Nagaoka and Sugiura [13], have worked on the same element, but they have confined their attention to the visible region only. Recently, however, Nagaoka and Mishima [14], Goudsmit and Back [15], and later Zeeman, Goudsmit, and Back [16], have extended the measurement of the hyperfine-structure of Bi-lines to the ultra-violet regions as far as 2627 Å.U. Nagaoka and Mishima [14] used two Lummer plates of quartz, giving a very high resolution ; while Goudsmidt and Back [15] made use of a concave grating in their investigation. Back and Goudsmit have also investigated the hyperfine components of the Zeeman separation of bismuth, and have thereby concluded that bismuth nucleus possesses a spin moment of $9/2.h/2\pi$.

In the absence of a suitable source of light, the authors could use only one quartz Lummer-Gehrcke plate at a time. The main difficulty with a single Lummer plate is that one cannot be certain whether a particular satellite of a line is positive or negative, and therefore, its wave-length is sometimes inaccurate. It may also happen that when the hyperfine separation of a particular line is greater than $\Delta\lambda_{max.}$ for that line, that particular hyperfine component may appear in the next order, and, consequently, its calculated wave-length come out to be smaller than what it is. The reverse may also happen. This difficulty is often met in the present investigation, and the problem appears almost incapable of solution by the use of one plate at a time. Crossed spectra will give the correct distribution of the satellites, but this would be wasteful in light and could not be used. This difficulty was, however, partially removed by the use of

* Communicated by the Authors.

another Lummer plate possessing greater resolving power, and the results of the two were combined together.

Experimental Procedure.

The experimental arrangement was the same as was described in the previous papers. A specially constructed arc-lamp [10] was employed as the source of light. Pure bismuth metal stick was used as the anode. The oxy-cathode in the lamp was heated to incandescence by a current which varied between 14 and 20 amperes at 40 volts, and a voltage of 220 was applied between the anode and the cathode to strike the arc. Bismuth melts at 270° C.: the arc is formed with a current of 0·5 amp. when the light is rather faint. The suitable thermionic current was found to be about 1·0 amp. The light of the arc was faintly bluish.

The spectrograph used was Hilger's 3-metre type with interchangeable optical systems. Two quartz Lummer plates, one 195 mm. long and 3·65 mm. thick and the other 130 mm. long and 4·593 mm. thick, were available for use. The fringes were photographed in the usual manner on the Wellington Iso- and Anti-screen plates. The exposure varied from 5 minutes for a bright line to 15 minutes for the faint line.

Calculation of Wave-length.

Von Baeyer's formula

$$\Delta\lambda_{\max.} = \frac{n\lambda^2}{n^2\lambda - 4t^2\mu\frac{d\mu}{d\lambda}}$$

has been employed to determine the distance between the two successive orders of the fringe-system, where n, the order of the fringe-system, is given by

$$n\lambda = 2t\sqrt{\mu^2 - 1},$$

t being the thickness of the plate.

The position of a satellite is found in the following way:

Fig. 1.

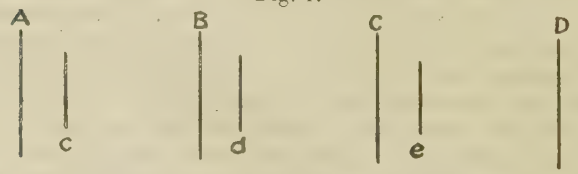

If "a" be the distance between two successive main fringes A and B, and if "b" be the distance between a

main fringe and its satellite—say between A and *c*—then the wave-length of the satellite is $\frac{b}{a}\Delta\lambda_{max.}$

If BC>AB and if $b<a/2$, then the satellite is negative, and if $b>a/2$, the satellite is positive, and in that case "*b*" is the distance between B and *c*.

This assumption is clearly hypothetical and so is liable to error. As pointed out previously, this was the main difficulty which had to be faced during the present investigation.

Measurement of the Structure.

1. λ 4722·43 $^2D_{3/2}-2s$.

This line has been investigated by all the previous investigators. Nagaoka and Mishima discovered as many as thirteen satellites to this line. The large Lummer plate produced only four satellites while the small plate gave only three, as indicated below :—

Large plate.	Small plate.
−0·018 (2)	−0·070 (2)
0·000 (10)	−0·057 (8)
+0·032 (7)	0·000 (10)
+0·068 (9)	+0·054 (8)
+0·109 (1)	

This, at first sight, appeared very curious, but a little extrapolation cleared the discrepancy. The pictures of the two Lummer patterns are as given below :

Fig. 2.

(*a*) Large plate.

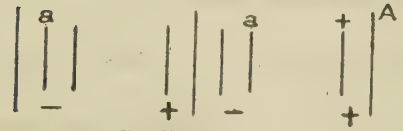

(*b*) Small plate.

If, in fig. 2 (*a*), the three positive satellites and the one negative satellite marked "*x*" be associated with the main

fringe C, it is found that the results agree fairly well with those of the previous investigators. This only gives four satellites, and the fifth satellite found by previous workers is found to be present in the pattern of the small plate only. Thus :

Large plate.		Small plate.	
$\Delta\lambda_{max.}$ = ·2577 Å.U.		$\Delta\lambda_{max.}$ = ·1697 Å.U.	
−0·018 = ·257 − ·018 = +·239		−0·070 = ·1697 − ·070 = +·100	
0·000	·000	−0·057 = 2 × ·1697 − ·057 = +·282	
+0·032 = ·257 + ·032 = +·289		0·000	·000
+0·068 = ·257 + ·066 = +·325		+0·054	+·054
+0·109	+·109		

By combining the two results we get a structure similar to the one found by others. It should be noted that the fringes were not very sharp but somewhat diffuse. It is highly probable that the satellite +0·054 found in the small plate pattern was mixed up in the large plate pattern with +0·068, since their intensities are also found to be the same.

2. λ 4121 95 $^2P_{1/2}-3d''''$.

The small Lummer-plate pattern of this line could not be measured satisfactorily. The large plate showed two satellites :—

+0·065 (5).
0·000 (10).
−0·066 (8).

This line has been examined by Gehrcke and Von Baeyer [7], Lunelund [8], Wali Mohammad [10], Nagaoka and Mishima [13], and Goudsmit and Back [15], but none of these results agree among themselves. By a calculation similar to that done in the case of λ 4722 a structure is obtained which agrees with that found by Goudsmit and Back. The two results are given below :—

Goudsmit and Back.	Authors. $\Delta\lambda_{max.}$ = ·1933.	
−0·119 (2)	+0·065 = −(·1933 − ·065) = −0·127 (5)	
0·000 (10)	0·000	0·000 (10)
+0·198 (9·5)		.....
+0·321 (5)	−0·066 = 2 × ·1933 − ·065 = +0·321 (8)	

Structure of 4722.

Gehrcke and Von Baeyer.	O. V. Baeyer.	Takamine.	Echelon grating.		Aronberg.	Nagaoka and Mishima.	Goudsmit and Back.	Authors.
			Lunelund.	W. Mohammad*.				
+0·316	+0·318	+0·320	+0·314	+0 316	+0·318	+0 3177	+0·3195 (8)	+0·325 (9)
+0·289	+0·283	+0·284	+0·283	+0·284	+0·284	+0·2847	+0·2855 (7)	+0·285 (7)
+0·242	+0·242	+0·238	+0·240	+0·242	+0·240	+0·2433	+0·2415 (4)	+0·239 (2)
						+0·1791		
+0·104	+0·100	+0·102	+0·103	+0·102	+0·102	+0·1026	+0·1005 (1)	+0·105 (1)
+0·057	+0·056	+0·056	+0·059	+0·057	+0·056	+0·0568	+0·0565 (8)	+0·054 (8)
0·000	0·000	0·000	0·000	0·000	0·000	0·0000	0·0000 (10)	0·000 (10)
			−0·144 (?)	−0·144 (?)		−0·0321		
			−0·166 (?)			−0·0721		
						−0·124		
						−0·165		
						−0·2183		
						−0·3191		
						−0·3281		

* Computed by Aronberg.

3. λ 3596·26 $^2P \quad -4d''$.

In the Lummer pattern of the large plate there appear four satellites to this line :—

$\Delta\lambda_{max.}$=0·1460 A.U.

−0·060 (6)
−0·026 (3)
−0·014 (1)
0·000 (10)
+0·040 (6)
+0·072 (5)

But in the small plate pattern there appear only three satellites :—

$\Delta\lambda_{max.}$=0·1159 Å.U.

−0·044 (5)
0·000 (10)
+0·020 (1)
+0·054 (5)

At first sight these results seem quite divergent, but with the help of a little calculation they are found to agree fairly well with those of the previous investigators.

Below is given a rough picture of the Lummer pattern due to the large and small plates as they appear on the photographic plate :—

Fig. 3.

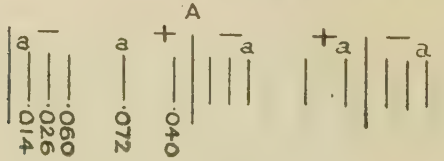

(*a*) Large plate.

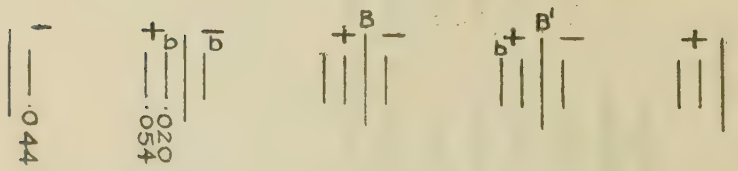

(*b*) Small plate.

If the satellites marked "*a*" in fig. 3 (*a*) be associated with the main fringe marked "A," then the wave-lengths of the satellites come out to be

−0·060		−0·060 (6)
−0·026	= −(0·1460+0·026)	= −0·172 (3)
−0·014	= 0·1460−0·014	= +0·132 (1)
0·000		0·000 (10)
+0·040	= −(0·1460−0·040)	= −0·106 (6)
+0·072		+0·072 (5)

In the case of the small plate pattern, fig. 3 (*b*), if the satellites marked "*b*" be associated with the main fringe marked "B," the wave-lengths of the satellites are

−0·044	= 0·1159−0·044	= +0·072 (5)
0·000		0·000 (10)
+0·020	= 0·1159−0·020	= +0·136 (1)
+0·054	= −(0·1159−0·054)	= −0·062 (5)

Combining the two results, a structure is obtained which is given in the following table together with the results obtained by Nagaoka and Mishima and Goudsmit and Back. The absence of the satellite −0·106 in the small plate pattern appears to be due to the fact that it very nearly coincides with the main fringe B′, since the difference between $\Delta\lambda$ for this satellite and $\Delta\lambda_{max.}$ is very small. Also the satellite −0·172 would appear just close to the satellite +0·054, since

$$-(2\times 0{\cdot}1159-0{\cdot}054)=-0{\cdot}177,$$

and it could not be measured separate from 0·054.

Nagaoka and Mishima.	Goudsmit and Back.	Authors.
+0·1361 (3)	+0·1340 (1)	+0·124 (1)
+0·0736 (6)	+0·0730 (6)	+0·072 (5)
0·0000 (10)	0·0000 (10)	0·000 (10)
−0·0599 (7)	−0·0595 (4)	−0·061 (6)
−0·1090 (8)	−0·1085 (5)	−0·106 (6)
−0·1705 (6)	−0·1700 (2)	−0·172 (3)

Our results agree fairly well with those of Nagaoka and Mishima and Goudsmit and Back.

4. λ 3511·00 $^2D_{5/2} - 3d'$.

The large quartz plate gives four satellites to this line.—

$\Delta\lambda_{max.} = 0{\cdot}1381$ Å.U.

$-0{\cdot}068$ (8)
$-0{\cdot}044$ (6)
0·000 (10)
$+0{\cdot}023$ (1)
+0 051 (3)

while the small plate gives only three satellites:—

$\Delta\lambda_{max.} = 0{\cdot}1103$ Å.U.

$-0{\cdot}028$ (1)
$-0{\cdot}019$ (9)
0·000 (10)
$+0{\cdot}044$ (7)

Rough pictures of the Lummer patterns were like the following:—

Fig. 4.

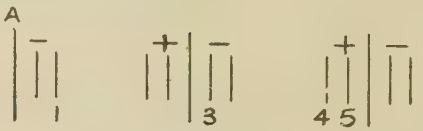

(*a*) Large plate.

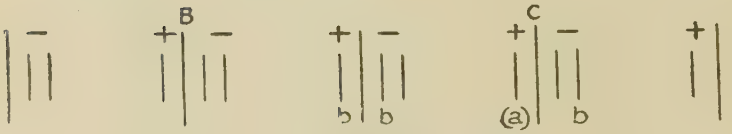

(*b*) Small plate.

If the satellites marked 1, 3, 4, 5 in fig. 4 (*a*) be associated with the main fringe marked "A," their wave-lengths come out to be

$$-0{\cdot}068 \qquad\qquad -0{\cdot}068\ (8)$$
$$-0{\cdot}044 = -\ (0{\cdot}1381 + 0{\cdot}044) = -0{\cdot}182\ (6)$$
$$0{\cdot}000 \qquad\qquad 0{\cdot}000\ (10)$$
$$+0{\cdot}023 = -(2 \times {\cdot}1381 - 0{\cdot}023) = -0{\cdot}253\ (1)$$
$$+0{\cdot}051 = -(2 \times {\cdot}1381 - 0{\cdot}051) = -0{\cdot}225\ (3)$$

On the other hand, if the satellites marked "*b*" in fig. 4(*b*) be associated with the main fringe marked "B," their wave-lengths are found to be

$$-0{\cdot}028 = -(2 \times {\cdot}1103 + 0{\cdot}028) = -0{\cdot}249\ (1)$$
$$-0{\cdot}019 = -\ (0{\cdot}1103 + 0{\cdot}019) = -0{\cdot}129\ (9)$$
$$0{\cdot}000 \qquad\qquad 0{\cdot}000\ (10)$$
$$+0{\cdot}044 = -\ (0{\cdot}1103 + 0{\cdot}044) = -0{\cdot}065\ (7)$$

The absence of the satellite $-0{\cdot}225$ in this pattern is perhaps due to the fact since $2 \times \Delta\lambda_{max.} = 0{\cdot}2206$, this satellite coincides with the main fringe marked "C." The satellite $-0{\cdot}129$ which appears in the small plate cannot be distinguished from the main fringe A′ of the large plate. Again, as in the case of the satellite $-0{\cdot}172$ of $\lambda\,3596$ given above, if the satellite $+0{\cdot}044$ of the small plate marked "*d*" be associated with the main fringe "B," its wave-length is found to be

$$-(2 \times 0{\cdot}1103 - 0{\cdot}044) = -0{\cdot}176.$$

Thus it appears that the satellites of wave-lengths $-0{\cdot}066$ and $-0{\cdot}176$ coincide with each other. Combining the two results, the following structure is obtained :—

Nagaoka and Mishima.	Goudsmit and Back.	Authors.
0·0000 (10)	0·0000 (10)	0·000 (10)
−0·0695 (8)	−0·0696 (8)	−0·067 (7)
−0·1300 (9)	−0·1293 (9)	−0·129 (9)
−0·1775 (4)	−0·1805 (4)	−0·178 (3)
−0·2160 (4)	−0·2204 (3)	−0·225 (3)
−0·2475 (1)	−0·2504 (2)	−0·251 (1)

5. λ 3397·31 $^2D_{5/2}-3d'''$.

This line is exactly similar to the previous line. The two plates give the satellites of the following wave-lengths :—

Large plate.	Small plate.
$\Delta\lambda_{max.}$=0·1297 Å.U.	$\Delta\lambda_{max.}$=·1030 Å.U.
−0·065 (8)	−0·038 (2)
−0·042 (5)	−0·022 (8)
0·000 (10)	0·000 (10)
+0·021 (2)	+0·033 (8)
+0·049 (5)	

The two results are treated just in the same way as in the previous case and the resulting wave-lengths are given in the table below :—

Nagaoka and Mishima.	Goudsmit and Back.	Authors.
0·0000 (9)	0·0000 (10)	0·000 (10)
−0·0712 (10)	−0·0680 (8)	−0·065 (8)
−0·1275 (8)	−0·1265 (7)	−0·125 (8)
−0·1785 (6)	−0·1757 (4)	−0·176 (6)
−0·2166 (7)	−0·2112 (5)	−0·210 (5)
−0·2456 (5)	−0·2465 (3)	−0·241 (2)

6. λ 3376·73 $3d'-{}^2D_{3/2}$.

Lummer patterns due to the large plate for this line were very weak and hence were not measurable. The smaller plate gave three satellites :—

$\Delta_{max.}$=0·0836 Å.U.

−0·031 (7)
−0·016 (2)
0·000 (10)
+0·028 (6)

It was, however, found that the experimental results fitted in with the term-scheme of this line if the two negative satellites had positive values. The computed values are given in the table below :—

Nagaoka and Mishima.	Goudsmit and Back.	Authors.
+0·0632 (3)	.....	−0·016=(0·0836−0·016)=+0·68 (2)
+0·0484 (5)	+0·0573 (9)	−0·031=(0·0836−0·031)=+0·053 (7)
+0·0274 (6)	+0·0255 (6)	+0·028 +0·028 (6)
0·0000 (10)	0·0000 (10)	0·000 0·000 (10)

7. λ 3067·81 $^4S_{3/2}-2s$.

The satellites of this line are very diffuse. Nagaoka and Mishima have measured some hazy components. Goudsmit and Back notice strong reversal in this line. They found a reversed doublet of the value $\Delta\nu \sim 0{\cdot}90$ cm.$^{-1}$.

The authors find three satellites to this line by using the large Lummer plate :—

$\Delta\lambda_{max.}=0{\cdot}1048$ Å.U.

−0·028=	0·1048−0·028	=+0·077 (6)
0·000		0·000 (10)
+0·010		+0·010 (2)
+0·020=−(·1048−0·020)=		−0·085 (7)

The patterns due to the small plate could not be measured.

8. λ 3024·75 $^2D_{5/2}-4d'$.

This line has many satellites which are very diffuse and are clustered together, hence they could not be measured. Nagaoka and Mishima have given twelve components of this line. The grating photograph of Goudsmit and Back gave five resolved lines and one unresolved group. They could not carry out the measurements accurately.

9. λ 2993·46 $^2D_{3/2}-3d''$.

Like the line 3076, it has three satellities of the following wave-lengths :—

−0·015 (9)
0·000 (10)
+0·018 (6)
+0·042 (3)

10. λ 2989·15 $^2D_{3/2}-3d''$.

This line is found to possess the following structure :—

$-0{\cdot}014$ (9)
$0{\cdot}000$ (10)
$+0{\cdot}019$ (6)
$+0{\cdot}046$ (4)

11. λ 2938·41 $^2D_{5/2}-4d''$.

In the case of this line, it was found that there were two groups of very broad and diffuse fringes. It appears that the satellites are very close together and so could not be separated by the Lummer plates. Nagaoka and Mishima give seven components to this line. Goudsmit and Back also found two unresolved groups of lines in their grating photograph.

12. λ 2898·08.

This line has three satellites. Their wave-lengths as found by means of the large and small plates are given below :—

Large plate.	Small plate.
$\Delta\lambda_{max.}=0{\cdot}0952$ Å.U.	$\Delta\lambda_{max.}=0{\cdot}0738$ Å.U.
$-0{\cdot}019=0{\cdot}0952-0{\cdot}019=+0{\cdot}076$ (8)	.....
.....	$-0{\cdot}015=0{\cdot}0738-0{\cdot}015=+0{\cdot}059$ (7)
0·040 (8)	.....
0·029 (0)	0·030 (8)
.....	0·018 (7)
0·000 (10)	0·000 (10)

It is seen that these results agree to a certain extent and that in all there are five satellites. It is not clear why all the five satellites should not appear in each pattern. The structure of this line is given in the following table, along

with the values found by Nagaoka and Mishima and Goudsmit and Back :—

Nagaoka and Mishima.	Goudsmit and Back.	Authors.
+0·0774 (8)	.....	+0·076 (8)
+0·0621 (9)	+0·0621 (6)	+0·059 (7)
	+0·0577 (7)	
+0·0399 (8)	+0·0358 (9)	+0·040 (8)
+0·0302 (10)	.....	+0·030 (9)
+0·0179 (9)	+0·0164 (8)	+0·018 (7)
0·0000 (8)	0·0000 (10)	0·000 (10)

It appears from the above that the authors' results agree fairly well with those of Nagaoka and Mishima.

13. λ 2780·53 $^2D_{3/2}-3s$.

The Lummer pattern of this line due to the large plate is very faint and hence it could not be measured. The smaller plate gives three satellites, while Nagaoka and Mishima and Goudsmit and Back found four each. The following table gives these results :—

Back and Goudsmit.	Authors.
+0·0618 (7)	.....
+0·0490 (6)	−0·020=0·0668−0·020=+0·047 (9)
+0·0345 (7)	−0·032=0·0668 - 0·032=+0·035 (3)
+0·0195 (8)	+0·021 (4)
0·0000 (10)	0·000 (10)

Conclusion.

The structure of thirteen lines of bismuth in the violet and the ultra-violet regions has been examined and the results compared with those of other authors. It is found that a single Lummer plate cannot enable one to determine the exact wave-length of a satellite. Two plates of different resolving powers prove of great assistance even if used

singly. The analysis of structure with a Lummer plate gives reliable results in the case of elements having a comparatively small atomic number and a small nuclear moment. But in the case of heavy elements having a comparatively larger nuclear moment, the analysis is not without ambiguity. The rational method appears to be that of crossed spectra, either with the help of two plates or with a plate and another interference apparatus or a grating. The intensities of the hyperfine components have been of great help in finding the relationship between the two patterns. Since the intensity-estimation is visual, certain discrepancies are bound to occur.

References.

(1) Wali Mohammad and Mathur, Phil. Mag. iv. p. 112 (1927).
(2) Wali Mohammad and Mathur, *ibid.* v. p. 1112 (1928).
(3) Wali Mohammad and Sharma, *ibid.* x. p. 916 (1930).
(4) Wali Mohammad and Sharma, *ibid.* xii. p. 726 (1931).
(5) Wali Mohammad and Sharma, *ibid.* xii. p. 1106 (1931).
(6) Wali Mohammad and Sharma, Ind. J. of Phy. vi. (I.) p. 75 (1931).
(7) Gehrcke and von Baeyer, *Ann. d Phys.* xx. p. 283 (1906).
(8) Lunelund, *ibid.* xxxiv. p. 524 (1911).
(9) O. V. Baeyer, *Vehr. d. Deutsch. Phys. Ges.* x. p. 739 (1908).
(10) Wali Mohammad, Astrophys. Jour. xliv. p. 189 (1914).
(11) Takamine, Proc. Tokyo Math. Phys. Soc. viii. p. 51 (1915).
(12) Aronberg, Astrophys. Jour. xlvii. p. 102 (1918).
(13) Nagaoka and Sugiura, *ibid.* liii. p. 339 (1921).
(14) Nagaoka and Mishima, Imp. Acad. Tokyo Proc. ii. p. 248 (1925).
(15) Goudsmit and Back, *Zeit. f. Phys.* xliii. p. 321 (1927).
(16) Zeeman, Back, and Goudsmit, *ibid.* xlvi. p. 1 (1930).

Department of Physics,
Lucknow University.
April 1932.

CI. *Measurement of Critical Velocity of Flow past Objects of small Section by means of a Pitot Tube.* *By* E. Tyler, *D.Sc., F.Inst.P., Physics Dept., College of Technology, Leicester* *.

Introduction.

THE utilization of a Pitot tube both as a velocity measurer and analyzer of regional vorticity in the wake of a body placed in an air stream is familiar in aerodynamics, but its application as a detector of critical eddy formation behind models such as cylinders and aerofoils does not appear to have been made hi herto.

* Communicated by the Author.

Its use in a somewhat similar direction has been attempted by Bond *, who sought for evidence of regular periodicity in the turbulent flow of air through a long circular pipe.

With an object of given section, placed in a steady stream of fluid and at right angles to the direction of flow, there is a critical speed at which streamline motion no longer exists and stationary eddies are formed in the wake of the body.

Beyond this speed is a higher critical value termed "critical velocity of flow," at which the eddies become alternately detached and pass down the stream at a definite rate dependent upon the size of the body and the speed of the fluid.

There are various methods suitable for examining such critical flow, namely: (1) Visual, photographic or kinematically † ‡ § ‖ ; (2) Vibrating Pendulums ¶ ; (3) Whirling Arm ** ; and (4) Hot Wire Amplifier, or String Galvanometer †† ‡‡.

In addition we may include the Pitot-tube method used aurally in conjunction with small models mounted in a wind tunnel, since it is capable of yielding results consistent with those obtained by other methods, and may be recommended by virtue of its cheapness and simplicity.

Method and Results using Pitot Tube.

Critical Velocities for Cylinders, Inclined Aerofoils, and Cords of Square Section.

As a consequence of the eddy formation in the wake of a body placed in a steady wind stream, there will

* Proc. Phys. Soc. xliii. no. 236 (1931).

† Townend, Aero. Res. Committee, Rep. and Mem. no. 1349 (Oct. 1930) and Phil. Mag., Oct. 1932.

‡ Nisi and Porter, Phil. Mag. xlvi. p. 754 (1923). Nisi, Japanese Journal of Physics, iv. no. 1 (1925). Farren, Aero. Soc. Journal (June 1932). Eden, Tech. Report, Advisory Committee for Aeronautics (1910–1) ; also R. and M. no. 31 (March 1911).

§ Tanner and Bairstow, Aero. Res. Comm., R. and M. no. 1352 (July 1930).

‖ Tietjens, Naturwissenschaften, xiii. p. 1050 (1925).

¶ Richardson, Proc. Phys. Soc. xxxvii. (April 1925). Kruger, *Ann. der Phys.* lx p. 279 (1919)

** Strouhal, *Ann. der Phys.* v. p. 216 (1878). Relf, Phil. Mag. xlii. p. 173 (1921).

†† Fage and Johansen, Proc. Roy. Soc. A, p. 116 (1927). Tyler, Journ. Scientific Inst. vii. (Nov. 1930).

‡‡ Tyler, *loc. cit.* ; also Phil. Mag. xi. p. 849 (1931).

exist within and just outside the vortex street, positions of fluctuating air-pressure.

If the object is of small section the periodicity of these fluctuations along each row of vortices will be the same

Fig. 1.

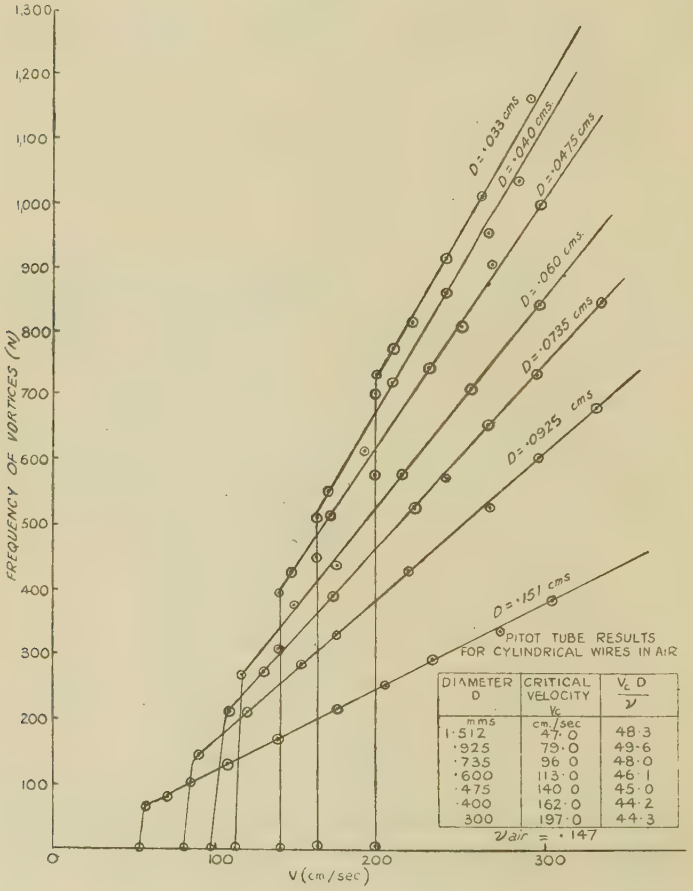

as that of the eddy formation, but for positions in the middle of the wake, double the frequency.

A Pitot tube placed end on to the stream or at right angles (preferably the former), and in a suitable position where the air-pressure variations are greatest, will be subject to these varying conditions, and upon listening

at the other end of the Pitot tube an audible note will usually be heard, equal in frequency to that of the production of the eddies.

The pitch of this note is easily determined by tuning it to a similar note produced on a monochord, calibrated with a standard fork.

Now by suitably choosing the size of the obstacle, the critical speed at which turbulence or eddy formation commences can be so arranged that a small increase in its value produces eddies whose rate of formation is well above the lower limit of audibility.

Fig. 2.

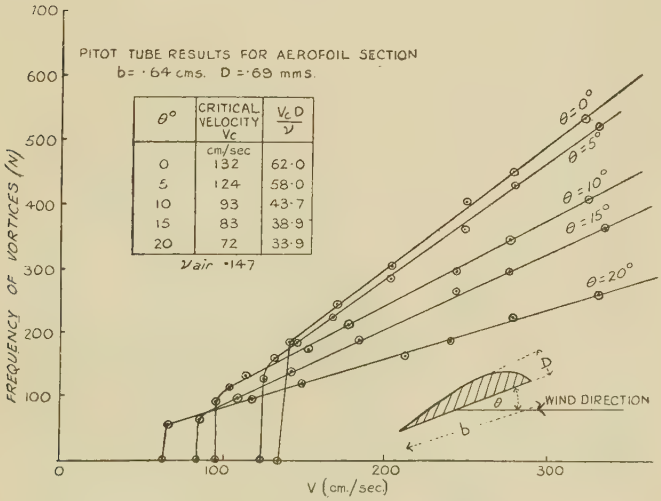

The audible note detected by the Pitot tube is thus in evidence for all speeds greater than the critical, and the speed at which audibility ceases is measured.

In order to estimate this speed accurately, a series of observations were made on the frequency of the eddy formation for different wind tunnel speeds, gradually reducing the latter until the lower limit had been reached. By plotting such results the critical values were easily interpolated. Incorporated in figs. 1, 2, and 3 are results for cylindrical wires, inclined aerofoil, and square section rubber cords.

It will be noticed that each graph exhibits similar characteristics, namely, a sudden drop in the frequency of eddy formation near the critical speed, and the change is more abrupt the smaller the model. Summaries of the interpolated critical speeds are included in the

Fig. 3.

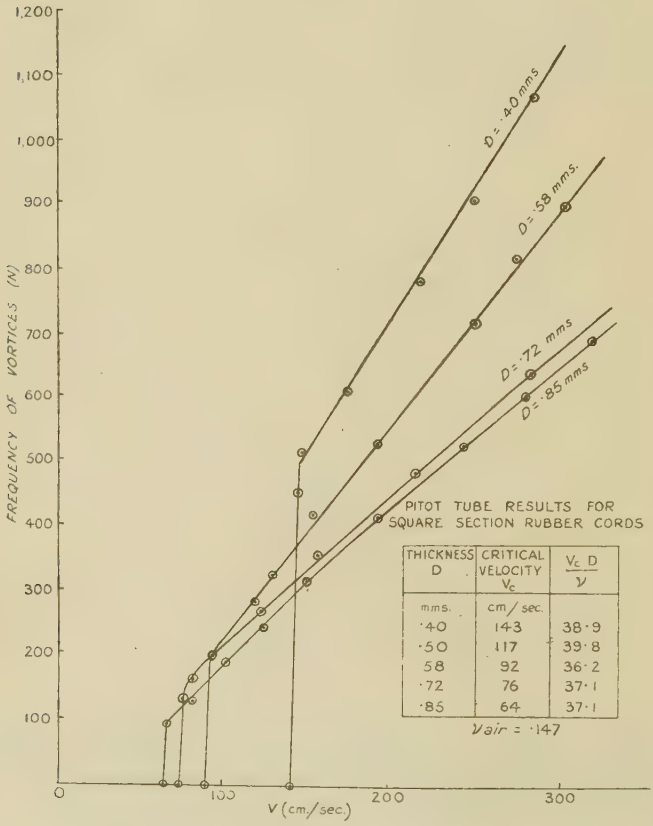

tables on figs. 1, 2, and 3. Good agreement is revealed particularly with the earlier data using the Hot wire amplifier method *. In view of the marked change in resistance † experienced by cylindrical wires

* Tyler, *loc. cit.*

† Powell, Aero. Res. Commitee, R. and M. No. 599, March 1919.

when inclined to an air current, it is to be expected that corresponding changes in the rate of eddy formation will also be produced, and in this respect the Pitot tube is capable of revealing such possible effects.

The wires, each of about 20 cm. long, were thus mounted at the ends of a thin metal frame, attached to a metal holder, capable of rotating about a horizontal axis.

Fig. 4.

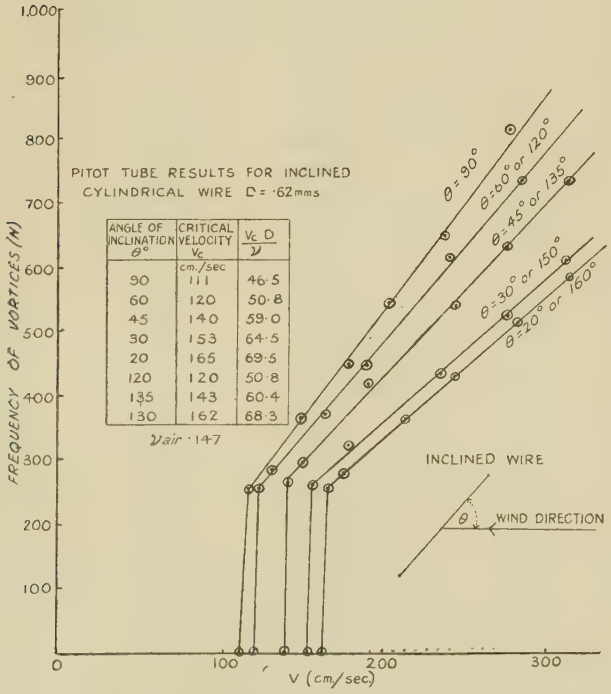

Yawing of the wires was thus effected by rotating the holder about an axis passing through the centre of a graduated circular scale which served to indicate the angle of inclination.

The frequency measurements shown in fig. 4 are a typical set for a wire of diameter ·062 cm., and clearly reveal the controlling influence of yawing. Critical flow data for wires of different diameters is included in

fig. 5 and Table I., and frequency measurements in Tables II. and III.

The method serves also to demonstrate the decay in the strength of the eddies as they pass dowstream, for the intensity of the sound heard diminishes as the Pitot tube is receded from the rear of the body along either vortex row.

TABLE I.

Critical Velocities for Inclined Cylindrical Wires in Air (Wind Tunnel Method).

Angle of inclination. $\theta°$.	Diameter D. mm.	Critical velocity V_c. cm./sec.	$\frac{V_c D}{\nu}$.
90°	·330	202	45·4
	·455	143	44·2
	·620	111	46·5
	·770	95	49·7
	·950	80	51·8
60°	·330	210	47·3
	·455	150	46·5
	·620	120	50·8
	·770	106	55·6
	·950	85	55·2
45°	·330	231	52·0
	·455	169	52·4
	·620	140	59·0
	·770	117	61·2
	·950	90	58·1
30°	·455	189	58·6
	·620	153	64·5
	·770	132	69·0
	·950	105	68·0
20°	·620	160	67·8
	·950	122	79·0

ν air= ·147

In addition, the overlapping of the vortex rows in the middle of the wake is also apparent, since on moving the Pitot tube across the vortex street the octave of the note corresponding to the frequency of the eddy formation was heard, thus confirming the measurements made by Fage and Johansen *, on the fluctuations

* Fage and Johansen, *loc. cit.*

TABLE II.

Frequency Measurements for Inclined Cylindrical Wires in Air (Wind Tunnel Method).

Diameter of wire D. mm.	Angle of inclination $\theta°$.	V. cm./sec.	N.	$\frac{V}{ND}$.	$\frac{VD}{\nu}$.
·770	90°	278	635	5·68	145
		240	530	5·73	126
		149	327	5·95	78·0
		119	240	6·45	62·5
		102	177	7·50	53·5
·770	60°	249	491	6·58	130
		215	424	6·59	113
		149	277	6·96	78·0
		115	196	7·70	60·5
		108	180	7·80	56·8
·770	45°	242	460	6·85	127
		158	300	6·84	83·0
		138	220	8·10	72·3
		117	190	8·00	61·5
		123	193	8·27	64·5
·770	30°	278	475	7·61	146
		250	408	7·97	131
		215	366	7·62	113
		174	285	7·90	91·2
		145	225	8·37	76·0
·770	20°	278	391	9·25	146
		257	365	9·16	135
		240	326	9·50	126
		202	267	9·85	106
·330	90°	280	1160	7·32	63·0
		260	1110	7·10	58·5
		240	955	7·62	54·0
		220	825	8·10	49·0
		213	770	8·35	47·8
·330	60°	279	982	8·60	62·5
		262	948	8·40	58·6
		247	880	8·52	55·5
		243	800	9·20	54·6
		225	400	(17·0)	50·5

ν air = ·147.

of air-flow behind an inclined plate, namely, the existence of a regular periodicity in velocity or pressure variations within the middle of a vortex street double that for positions just outside.

TABLE III.

Frequency Measurements for Inclined Cylindrical Wires in Air (Wind Tunnel Method) (*cont.*).

Diameter of wire D. mm.	Angle of inclination. θ.	V. cm./sec.	N.	$\frac{V}{ND}$.	$\frac{VD}{\nu}$.
·950	90°	278	506	5·80	180
		157	281	5·90	101
		108	166	6·81	70·0
		87	117	7·84	56·2
·950	60°	278	479	6·12	180
		191	318	6·33	123
		97	142	7·20	62·5
		91	125	7·65	58·8
·950	45°	278	448	6·54	180
		173	276	6·60	112
		127	192	7·00	82·5
		105	127	8·68	68·0
		98	93·5	11·00	63·5
·950	30°	278	380	7·70	180
		171	217	8·30	110
		143	194	7·78	92·5
		123	128	10·10	79·5
·950	20°	278	280	10·4	180
		210	235	9·40	133
		171	195	9·25	116
		145	130	12·80	98·5
·450	90°	278	923	6·62	86·0
		239	740	7·10	74·0
		159	477	7·35	49·3
		143	400	7·85	44·3
·450	60°	278	850	7·19	86·0
		240	720	7·31	74·2
		175	502	7·63	54·1
		159	413	8·45	49·2
·450	45°	278	730	8·39	86·0
		242	633	8·39	75·0
		210	527	8·76	65·0
		196	447	9·65	60·7
·450	30°	278	666	9·20	86·0
		241	590	9·00	74·5
		232	555	9·20	71·5
		215	460	10·30	66·5

The possibility of Aeolian tones arising from the presence of the Pitot tube, thus interfering with the

TABLE IV.

Frequency Measurements for Inclined Aerofoil in Air.

Type of aerofoil.	Angle of incidence.	V. cm./sec.	N.	$\frac{ND}{V}$ ·	$\frac{Nb}{V}$ ·
Width b= ·64 cm. max thickness D= ·69 mm.	0°	constant speed V= 278	463	8·70	1·06
	2°		463	8·70	1·06
	5°		440	9·15	1·01
	7°		426	9·47	·98
	10°		365	11·02	·84
	12°		340	11·85	·78
	15°		284	14·20	·65
	20°		226	17·80	·52
	25°		203	19·90	·47
	30°		153	26·40	·35
b= ·64 cm. D= ·69 mm.	0°	283	463	8·85	1·04
		250	410	8·85	1·05
		205	305	9·78	·95
		169	250	9·81	·94
	5°	278	435	9·26	1·00
		250	358	10·10	·91
		200	292	9·97	·93
		165	235	10·20	·91
	10°	258	333	11·20	·83
		177	213	12·05	·77
		133	162	11·90	·78
		113	134	12·20	·76
	15°	232	229	14·70	·63
		172	166	15·00	·61
		142	136	15·10	·61
	20°	256	201	18·45	·50
		148	123	17·40	·53
		118	93	18·30	·50
		95	74	18·60	·49

general phenomena, was looked for, but since no sound was heard when the tube was placed end on to the wind stream, it may be assumed that such an effect is remote.

Discussion of Aerofoil and Cylinder Results.

Referring to the critical Reynolds number, $\frac{VD_c}{\nu}$, for the inclined aerofoil exhibited in figs. 2 and 6, it will be observed that with an object of effective width D

Fig. 5.

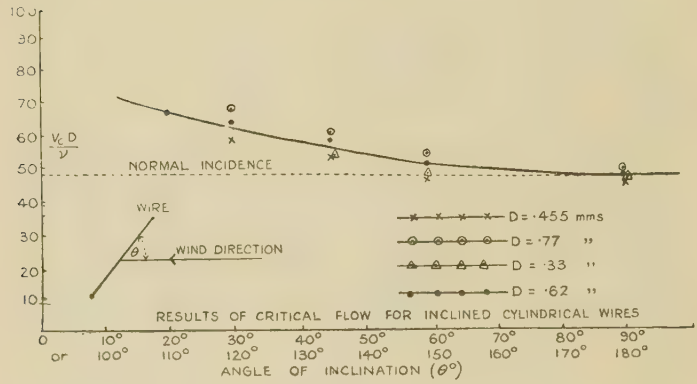

Fig. 6.

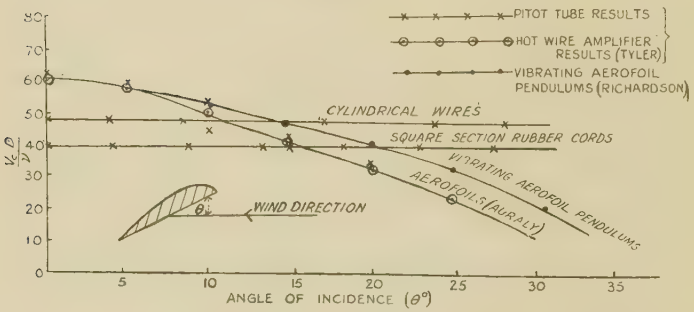

in a given fluid, the advantage of the aerofoil section at grazing incidence over a circular or square section rod is most marked.

At grazing incidence a much higher velocity (about 50 per cent. increase) is necessary for streamline motion to pass into turbulence. Whereas the critical $\frac{V_c D}{\nu}$ is about 62 for an aerofoil at grazing incidence, it is

about 46 and 38 for a cylindrical wire and square cord respectively.

The aerofoil continues to hold this advantage as it is yawed, until about 12° is reached, after which the cylindrical wire is better for the same D. Comparing with the square cords this advantage is maintained up to about 16°.

There is a steady drop in the critical $\frac{V_c D}{\nu}$ for an aerofoil section, from 62 at grazing incidence to about 46 at 12°, followed by a more sudden change to 25 at 25°.

Concerning the results obtained with inclined cylindrical wires, it is clearly evident that the decrease in resistance experienced by such bodies is an attribute of the resulting decrease in rate of eddy formation at a constant air speed. The graphs in fig. 4 bring out this effect most clearly, since when the axis of the wire approaches the direction of grazing incidence, a much higher velocity of flow is required to produce eddies at the same rate as under normal incidence.

In view of this modification, it is to be expected that the critical $\frac{V_c D}{\nu}$ for inclined wires would be larger than for normal inclination, and this fact is borne out by the critical data in fig. 5 and Table I.

There is a slight increase in $\frac{V_c D}{\nu}$ as the angle of incidence changes from 90° to 60°, the respective values being 47 and 50.

For smaller angles of inclination the change in $\frac{V_c D}{\nu}$ is more rapid, its value increasing from 50 at 60° to 68 at 20°.

The aerofoil at grazing incidence still holds the advantage over the inclined wire until the latter is set at an angle as low as 35°. Below this inclination the inclined wire is preferable.

With reference to the frequency measurements, the results for the cylindrical wires indicate a cut off frequency of constant value for a wire of given diameter, even though it is yawed.

This cessation frequency is the same for a given wire, whether inclined forward or backwards with respect

to the direction of flow, likewise the eddy formation frequency for a given speed and angle of yaw. There only appears to be a change in both the critical velocity of flow and rate of formation of eddies as a result of altering the angle of inclination.

The frequency measurements both for the cylindrical wires and square section cords are in good agreement with results formerly obtained by different observers, and at low values of $\frac{V_c D}{\nu}$ exhibit the usual apparent rise in $\frac{V}{ND}$, associated with such small models. At normal incidence the results for the circular wires are well represented by the relation

$$\frac{ND}{V} = \cdot 198\left(1 - 19\cdot 7\ \frac{\nu}{VD}\right),$$

while the average results for the square section cords satisfy the equation

$$\frac{ND}{V} = \cdot 190\left(1 - 14\cdot 0\frac{\nu}{VD}\right).$$

The aerofoil results in Table IV. exhibit the usual fall in eddy frequency formation at constant speed as the angle of incidence is increased, and agree well with the earlier Hot wire amplifier values.

The results given are of interest, since they afford an example of the use of simple apparatus capable of yielding reliable information concerning eddy formation. The fact that the production of periodic eddies behind models gives rise to sound waves of audible frequency under certain conditions, enhances the use of the Pitot tube as a detector in this respect. The existence of such periodic eddies means also the production of periodic cross forces which exert their influence on the wire, and if these forces are of same frequency as the vibrations natural to the wire, a forced oscillation of considerable amplitude is possible with resulting fracture.

Summary.

By means of aural observation of the frequency of formation of Aeolian tones behind models of small section such as aerofoils, cylindrical wires, and square

section cords, using a Pitot tube as detector, critical values of $\frac{V_c D}{\nu}$ have been obtained at which the detachment of eddies from the rear of the body begins.

The minimum value of $\frac{V_c D}{\nu}$ for such flow is found to be about 62 at grazing incidence for an aerofoil section, whereas for wires of circular and square section $\frac{V_c D}{\nu}$ is about 46 and 38 respectively.

The critical $\frac{V_c D}{\nu}$ for an aerofoil section falls from 62 at grazing incidence to 46 at 12°, and then more rapidly to 25 at 25°, in good agreement with data obtained for similar models employing a Hot wire Amplifier method.

The effect of yawing cylindrical wires in an air stream and the consequent change in eddy frequency formation is also exhibited, together with critical flow data. At normal incidence $\frac{V_c D}{\nu}$ is about 47 and increases to 50 at 60°, and then more suddenly to 68 at 20°.

CII. *The Diamagnetic Susceptibilities of some Sulphur Compounds.* By John Farquharson, *B.Sc., Ph.D., Senior* 1851 *Student* *.

I. Introduction.

THE susceptibilities of a series of sulphur compounds have been measured in order to test some of the modern theories of magnetism. The measurements have been made on a Curie-Chéneveau Magnetic Balance similar to that described by Gray and Farquharson [1]. The standard for these measurements was conductivity water of which the mass susceptibility was taken to be $-0{\cdot}72 \times 10^{-6}$. All measurements were made at 18° C. The solids were measured in finely powdered form.

* Communicated by Prof. F. G. Donnan, C.B.E., M.A., F.R.S.

II. Experimental.

(1) *The Substances measured and their Susceptibilities.*

The experimental values found in this investigation are given in Table I. The average deviation from the mean is shown for each substance. The figures in parentheses indicate the number of measurements.

Table I.

Experimental Molecular Susceptibilities.

Substance.	$-\chi_M \times 10^6$.	
SO_3	$28{\cdot}54 \pm 0{\cdot}13$	(3)
H_2SO_4	$39{\cdot}00$	
$KHSO_4$	$49{\cdot}77 \pm 0{\cdot}61$	(4)
K_2SO_4	$65{\cdot}00 \pm 0\ 44$	(6)
$K_2S_2O_3$	$75{\cdot}88 \pm 0{\cdot}23$	(5)
$K_2S_2O_7$	$92{\cdot}04 \pm 0{\cdot}82$	(5)
$K_2S_2O_8$	$102{\cdot}4 \pm 0{\cdot}80$	(4)
$K_2S_4O_6$	$118{\cdot}4 \pm 0{\cdot}30$	(3)
	$120{\cdot}9 \pm 0{\cdot}60$	(3)

(2) *Preparation and Purification of the Substances.*

It is necessary that the substances should be in their purest possible state, for a trace of impurity, especially if paramagnetic, may appreciably alter the result.

Sulphur trioxide.—This substance was redistilled through a narrow glass tube straight into the measuring tube of the balance. Three samples in all were distilled, collected, and measured. The measurements agreed very well, and the figure so obtained was taken to be correct, although a lower value of $-23{\cdot}04$ was reported by Pascal in 1912.

Sulphuric acid.—The figure for H_2SO_4 is that found by the author [2]. Pure H_2SO_4 was obtained by recrystallization.

Potassium bisulphate.—This substance was obtained from B.D.H. Ltd. A sample was also prepared by heating together the necessary quantities of pure H_2SO_4 and pure K_2SO_4. The figure for $KHSO_4$ is not very reliable.

Potassium sulphate.—Figures of the order of $-70{\cdot}0 \times 10^{-6}$ are given in the literature for the molecular susceptibility of K_2SO_4. Great pains were taken in this investigation to repeat this figure, but no value was obtained higher than $-65{\cdot}74 \times 10^{-6}$. Samples of the A.R. chemical were obtained from reputable firms, were measured, recrystallized, measured again, and a sample was also recrystallized from conductivity water, but all with the same result.

Potassium thiosulphate.—This substance was recrystallized from water, washed with alcohol, and dehydrated in a tube furnace under a current of dry air.

Potassium metabisulphate.—The sample measured was supplied by B.D.H. Ltd. Analysis by means of barium chloride showed it to be chemically pure.

Potassium persulphate.—This was recrystallized several times from water.

Potassium tetrathionate.—Two values are given for this substance. They were obtained from different samples prepared from purified thiosulphate and iodine. The higher value is probably the more accurate.

Chemical analyses were made of all the substance showing each to be chemically pure.

III. Theoretical Considerations.

(1) *The Theoretical Diamagnetism of Molecules.*

Van Vleck[3], by a system of quantum mechanics, has developed an expression for molecular magnetism, which may be written simply

$$\chi = P_x + P_y - D,$$

where

P_x is paramagnetism dependent on temperature,

P_y is a weak paramagnetism independent of temperature,

D is pure diamagnetism.

When a polyatomic molecule has a spin quantum number zero, the commonest value for even molecules, the P_x part of this expression vanishes and the susceptibility of a diamagnetic molecule becomes

$$\chi = P_y - D.$$

The P_y part of this expression will never vanish for polyatomic molecules. The experimental value will always be less than the theoretical by this amount, which is due to the fluctuations of electronic angular momentum and the formation of bonds.

(2) *The Evaluation of the Diamagnetic Term* D.

Pauli[4] derived classically, a formula for the susceptibility of a gram atom,

$$\chi = -\frac{e^2}{6mc^2}\bar{\Sigma}r^2$$

Van Vleck obtained a similar formula by quantum mechanical treatment.

Pauling [5] obtained an expression for $\overline{r^2}$ in terms of the quantum numbers, and after giving the constants their appropriate values found the expression

$$\chi = -2{\cdot}010 \times 10^{-6} \Sigma \frac{n_\kappa^4}{(Z - S_{M_\kappa})^2} \left[1 - \frac{3i_\kappa(l_\kappa + 1) - 1}{5n_\kappa^2} \right].$$

The screening contant S was determined by Pauling for different electron groups, and he calculated the susceptibilities of a large number of atoms and ions. Gray and Farquharson [6], whose method is being followed here, show how to interpolate values for ions from those given by Pauling.

More recently Slater [7] gives an expression for $\overline{r^2}$ in terms of effective principal quantum numbers and of screening constants. He gives rules by means of which the screening constant and effective quantum number may be obtained for any electron group.

Brindley [8] following this shows that the susceptibility of a gram atom, using Slater's notation, is

$$\chi_A = -0{\cdot}807 \times 10^{-6} \Sigma \frac{(n^*)^2(n^* + \frac{1}{2})(n^* + 1)}{(Z - S)^2},$$

where n^* is the effective principal quantum number and s is the screening constant.

In Table II. are given ionic susceptibilities necessary for the present discussion. These have been calculated by Pauling's and Slater's methods. By adding together the appropriate ionic values it is possible to arrive at a value for D.

TABLE II.

Theoretical Ionic Susceptibilities after Pauling and Slater.

	O^{+6}.	O^{+4}.	O^{+2}.	O^{0}.	O^{-2}.
Pauling	0·08	2·09	4·09	7·19	12·60
Slater	0·08	1·45	3·60	7·10	13·14
	S^{+6}.	S^{+4}.	S^{+2}.	S^{0}.	S^{-2}.
Pauling	1·40	7·40	14·70	25·50	40·00
Slater	1·40	5·73	12·15	21·94	37·46
	K^{+1}.	H^{+1}.			
Pauling	16·70	0			
Slater	14·44	0			

(3) *The Magnitude of the Paramagnetic Term* P_y.

The hydrogen molecule is the only one for which a theoretical deduction of P_y has been made. Van Vleck [9]

has calculated P_y for the hydrogen molecule and finds it to be $0{\cdot}51 \times 10^{-6}$.

Wang [10] calculated D for the hydrogen molecule to be $-4{\cdot}7 \times 10^{-6}$.

Two experimental values for hydrogen have been found,

$-3{\cdot}94 \times 10^{-6}$, Wills and Hector [11],
Hector,
$-3{\cdot}99 \times 10^{-6}$, Soné [12].

The relationship of P_y and D for H_2 is

D. Calculated.	P_y. Calculated.	P_y—D. Experimental.	P_y. Experimental.
		$-3{\cdot}94 \times 10^{-6}$	$0{\cdot}76 \times 10^{-6}$
$-4{\cdot}7 \times 10^{-6}$	$0{\cdot}51 \times 10^{-6}$	or	or
		$-3{\cdot}99 \times 10^{-6}$	$0{\cdot}71 \times 10^{-6}$

so that

calculated P_y is 11 per cent. of D,
experimental P_y is 16·4 per cent of D,
or 15·1 per cent of D.

It is expected that for more complicated molecules, such as those under discussion in the present investigation, the effect of P_y will be relatively greater.

It is of interest, then, to compare the experimental values with the sum of the theoretical susceptibilities of the ions which go to make up the neutral molecule of the substance under discussion. This is done in Table III. for Pauling's and Slater's theoretical ionic susceptibilities. The results are in good agreement with each other. The magnitude of P_y is in quite good agreement with that for the H_2 molecule.

(4) *Addition Reactions and the Relative Increase in* P_y.

The reactions involving the formation of some of the sulphur compounds under discussion may be regarded as addition reactions. In the process of formation of the new molecule, there will be the formation of a new bond. This will give rise to a relatively greater increase in P_y, and there will be a fall in diamagnetism. This is shown in Table IV.

This table is of great importance, because it depends entirely on experimental results and not at all on theoretical susceptibilities. It shows how departure from additivity is to be expected as a result of chemical action. The occurrence of such departure from additivity is demonstrated clearly from experimental data only and cannot be ascribed to experimental errors (unless there is a good reason for doing so). Rather, the deviations should be welcomed as valuable aids to the understanding of molecular magnetism.

TABLE III.

Estimated Effect of P_y for some Sulphur Compounds.

Neutral group.		Molecular diamagnetism of neutral group.			Fall in diamagnetism.		Percentage fall.	
		Experimental.	Pauling.	Slater.	Pauling.	Slater.	Pauling.	Slater.
SO_3	$S^{+6}+3O^{-2}$	28·54	39·2	40·82	10·66	12·28	27·19	29·88
H_2SO_4	$2H^{+1}+S^{+6}+4O^{-2}$	39·00	51·8	53·96	12·80	14·96	24·71	27·77
$KHSO_4$ ...	$K^{+1}+H^{+1}+S^{+6}+4O^{-2}$	49·77	68·5	68·40	18·73	18·63	27·34	27·24
K_2SO_4	$2K^{+1}+S^{+6}+4O^{-2}$	65·00	85·2	82 84	20·20	17·84	23·71	21·54
$K_2S_2O_3$ ...	$2K^{+1}+S^{+6}+3O^{-2}+S^{-2}$	75·88	112·6	107·16	36·72	31·28	32·61	29·18
$K_2S_2O_7$ ...	$2K^{+1}+2S^{+6}+7O^{-2}$	92·04	124·4	123·66	32·36	31·62	26·01	25·57
$K_2S_2O_8$ ...	$2K^{+1}+2S^{+6}+7O^{-2}+O^{\circ}$	102·4	131·6	130·76	29·20	28·36	22·19	21·69
$K_2S_4O_6$ ...	$2K^{+1}+2S^{+6}+2S^{-2}+5O^{-2}+O^{\circ}$	118·4	186·4	179·32	68·00	60·92	36·49	33·97
		for 120·9			65·50	58·42	35·14	32·58

The reaction involving the formation of tetrathionate can be treated in the same way, but here, there is no simple addition reaction, and a fall in diamagnetism may not result; in fact, there is a rise. This may be readily explained if the

TABLE IV.

Equation.	New bond.	Fall in diamagnetism.
$H_2O+SO_3\rightarrow H_2SO_4$ 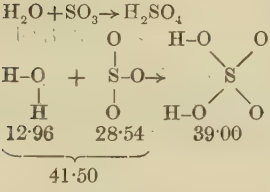 12·96 28·54 39·00 41·50	Sulphur-oxygen.	2·5
$H_2SO_4+K_2SO_4\rightarrow 2KHSO_4$ 39·00 65·00 104·0 99·54	Rearrangement.	4·56
$K_2SO_4+SO_3\rightarrow K_2S_2O_7$ 65·00 28·54 93·54 92·04	Sulphur-oxygen.	1·50

diamagnetic changes accompanying the reaction are analysed.

The equation usually given for the reaction is

		Diamagnetic change.
$2K_2S_2O_3+I_2$	$K_2S_4O_6+2KI$	
$2\times75\cdot88+88\cdot8$	$118\cdot4+2\times63\cdot9$	
	or 120·9	
240·56	246·2	gain 5·64
	or 248·7	or 8·14

The reaction involves the following changes:

loss of (I–I) bond ..... homopolar [5]
gain of 2(K–I) bonds ... heteropolar [5]
gain of (0–0) bond
} gain in diamagnetism.

The net result of these changes is a rise in diamagnetism, and theory and experiment are in agreement.

(5) *The Relative Polarities of some of the Bonds.*

By an application of the theoretical susceptibilities in Table II. and the comparison of molecules with similar structures, it is possible to draw conclusions as to the polarities of some of the bonds. This becomes clear after examination of one or two examples.

H_2SO_4 and K_2SO_4 have a similar structure, only in K_2SO_4

two potassium ions are substituted for the two hydrogen ions of H_2SO_4, thus

$H_2SO_4 \rightarrow K_2SO_4$	rise 26
core change	
$2H^{+1} \rightarrow 2K^{+1}$	rise 33·4 (L. P.)
	„ 28·88 (J.C.S.)
bond change	
$2(H–O) \rightarrow 2(K–O)$	fall 7·40 (L. P.)
	„ 2·88 (J.C.S.)

This considerable fall in diamagnetism of the bonds indicates that there has been a relative increase in P_y, and that the (K–O) bond is more homopolar than the (H–O) bond.

Similiarly,

$H_2SO_4 \rightarrow KHSO_4$	rise 10·77
$H^{+1} \rightarrow K^{+1}$	„ 16·70 (L. P.)
	„ 14·44 (J. C. S.)
$(H–O) \rightarrow (K–O)$	fall 5·93 (L. P.)
	„ 3·67 (J. C. S.)

Also,

$KHSO_4 \rightarrow K_2SO_4$	rise 15·23
$H^{+1} \rightarrow K^{+1}$	„ 16·70 (L. P.)
	„ 14·44 (J. C. S.)
$(H–O) \rightarrow (K–O)$	fall 1·47 (L. P.)
	rise 0·79 (J. C. S.)

Here again the application of Pauling's value indicates that (K–O) is more homopolar than (H–O), and the fact that Slater's value shows a rise, can be explained away by the fact that the experimental value for $KHSO_4$ is a little uncertain.

This result is in good agreement with that of Gray and Farquharson [5] for HIO_3 and KIO_3, and HIO_4 and KIO_4.

(6) *The Relationship of the Sulphur-Oxygen and Sulphur-Sulphur Bonds.*

Consider K_2SO_4 and $K_2S_2O_3$. These molecules may be regarded as having the same structure, but with one S replacing an O.

	Diamagnetic change in whole molecule. Theoretical.	Actual.	Change in bond.
$K_2SO_4 \rightarrow K_2S_2O_3$			
$XS^{+6}O^{-2} \rightarrow XS^{+6}S^{-2}$	rise 27·40 (L.P.)	rise 10·88	fall 16·52
65·00 76·88	„ 24·32 (J.C.S.)	„ 10·88	„ 13·44

This fall in the bond is due to the change from a sulphur-oxygen to a sulphur-sulphur bond and shows the sulphur-sulphur to be much more homopolar.

Again, with $K_2S_2O_8$ and $K_2S_4O_6$.

	Diamagnetic change in whole molecule.		Change in bond.
	Theoretical.	Actual.	
$K_2S_2O_8 \rightarrow K_2S_4O_6$			fall 38·8
$K_2S_2O_8$ $K_2S_2O_6S_2$	rise 54·80 (L. P.)	rise 16·0 or	or 36·3
$\times^{S^{+6}O^{-2}}_{S^{+6}O^{-2}} \rightarrow \times^{S^{+6}S^{-2}}_{S^{+6}S^{-2}}$	,, 48·64 (J.C.S.)	rise 18·5	fall 32·64 or 30·14
102·4 118·4 or 120·9			

This large fall is due to the change from two sulphur-oxygen bonds to two sulphur-sulphur bonds, and shows that the sulphur-sulphur bond is much the more homopolar.

The following table sums up the relationship of these bonds.

	Fall in diamagnetism due to change from sulphur-oxygen to sulphur-sulphur bonds.		
$K_2SO_4 \rightarrow K_2S_2O_3$	16·52		13·44
$K_2S_2O_8 \rightarrow K_2S_4O_6$	$2 \times 19{\cdot}40$		$2 \times 16{\cdot}32$
(with twice the number of bonds).	or $2 \times 18{\cdot}52$	or	$2 \times 15{\cdot}07$

The figures in the table show good agreement.

Summary.

Experimental magnetic susceptibilities are given for a series of sulphur compounds.

Theoretical ionic susceptibilities are calculated for ions by Pauling's and Slater's methods for ions required in the interpretation of the results.

The percentage differences between the experimental and theoretical figures are in good agreement with each other and with theory.

A study of addition reactions shows a good agreement with theory.

Comparison of molecules with similar structures, and the use of theoretical ionic susceptibilities give the polarities of some of the bonds. These are in good agreement with those found previously and with each other.

The author wishes to express his thanks to Professor F. G. Donnan, F.R.S., for his interest and advice throughout this investigation, to Dr. F. W. Gray, Aberdeen, for his helpful criticism of the discussion, and to the Royal Commissioners of the Exhibition of 1851 for a Senior Studentship.

References.

(1) Gray and Farquharson, J. Scientific Inst. ix. p. 1 (1932).
(2) Farquharson, Phil. Mag. xii. p. 283 (1931).
(3) Van Vleck, Phys. Rev. xxxi. p. 587 (1928).
(4) Pauli, *Zeit. f. physik*, ii. p. 201 (1920).
(5) Pauling, Proc. Roy. Soc. A, xii. p. 662 (1927).
(6) Gray and Farquharson, Phil. Mag. x. p. 191 (1930).
(7) Slater, Phys. Rev. xxxvi. p. 57 (1930).
(8) Brindley, Phil. Mag. xi. p. 786 (1931).
(9) Van Vleck, 'Electric and Magnetic Susceptibilities,' pp. 278–279 (1932).
(10) Wang, Proc. Nat. Acad. Sciences, xiii. p. 798 (1927).
(11) Wills and Hector, Phys. Rev. xxiii. p. 209 (1924); Hector, Phys. Rev. xxiv. p. 418 (1924).
(12) Soné, Phil. Mag. xxxix. p. 305 (1920).

Sir William Ramsay Laboratories of Inorganic and Physical Chemistry, University College, London, W.C. 1.

CIII. *The Acoustic and Inertia Pressure at any Point on a Vibrating Circular Disk.* *By* N. W. McLachlan, *D.Sc., M.I.E.E.* *

Abstract.

A formula is obtained for the acoustic pressure at *any* point on a rigid circular disk vibrating in an infinite plane. The analysis is extended to flexible disks whose dynamic deformation curve is taken to be of the form

$$w = A\left(1 - p_1 \frac{r^2}{a^2}\right),$$

where p_1 is a variable parameter. It is shown that the acoustic and inertia components, into which the pressure can be resolved, vary from the centre to the edge. The expressions derived for the pressure in the cases considered involve Bessel, Struve, and hypergeometric functions.

* Communicated by the Author.

The results obtained are discussed with reference to the distribution of sound from the mouth of a long loud speaker horn. By integrating the product of pressure and velocity over the surface of the disk the radiated power can be evaluated. As an example, the case of a free-edge disk vibrating with free centre and one nodal circle is treated.

---

1. *Rigid Disk.*

THE formula for the *total* pressure on the surface of a rigid circular disk vibrating in an equal aperture in an infinite plane was obtained by the late Lord Rayleigh many years ago*. In modern acoustical work it is sometimes necessary to know the pressure at *any point* on the disk. As this cannot be extracted from Rayleigh's analysis, the solution to the problem, together with an extension to *flexible* disks, is given below.

Fig. 1.

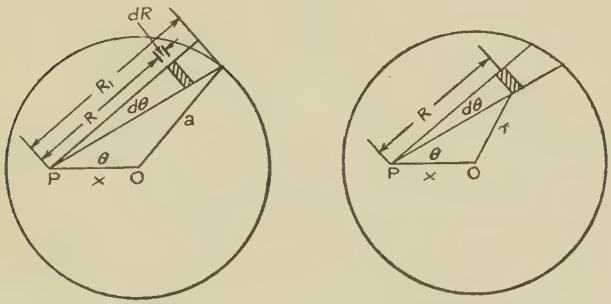

Diagrams showing geometrical relationships to which reference is made in the text. The elemental shaded area is $R dR\, d\theta$.

Referring to fig. 1, the maximum pressure at P, due to the elemental area $R dR\, d\theta$ moving harmonically with axial velocity $\dot{A}$ and frequency $\frac{\omega}{2\pi}$ is,

$$dp = \frac{i\rho\omega\dot{A}}{2\pi} \cdot \frac{e^{-ikR}}{R} \cdot R dR\, d\theta, \quad . \quad . \quad . \quad . \quad (1)$$

where ρ = density of fluid, $k = \frac{\omega}{c} = \frac{2\pi}{\lambda}$, λ = wave-length, $i = \sqrt{-1}$, and c = velocity of sound.

* 'Sound,' ii. p. 164 (1894).

The total pressure at P is, therefore,

$$p = \frac{i\rho c\dot{A}}{\pi}\int_0^{\pi} d\theta \int_0^{R_1} ke^{-ikR}\,dR. \quad . \quad . \quad . \quad (2)$$

From the geometry of fig. 1 we have

$$R_1^2 - 2R_1 x\cos\theta + (x^2 - a^2) = 0$$

or

$$R_1 = x\cos\theta \pm a(1 - b^2\sin^2\theta)^{\frac{1}{2}}, \quad \text{where } b = x/a;$$
$$= \mu \pm \chi.$$

The limits of R_1 being 0 and $\mu+\chi$, the first integral in (2) is:

$$I_1 = k\int_0^{\mu+\chi} e^{-ikR}\,dR$$
$$= i[e^{-ik(\mu+\chi)} - 1]. \quad . \quad . \quad . \quad . \quad . \quad (3)$$

Expanding (3), the second integral in (2) becomes

$$I_2 = \int_0^{\pi}\Big[\Big\{k(\mu+\chi) - \frac{k^3}{3!}(\mu+\chi)^3 + \frac{k^5}{5!}(\mu+\chi)^5 - \text{etc.}\Big\}$$
$$-i\Big\{\frac{k^2}{2!}(\mu+\chi)^2 - \frac{k^4}{4!}(\mu+\chi)^4 + \text{etc.}\Big\}\Big]\,d\theta. \quad . \quad (4)$$

As a first step in evaluating (4) we require the following expansions :—

$$\chi = a(1 - b^2\sin^2\theta)^{\frac{1}{2}} = a\Big(1 - \frac{b^2}{2}\sin^2\theta - \frac{b^4}{8}\sin^4\theta - \frac{b^6}{16}\sin^6\theta\ldots\Big),$$
$$. \quad . \quad . \quad (5)$$

$$\chi^2 = a^2(1 - b^2\sin^2\theta), \quad . \quad . \quad . \quad . \quad . \quad . \quad . \quad . \quad . \quad . \quad (6)$$

$$\chi^3 = a^3\Big(1 - \frac{3}{2}b^2\sin^2\theta + \frac{3}{8}b^4\sin^4\theta + \frac{b^6}{16}\sin^6\theta + \text{etc.}\Big), \quad . \quad (7)$$

$$\chi^4 = a^4(1 - 2b^2\sin^2\theta + b^4\sin^4\theta), \quad . \quad . \quad . \quad . \quad . \quad . \quad . \quad (8)$$

$$\chi^5 = a^5\Big(1 - \frac{5}{2}\sin^2\theta + \frac{15}{8}b^4\sin^4\theta - \frac{5}{16}b^6\sin^6\theta\ldots\Big). \quad . \quad . \quad (9)$$

Taking the integrals in (4) individually, we find

$$k\int_0^{\pi}(\mu+\chi)\,d\theta = 2k\int_0^{\frac{\pi}{2}} a\Big(1 - \frac{b^2}{2}\sin^2\theta$$
$$- \frac{b^4}{8}\sin^4\theta - \frac{b^6}{16}\sin^6\theta\ldots\Big)\,d\theta.$$

Using the sine reduction formula the above yields,

$$k\int_0^{\pi}(\mu+\chi)d\theta=\pi z\left(1-\frac{b^2}{4}-\frac{3}{64}b^4-\frac{5}{256}b^6\ldots\right),$$
$$=\pi z\mathrm{F}\left(-\frac{1}{2},\frac{1}{2},1,b^2\right), \quad . \quad . \quad . \quad (10)$$

where $z=ka$ and F indicates the hypergeometric function. Similarly,

$$\frac{k^3}{3!}\int_0^{\pi}(\mu+\chi)^3d\theta$$
$$=\frac{\pi z^3}{3!}\left(1-\frac{3}{4}b^2+\frac{9}{64}b^4+\frac{5}{256}b^6\ldots\right)$$
$$+\frac{3b^2}{2}\cdot\frac{\pi z^3}{3!}\left(1-\frac{b^2}{8}-\frac{b^4}{64}-\frac{5}{1024}b^6\ldots\right)$$
$$=\frac{\pi z^3}{3!}\left\{\mathrm{F}\left(-\frac{3}{2},\frac{1}{2},1,b^2\right)+\frac{3}{2}b^2\mathrm{F}\left(-\frac{1}{2},\frac{1}{2},2,b^2\right)\right\}, \quad (11)$$

$$\frac{k^5}{5!}\int_0^{\pi}(\mu+\chi)^5d\theta=\frac{\pi z^5}{5!}\left(1-\frac{5}{4}b^2+\frac{45}{64}b^4-\frac{25}{256}b^6\ldots\right)$$
$$+5b^2\cdot\frac{\pi z^5}{5!}\left(1-\frac{3}{8}b^2+\frac{3}{64}b^4+\frac{5}{1024}b^6\ldots\right)$$
$$+\frac{15b^4}{8}\cdot\frac{\pi z^5}{5!}\left(1-\frac{b^2}{12}-\frac{b^4}{128}\ldots\right)$$
$$=\frac{\pi z^5}{5!}\left\{\mathrm{F}\left(-\frac{5}{2},\frac{1}{2},1,b^2\right)+5b^2\mathrm{F}\left(-\frac{3}{2},\frac{1}{2},2,b^2\right)\right.$$
$$\left.+\frac{15}{8}b^4\mathrm{F}\left(-\frac{1}{2},\frac{1}{2},3,b^2\right)\right\}, \quad . \quad . \quad . \quad (12)$$

$$\frac{k^2}{2!}\int_0^{\pi}(\mu+\chi)^2d\theta=\frac{\pi z^2}{2!}, \quad . \quad . \quad . \quad . \quad . \quad . \quad . \quad (13)$$

$$\frac{k^4}{4!}\int_0^{\pi}(\mu+\chi)^2d\theta=\frac{\pi z^4}{4!}(1+2b^2), \quad . \quad . \quad . \quad (14)$$

$$\frac{k^6}{6!}\int_0^{\pi}(\mu+\chi)^6d\theta=\frac{\pi z^6}{6!}(1+6b^2+3b^4). \quad . \quad (15)$$

Adding the various integrals in (4) and multiplying throughout by the common factor $\frac{i\rho c\dot{A}}{\pi}$, the pressure at any

point distant x from the centre of the disk $\left(b=\frac{x}{a}\right)$ is given by the expression

$$p=\rho c\dot{\mathrm{A}}\left\{\frac{z^2}{2!}f_2-\frac{z^4}{4!}f_4+\frac{z^6}{6!}f_6\cdots\right.$$
$$\left.+i\left(zf_1-\frac{z^3}{3!}f_3+\frac{z^5}{5!}f_5\cdots\right)\right\}, \quad (16)$$

where

$$f_2=1,$$
$$f_4=1+2b^2,$$
$$f_6=1+6b^2+3b^4,$$
$$f_8=1+12b^2+18b^4+4b^6,$$
$$f_{10}=1+18b^2+66b^4+36b^6+b^8.$$

. . . . . .

For general term see (38) in Appendix.

$$f_1=\mathrm{F}\left(-\frac{1}{2},\frac{1}{2},1,b^2\right),$$

$$f_3=\mathrm{F}\left(-\frac{3}{2},\frac{1}{2},1,b^2\right)+\frac{3}{2}b^2\mathrm{F}\left(-\frac{1}{2},\frac{1}{2},2,b^2\right),$$

$$f_5=\mathrm{F}\left(-\frac{5}{2},\frac{1}{2},1,b^2\right)+5b^2\mathrm{F}\left(-\frac{3}{2},\frac{1}{2},2,b^2\right)$$
$$+\frac{15}{8}b^4\mathrm{F}\left(-\frac{1}{2},\frac{1}{2},3,b^2\right),$$

$$f_7=\mathrm{F}\left(-\frac{7}{2},\frac{1}{2},1,b^2\right)+\frac{21}{2}b^2\mathrm{F}\left(-\frac{5}{2},\frac{1}{2},2,b^2\right)$$
$$+\frac{105}{8}b^4\mathrm{F}\left(-\frac{3}{2},\frac{1}{2},3,b^2\right)+\frac{35}{16}b^6\mathrm{F}\left(-\frac{1}{2},\frac{1}{2},4,b^2\right),$$

$$f_9=\mathrm{F}\left(-\frac{9}{2},\frac{1}{2},1,b^2\right)+18b^2\mathrm{F}\left(-\frac{7}{2},\frac{1}{2},2,b^2\right)$$
$$+\frac{189}{4}b^4\mathrm{F}\left(-\frac{5}{2},\frac{1}{2},3,b^2\right)+\frac{105}{4}b^6\mathrm{F}\left(-\frac{3}{2},\frac{1}{2},4,b^2\right)$$
$$+\frac{315}{128}b^8\mathrm{F}\left(-\frac{1}{2},\frac{1}{2},5,b^2\right).$$

. . . . . .

For general term see (39) in Appendix.

2. *Pressure at Centre and at Edge.*

As a check on the preceding analysis, suppose we ascertain the pressure in two particular cases. At the centre of the disk $b = \frac{x}{a} = 0$, and (16) becomes

$$p_c = \rho c \dot{A}(1 - \cos z + i \sin z). \quad . \quad . \quad . \quad (17)$$

Evidently the central acoustic pressure vanishes when $\cos z = 1$ or $z = 2n\pi$, whilst the inertia pressure does likewise when $\sin z = 0$, or $z = n\pi$, where $n = 0, 1, 2 \ldots$. The latter has therefore twice as many zeros in a given range of z as the former. At the edge of the disk $b = 1$, and the pressure is given by

$$p_e = \frac{\rho c \dot{A}}{2} \{1 - J_0(2z) + iH_0(2z)\}, \quad . \quad . \quad (18)$$

where J_0 and H_0 are, respectively, Bessel and Struve Functions of zero order.

In obtaining (18), Gauss's formula

$$F(\alpha, \beta, \gamma, 1) = \frac{\Gamma(\gamma)\,\Gamma(\gamma - \alpha - \beta)}{\Gamma(\gamma - \alpha)\,\Gamma(\gamma - \beta)},$$

was used for the evaluation of the hypergeometric functions with argument unity.

Formulæ (17) and (18) agree with those given by Warren *.

The acoustic pressure at the edge vanishes when $J_0(2z) = 1$, a condition which occurs only when $z = 0$, *i. e.*, at zero frequency. Above this frequency the pressure oscillates but is always positive. The inertia pressure is zero when $H_0(2z) = 0$ or $z = 2{\cdot}166$, $3{\cdot}391$, $5{\cdot}235$, and so on.

3. *Total Pressure on one Side of Disk.*

As an additional check on formula (16) for the pressure at any point on the disk, it is of considerable interest to integrate over the surface in order to determine the total pressure. Ultimately we ought to reproduce Rayleigh's formula.

The total pressure on the disk is

$$2\pi \int_0^a px\,dx = 2\pi a^2 \int_0^1 pb\,db,$$

where p is given by (16). Taking the real and imaginary

* Proc. Phys. Soc. xl. p. 296 (1928).

parts individually, the integration of the former is straightforward and gives

$$\rho c\dot{A}\int \text{real part} = \rho c\dot{A}\pi a^2 \left\{ \frac{(2z)^2}{2.4} - \frac{(2z)^4}{2.4^2.6} + \frac{(2z)^6}{2.4^2.6^2.8\ldots} \right\}$$

$$= \rho c\dot{A}\pi a^2 \left\{ 1 - \frac{J_1(2z)}{z} \right\}. \quad . \quad . \quad . \quad . \quad (19)$$

To integrate the imaginary part we require the following integrals :—

$$\int_0^1 F(\alpha, \beta, 1, b^2) b\,db = \frac{1}{2} F(\alpha, \beta, 2, 1), \quad . \quad . \quad (20)$$

$$\int_0^1 F(\alpha, \beta, 2, b^2) b^3\,db = \frac{1}{4} F(\alpha, \beta, 3, 1), \quad . \quad . \quad (21)$$

$$\int_0^1 F(\alpha, \beta, 3, b^2) b^5\,db = \frac{1}{6} F(\alpha, \beta, 4, 1) \quad . \quad . \quad (22)$$

Performing the requisite sequence of operations and evaluating the integrated hypergeometric functions by aid of Gauss's formula given above, we obtain

$$\rho c\dot{A}\int \text{imaginary part} = \frac{\rho c\dot{A}}{k^2} \left\{ \frac{(2z)^3}{1^2.3} - \frac{(2z)^5}{1^2.3^2.5} + \frac{(2z)^7}{1^2.3^2.5^2.7\ldots} \right\}$$

$$= \frac{\pi \rho c\dot{A}}{2k^2} . (2z) . H_1(2z), \quad . \quad . \quad . \quad (23)$$

where $H_1(z)$ is Struve's function of unit order *. Adding the real and imaginary parts of the total pressure from (19) and (23), we find that on one side of the disk,

$$\Sigma pds = \rho c\dot{A} \left\{ \pi a^2 \left[1 - \frac{J_1(2z)}{z} \right] + \frac{i\pi}{2k^2} . (2z) . H_1(2z) \right\}, \quad (24)$$

This expression is identical with that found by Rayleigh, so that the validity of (16) has been completely established.

4. *Variation in Pressure along any Radius.*

From (16) the acoustic pressure at any radius is

$$p_a = \rho c\dot{A} \left\{ \frac{(ka)^2}{2!} - \frac{(ka)^4}{4!}(1 + 2b^2) + \frac{(ka)^6}{6!}(1 + 6b^2 + 3b^4) \right.$$

$$\left. - \frac{(ka)^8}{8!}(1 + 12b^2 + 18b^4 + 4b^6) \right.$$

* Rayleigh's $K_1(z) = zH_1(z)$. Struve's function is tabulated in G. N. Watson's Bessel Functions, and gives greater generality.

$$+\frac{(ka)^{10}}{10!}(1+18b^2+66b^4+36b^6+b^8)\ldots\Big\}, \quad (25)$$

where

$$b=\frac{x}{a}.$$

This formula, as given above in (25), can be used to evaluate p_a for values of $ka \leqq 2$. For greater values of ka additional terms must be incorporated to attain accuracy *.

The acoustic pressure variation over the surface of a rigid disk for several values of ka is portrayed graphically in

Fig. 2.

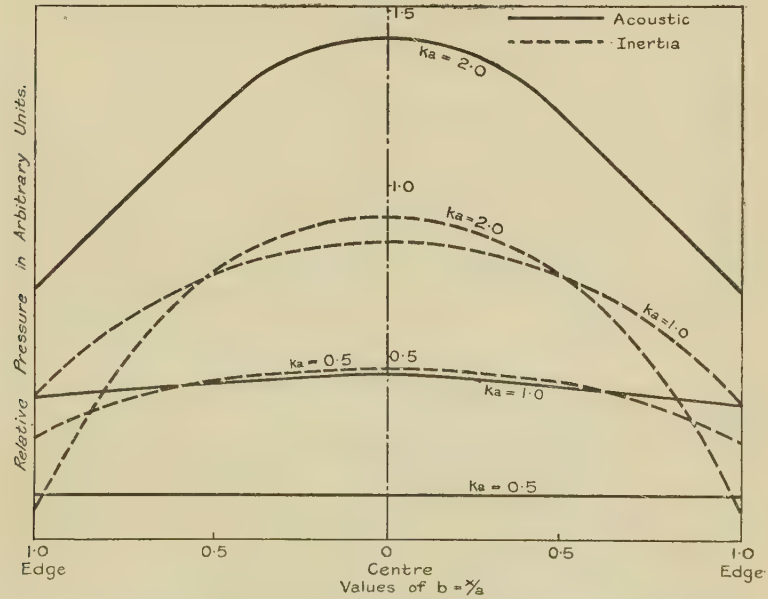

Curves showing acoustic and inertia pressure over the surface of a rigid disk vibrating in an infinite rigid plane for various values of ka.

fig. 2. At low frequencies the pressure is constant, but the edge pressure falls off relatively as the frequency rises. Beyond a certain frequency the central pressure decreases, and ultimately vanishes when $ka=2\pi$ or $f=3400$ cycles per second for a disk 10 cm. radius. Above this frequency it oscillates between zero and a constant maximum.

The inertia component of the pressure calculated from the imaginary part of expression (16) is also shown in fig. 2.

* When $ka=2$, the error in (25) using only 5 terms is about 1 per cent. In acoustical work this is quite negligible.

At the centre it is about three times the acoustic pressure for $ka=0{\cdot}5$, but falls away towards the edge.

As ka increases the acoustic pressure rises more rapidly than the inertia pressure, whilst at $ka=2{\cdot}0$ it is definitely greater.

The total pressure and its phase angle, with the axial velocity $\theta_1=\tan^{-1}\left(\frac{p_i}{p_a}\right)$, are plotted in fig. 3. Even at low

Fig. 3.

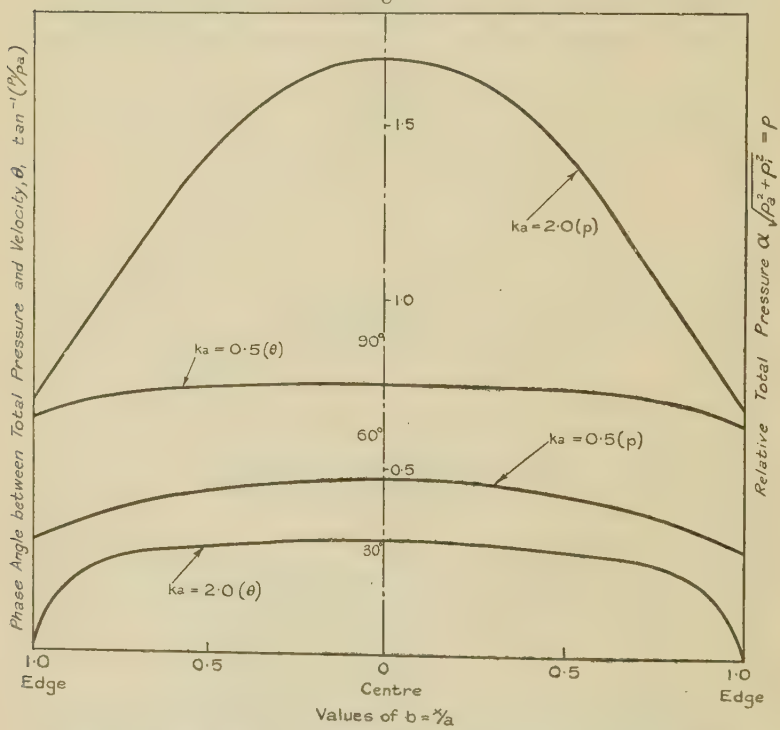

Curves showing the total pressure $\sqrt{p_a^2+p_i^2}$ and the phase angle θ_1 between it and the velocity for various values of ka.

frequencies the pressure is not constant but falls off towards the edge. To preserve constant pressure at small values of ka the velocity of the disk would have to increase with the radius ultimately becoming infinite at the edge.

5. *Pressure at Centre and at Edge of Flexible Disk.*

The dynamic deformation curve of the disk vibrating in an infinite plane will be assumed as

$$w=\mathrm{A}\left(1-p_1\frac{r^2}{a^2}\right),$$

where p_1 is a variable parameter, r is the radius of the vibrating element (fig. 1 *b*), and at the centre $A = X \cos \omega t$.

Taking the case of simple harmonic motion for the disk, the axial velocity at a radius r is given by

$$\frac{\partial w}{\partial t} = \dot{w} = \dot{A}\left(1 - p_1 \frac{r^2}{a^2}\right), \quad . \quad . \quad . \quad . \quad (26)$$

where

$$\dot{A} = -\omega X \sin \omega t.$$

From expression (2) it follows that the pressure at any point on the disk is

$$p = \frac{i\rho c \dot{A} k}{\pi} \int_0^{\pi} d\theta \int_0^{R_1} \left(1 - p_1 \frac{r^2}{a^2}\right) e^{-ikR}\, dr, \quad . \quad (27)$$

where

$$r^2 = R^2 - 2Rx \cos \theta + x^2$$

and

$$R_1 = x \cos \theta + a(1 - b^2 \sin^2 \theta)^{\frac{1}{2}}.$$

The evaluation of (27) is more laborious than it is difficult. We shall, therefore, initially give two particular solutions, namely, (*a*) for the central pressure, (*b*) for the edge pressure. For the central case $R_1 = a$, $R = r$, and (27) becomes :

$$p_c = \frac{i\rho c \dot{A} k}{\pi} \int_0^{\pi} d\theta \int_0^{a} \left(1 - p_1 \frac{R^2}{a^2}\right) e^{-ikR}\, dR$$

$$= \rho c \dot{A} \{a_1 + (b_1 + ic_1) e^{-iz}\}, \quad . \quad . \quad . \quad . \quad . \quad (28)$$

where

$$a_1 = 1 + \frac{2p_1}{z^2},$$

$$b_1 = 1 - p_1\left(1 - \frac{2}{z^2}\right),$$

$$c_1 = \frac{2p_1}{z},$$

$$z = ka.$$

The modulus $|p_c| = \sqrt{P^2 + Q^2}$, where

$$P = a_1 - b_1 \cos z + c_1 \sin z \quad . \quad . \quad . \quad . \quad (29)$$

and

$$Q = b_1 \sin z - c_1 \cos z. \quad . \quad . \quad . \quad . \quad . \quad (30)$$

At the edge,

$$R_1 = 2a \cos \theta\ ; \quad r^2 = a^2 - 2aR \cos \theta + R^2,$$

the limits of θ are 0 and $\frac{\pi}{2}$, and (27) can be written

$$p_e = \frac{i\rho c\dot{A}k}{\pi}\int_0^{\frac{\pi}{2}} d\theta \int_0^{2a\cos\theta}\left[(1-p_1)+p_1\left(\frac{2R\cos\theta}{a}-\frac{R^2}{a^2}\right)\right]e^{-ikR}\,dR. \quad (31)$$

The first integral in (31) is

$$-\frac{i}{k}\{b_1(1-e^{-2iz\cos\theta})+ic_1\cos\theta(1+e^{-2iz\cos\theta})\}, \quad (32)$$

b_1 and c_1 having the same values as in (28), whilst $z=ka$.

Integrating (32) with respect to θ from 0 to $\frac{\pi}{2}$ we obtain:

$$-\frac{\pi i}{2k}\left\{b_1[1-J_0(2z)+iH_0(2z)]+ic_1\left[\frac{4}{\pi}-H_1(2x)-iJ_1(2z)\right]\right\}. \quad (33)$$

Multiplying (33) by $\frac{i\rho c\dot{A}k}{\pi}$, we find that the edge pressure

$$p_e = \frac{\rho c\dot{A}}{2}\left\{b_1[1-J_0(2z)] + c_1J_1(2z)+i\left[b_1H_0(2z)+c_1\left(\frac{4}{\pi}-H_1(2z)\right)\right]\right\}. \quad (34)$$

For a rigid disk $p_1=0$, and so $b_1=1$ and $c_1=0$. Inserting these values in (34) we obtain

$$p_e=\rho c\dot{A}\{1-J_0(2z)+iH_0(2z)\},$$

which is identical with expression (18). In (34) the acoustic and inertia components of the pressure vanish respectively, when the real and imaginary parts are zero. Formulæ (28) and (34) can be used for any value of p_1 from $-\infty$ to $+\infty$. Several typical dynamic deformation curves for various values of p_1 are illustrated in fig. 4.

6. *Pressure at any Point on Flexible Disk.*

The pressure at *any* point on the disk is found by evaluating (27) for the general case. The procedure is akin to that adopted in connexion with (4), and the result can be expressed in the same form as (16). Thus:

$$p=\rho c\dot{A}\left\{\frac{z^2}{2!}g_2-\frac{z^4}{4!}g_4+\frac{z^6}{6!}g_6\ldots, \text{ etc.} + i\left(zg_1-\frac{z^3}{3!}g_3+\frac{z^5}{5!}g_5\ldots\right)\right\}, \quad (35)$$

where

$$g_2=1-\frac{p_1}{2},$$

$$g_4=1+2b^2-p_1\left(\frac{2}{3}+b^2\right),$$

$$g_6=1+6b^2+3b^4-p_1\left(\frac{3}{4}+4b^2+\frac{3}{2}b^4\right).$$

. . . . . .

Fig. 4.

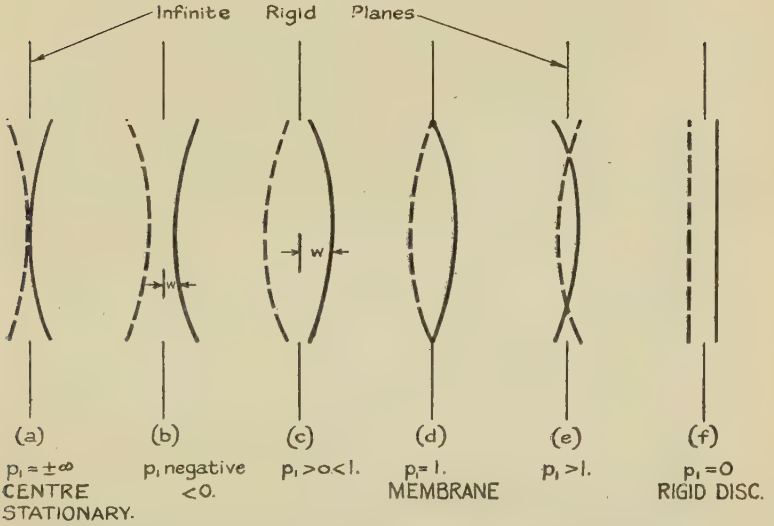

Diagram illustrating the different dynamic deformation curves which can be obtained by varying the parameter p_1 in the formula $\dot{A}\left(1-p_1\frac{r^2}{a^2}\right)$ for the axial velocity. In case (a) Ap_1 is to be finite.

$$g_1=\mathrm{F}\left(-\frac{1}{2},\frac{1}{2},1,b^2\right)-p_1\left\{\frac{1}{3}\mathrm{F}\left(-\frac{3}{2},\frac{1}{2},1,b^2\right)\right.$$
$$\left.+b^2\left[\mathrm{F}\left(-\frac{1}{2},\frac{1}{2},1,b^2\right)-\frac{1}{2}\mathrm{F}\left(-\frac{1}{2},\frac{1}{2},2,b^2\right)\right]\right\},$$

$$g_3=\mathrm{F}\left(-\frac{3}{2},\frac{1}{2},1,b^2\right)+\frac{3}{2}b^2\mathrm{F}\left(-\frac{1}{2},\frac{1}{2},2,b^2\right)$$

$$-p_1\left\{\frac{3}{5}\mathrm{F}\left(-\frac{5}{2},\frac{1}{2},1,b^2\right)+b^2\mathrm{F}\left(-\frac{3}{2},\frac{1}{2},1,b^2\right)\right.$$
$$\left.+\frac{3}{2}b^4\left[\mathrm{F}\left(-\frac{1}{2},\frac{1}{2},2,b^2\right)-\frac{3}{4}\mathrm{F}\left(-\frac{1}{2},\frac{1}{2},3,b^2\right)\right]\right\},$$

$$g_5=\mathrm{F}\left(-\frac{5}{2},\frac{1}{2},1,b^2\right)+5b^2\mathrm{F}\left(-\frac{3}{2},\frac{1}{2},2,b^2\right)$$
$$+\frac{15}{8}b^4\mathrm{F}\left(-\frac{1}{2},\frac{1}{2},3,b^2\right)-p_1\left\{\frac{5}{7}\mathrm{F}\left(-\frac{7}{2},\frac{1}{2},1,b^2\right)\right.$$
$$+b^2\left[\mathrm{F}\left(-\frac{5}{2},\frac{1}{2},1,b^2\right)+\frac{5}{2}\mathrm{F}\left(-\frac{5}{2},\frac{1}{2},2,b^2\right)\right]$$
$$+5b^4\left[\mathrm{F}\left(-\frac{3}{2},\frac{1}{2},2,b^2\right)-\frac{5}{8}\mathrm{F}\left(-\frac{3}{2},\frac{1}{2},3,b^2\right)\right]$$
$$\left.+\frac{5}{8}b^6\left[3\mathrm{F}\left(-\frac{1}{2},\frac{1}{2},3,b^2\right)-\frac{5}{2}\mathrm{F}\left(-\frac{1}{2},\frac{1}{2},4,b^2\right)\right]\right\}.$$

When $p_1=0$ we have the case of a rigid disk as given in (16), and the corresponding values of f_n and g_n are identical. When $p_1=2$ the disk has a nodal circle whose radius $r=\frac{a}{\sqrt{2}}$, and this corresponds closely to its first centre moving mode of vibration. By integrating the product of acoustic pressure (real part of (35)) and the velocity $\dot{\mathrm{A}}(1-2b^2)$ over the surface, we obtain the radiated power,

$$w=\frac{\pi\rho a^4\omega^4\mathrm{X}^2}{2c}\left\{\frac{1.2}{3!\,6!}z^4-\frac{2.3}{4!\,7!}z^6+\frac{3.4}{5!\,8!}z^8\ldots\text{ etc.}\right\}, \quad (36)$$

where X is the central amplitude and $z=ka$.

Neither of the terms in z^2 nor z^4 from (35) contribute anything to the result. That in z^2 is zero, whilst that in z^4 represents a constant pressure over the disk. Since the two *equal* areas on either side of the nodal circle vibrate in anti-phase, the integral over the surface for the z^4 term is evanescent. If $p_1\neq 2$ both terms contribute to the result and the radiation for a given central amplitude is enhanced. Whatever the value of p_1—including 2—the term in z^2 represents a constant pressure over the disk.

When $p_1=2$ and $z<0{\cdot}5$ the inertia pressure at any point on the disk is

$$p_i=\rho c\dot{\mathrm{A}}z\left\{(1-p_1b^2)\mathrm{F}\left(-\frac{1}{2},\frac{1}{2},1,b^2\right)\right.$$
$$\left.-p_1\left[\frac{1}{3}\mathrm{F}\left(-\frac{3}{2},\frac{1}{2},1,b^2\right)-\frac{b^2}{2}\mathrm{F}\left(-\frac{1}{2},\frac{1}{2},2,b^2\right)\right]\right\}$$

$$=\rho c A z\left\{(1-p_1)\mathrm{F}\left(-\frac{1}{2},\frac{1}{2},1,b^2\right)+\frac{2}{3}p_1\mathrm{F}\left(-\frac{3}{2},\frac{1}{2},1,b^2\right)\right\} \quad . \quad . \quad . \quad (37)$$

This is identical with the value found previously by the author—using a different method *—when evaluating the reduction in the natural frequency of a disk vibrating in water. By using several terms of the imaginary part of (35), the analysis can be extended to values of $z>0{\cdot}5$, that is, to higher frequencies.

In dealing with the power radiated from the mouth of a long loud-speaker horn, and also with the distribution of radiation throughout the surrounding space, it is sometimes assumed that the horn can be replaced by a rigid disk of equal radius. By making measurements of the pressure and its phase relationship with the air-particle velocity and comparing the results with the foregoing analysis, it will be possible to ascertain the accuracy of this assumption. If the accuracy is of a low order, then by giving p_1 in (35) some suitable value, a closer approximation may possibly be found.

Appendix.

The following formulæ can be used for evaluating the coefficients in (16) :—

When n is *even* $f_n=\dfrac{1}{\pi a^n}\displaystyle\int_0^{\pi}(\mu+\chi)^n d\theta,$

$$=\left\{\sum_{p=0,\ 2\ldots n}\frac{n(n-1)\ldots(n-p+1)}{p\,!}\cdot\frac{(n-p-1)(n-p-3)\ldots 1}{(n-p)(n-p-2)\ldots 2}\cdot b^{n-p}\right\}$$

$$\left\{1+\sum_{r=1}^{\frac{p}{2}}(-1)^r\frac{\frac{p}{2}\ldots\left(\frac{p}{2}-r+1\right)}{r\,!}\cdot\frac{(2r-1)\ldots 1}{(n-p+2r)\ldots(n-p+2)}\cdot b^{2r}\right\} \quad . \quad . \quad . \quad (38)$$

When n is *odd*

$$f_n=\sum_{p=1,\ 3\ldots n}\frac{n(n-1)\ldots(n-p+1)}{p\,!}\cdot\frac{(n-p-1)\ldots 1}{(n-p)\ldots 2}\cdot b^{n-p}\,\mathrm{F}\left(-\frac{p}{2},\frac{1}{2},\frac{n-p+2}{2},b^2\right) \quad . \quad . \quad . \quad . \quad (39)$$

September 1932.

* Proc. Phys. Soc. xliv. p. 546 (1932).

CIV. *Rotary Oscillation of a Long Circular Cylinder in a Viscous Fluid.* *By* H. F. Winny, *Ph.D.**

Introduction.

THE problem of a long circular cylinder oscillating in a viscous fluid was first discussed mathematically by Stokes † in connexion with his classical work on the motion of pendulums for determining the viscosity of air. The analysis permitted a correction to be applied to the deduced value of the coefficient of viscosity, by taking into account the rotation of the cylindrical bobs about their axes. Subsequently experiments were carried out by Tomlinson ‡, at the suggestion of Stokes, to verify the theory for pure oscillatory rotation. These latter experiments investigated the damping of the rotatory oscillation of paper cylinders in air, and led to values of the coefficient of viscosity in close agreement with those obtained by other methods. More recently the mathematics has been recast by Coster § using the usual notation for Bessel functions with complex arguments, but no further advance appears to have been made on the experimental side.

The two-dimensional case has often been cited as an approximate solution, and it is perhaps not generally appreciated that the solution is, in fact, exact for an incompressible fluid. The number of cases of viscous fluid motion that have as yet been solved exactly being small, the present problem has a peculiar interest, and may be expected to hold exactly, for all frequencies of oscillation of a long cylinder until a critical speed may be reached and instability appear. The present note describes some preliminary experiments designed to study in detail the rotatory oscillation of circular cylinders.

Theoretical.

Considering two-dimensional incompressible motion independent of θ, where r and θ are the cylindrical coordinates and u and v the velocity components along and perpendicular to r, respectively, the equation of continuity together with the boundary condition $u=0$ when $r=a$, where

* Communicated by Dr. N. A. V. Piercy.
† 'Collected Papers,' v. p. 197.
‡ Phil. Trans. clxxvii. p. 795 (1886).
§ Phil. Mag. xxxvii. p. 587 (1919).

a is the radius of the cylinder, gives $u=0$ throughout the plane. The general equations of motion then reduce to

$$-\frac{v^2}{r}=-\frac{1}{\rho}\frac{\partial p}{\partial r} \quad . \quad . \quad . \quad . \quad . \quad . \quad (1)$$

and

$$\frac{\partial v}{\partial t}=\nu\left(\frac{\partial^2 v}{\partial r^2}+\frac{1}{r}\frac{\partial v}{\partial r}-\frac{v}{r^2}\right) \quad . \quad . \quad . \quad . \quad (2)$$

where p is the pressure and is determined by equation (1), and ν is the coefficient of kinematic viscosity.

Putting $v=e^{i\sigma t}v_1$, where v_1 is a function of r only, equation (2) becomes :—

$$\frac{d^2v_1}{dr^2}+\frac{1}{r}\frac{dv_1}{dr}-\frac{v_1}{r^2}-\frac{i\sigma}{\nu}v_1=0 \quad . \quad . \quad . \quad . \quad (3)$$

of which the solution expressed in Bessel functions is :—

$$v_1=\mathrm{A}\mathrm{K}_1\left(r\sqrt{\frac{i\sigma}{\nu}}\right)+\mathrm{B}\mathrm{I}_1\left(r\sqrt{\frac{i\sigma}{\nu}}\right) \quad . \quad . \quad . \quad (4)$$

Attention is confined to the simple case of a cylinder of radius a oscillating in simple harmonic motion with frequency $\frac{\sigma}{2\pi}$ in an infinite expanse of fluid, so that B vanishes. Adopting Kelvin's notation for Bessel functions of complex argument, we finally obtain for v, rejecting the imaginary part since equation (2) is a linear differential equation with real coefficients :—

$$v=\frac{\mathrm{V}}{\left\{\mathrm{Ker}_1^2\left(a\sqrt{\frac{\sigma}{\nu}}\right)+\mathrm{Kei}_1^2\left(a\sqrt{\frac{\sigma}{\nu}}\right)\right\}^{\frac{1}{2}}}$$

$$\left\{\cos\sigma t\,.\,\mathrm{Ker}_1\left(r\sqrt{\frac{\sigma}{\nu}}\right)-\sin\sigma t\,.\,\mathrm{Kei}_1\left(r\sqrt{\frac{\sigma}{\nu}}\right)\right\} \quad (5)$$

where $\mathrm{K}_1(x\sqrt{i})=\mathrm{Ker}_1(x)+i\mathrm{Kei}_1(x)$, and v is the maximum velocity of the boundary. Tables of $\mathrm{Ker}_1(x)$ and $\mathrm{Kei}_1(x)$ have been calculated by Savidge *, and when x is large the asymptotic expansions may be written approximately in the form

$$\mathrm{Ker}_1(x)=\sqrt{\frac{\pi}{2x}}\,e^{-\frac{x}{\sqrt{2}}}\cos\left(\frac{\pi}{8}-\frac{x}{\sqrt{2}}\right),$$

$$\mathrm{Kei}_1(x)=\sqrt{\frac{\pi}{2x}}\,e^{-\frac{x}{\sqrt{2}}}\sin\left(\frac{\pi}{8}-\frac{x}{\sqrt{2}}\right). \quad . \quad . \quad (6)$$

* Brit. Assoc., 1915, pp. 36–38.

It is seen from equation (5) that the motion consists of a series of concentric velocity waves, and hence pressure waves, of decreasing amplitude propagated outwards from the cylinder, the amplitude α of the motion of the particles at any radius r being given by

$$\alpha = \frac{2v}{\sigma}\left\{\frac{\mathrm{Ker}_1^2\left(r\sqrt{\frac{\sigma}{\nu}}\right)+\mathrm{Kei}_1^2\left(r\sqrt{\frac{\sigma}{\nu}}\right)}{\mathrm{Ker}_1^2\left(a\sqrt{\frac{\sigma}{\nu}}\right)+\mathrm{Kei}_1^2\left(a\sqrt{\frac{\sigma}{\nu}}\right)}\right\}^{\frac{1}{2}} \quad . \quad (7)$$

Experimental.

The apparatus consisted of a cylindrical vessel 30 cm. diameter and 15 cm. deep, which served as a container for the oil or water used in the experiments as fluid. A cylinder 2·54 cm. diameter could be concentrically oscillated very nearly in simple harmonic motion by means of an electrically driven crank mechanism connected by wires 100 cm. long. The amplitude was maintained at 2·54 cm. measured round the boundary, while the frequency varied from 0·2 to 0·5 per sec. The method adopted was to observe through a thin celluloid polar scale, or a graduated microscope when necessary, the motion of aluminium powder sprinkled on the surface of the liquid after the steady state of oscillation had been attained. The amplitude of the flow at various radii was thus measured with fair accuracy, care being taken to keep the frequency constant. The results are given in figs. 1, 2, and 3, where fig. 3 conveniently contains on one curve the results for oil at two frequencies, the abscissa in all figures being $r\sqrt{\frac{\sigma}{\nu}}$ as suggested by equation (7). The values of ν used were taken from tables in the case of water and found experimentally by Redwood's viscometer for the oil at the required temperature.

The theoretical amplitude was calculated from equation (7), since the influence of the finite diameter of the containing vessel was found from equation (4) to be negligible, the present experiment thus closely approximating to a cylinder oscillating in an infinite fluid. These theoretical results are shown as broken curves in the figures, and agreed within experimental errors with those observed.

Conclusion.

It follows from equation (7), and is seen to be justified within the range of the experiments, that the amount of fluid influenced by an oscillating cylinder decreases with increase

of speed. The expression for the thickness δ of the fluid appreciably affected takes a simple form when it is small compared with a, the radius of the cylinder, and may be regarded as a boundary layer. Making use of equations (6) and (7) and agreeing to define the outer edge of the boundary

Fig. 1.

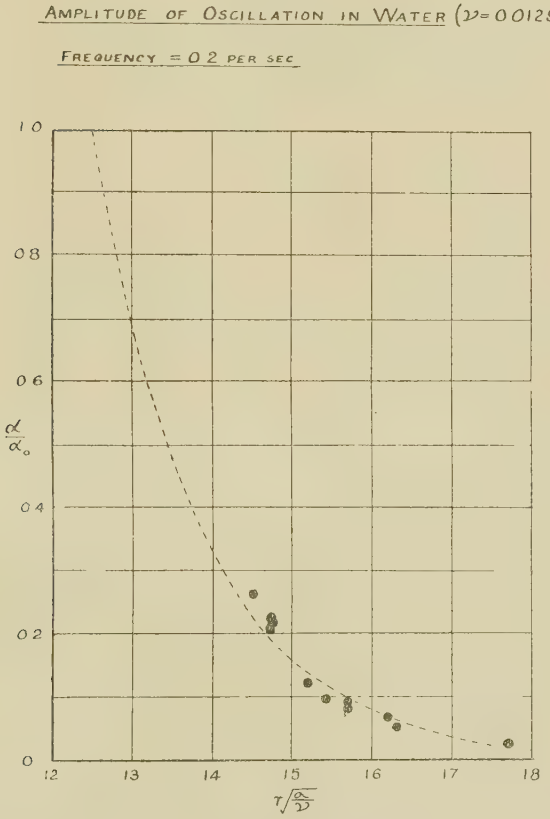

layer as the circle at which the amplitude α has decreased to 1 per cent. of its maximum value, we have

$$\delta = 4{\cdot}6\frac{\alpha_0}{\sqrt{\frac{V\alpha_0}{\nu}}} \quad . \quad . \quad . \quad . \quad . \quad . \quad (8)$$

where α_0 is the total amplitude of the boundary of the circular cylinder. Equation (8) becomes of the same form

as that found by Blasius for the thickness of the boundary layer of a flat plate moving with uniform velocity V, if α_0 be substituted for the length of the plate ; the change of the numerical coefficient is from 5·5 to 4·6.

A drag coefficient k_D is often employed to measure the force retarding uniform translational motion, and for a flat

Fig. 2.

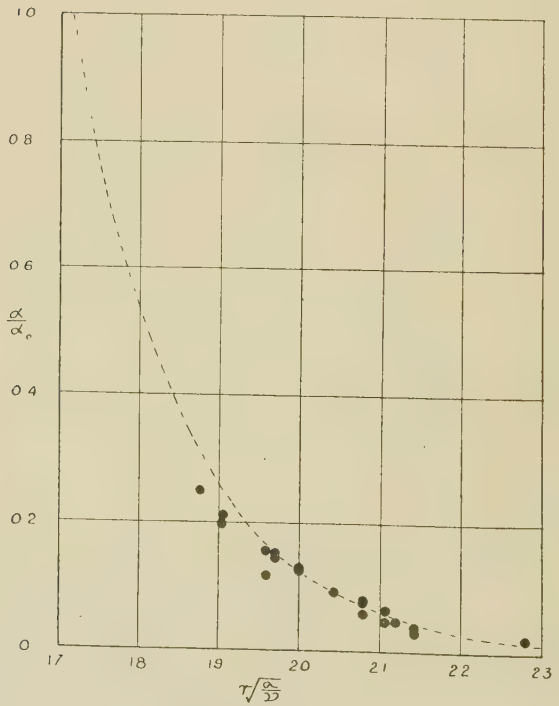

plate of length l moving edgewise with velocity v through a fluid of density ρ may be defined as

$$k_D = \frac{F}{\rho v^2} \quad . \quad . \quad . \quad . \quad . \quad . \quad . \quad (9)$$

where F is the force per unit *surface* area. The approximate solution of Prandtl's boundary layer equations for flat plates moving edgewise enabled Blasius to give the following expression for k_D

$$k_D = \frac{0{\cdot}66}{\sqrt{\frac{vl}{\nu}}} \quad . \quad . \quad . \quad . \quad . \quad . \quad (10)$$

On the assumption δ is small compared with a, equation (5) also yields a simple expression for a representative drag

Fig. 3.

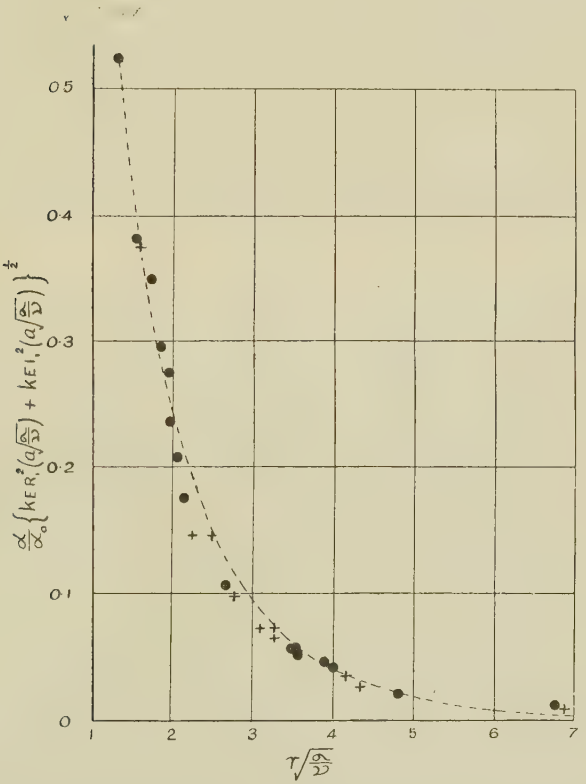

coefficient, defined as the maximum retarding force on the boundary per unit area divided by the density and the square of the maximum velocity of the boundary, as follows :—

$$k_D = \frac{1{\cdot}414}{\sqrt{\frac{V\alpha_0}{\nu}}} . \quad . \quad . \quad . \quad . \quad . \quad (11)$$

For steady translation of flat plates turbulence is known to set in when the Reynolds number, $\frac{vl}{\nu}$, is 10^5 to 5×10^5. So far as this case may tentatively be compared with cylinders in rotatory oscillation it has appeared that the quantity $\frac{V\alpha_0}{\nu}$ might suitably define the Reynolds number. It would be of interest to extend the experiments with other apparatus to values of $\frac{V\alpha_0}{\nu}$, at present limited to 600, as far as 10^5 to see if any correspondence may exist in the range for streamline flow.

The author is indebted to Dr. Piercy, under whose direction the investigation was carried out at East London College.

CV. *Notice respecting New Book.*

The Foundations of Differential Geometry. By O. Veblen and J. H. C. Whitehead. (Cambridge Tracts in Mathematics and Physics, no. 29, 1932. Price 6*s.* 6*d.*)

THIS is a welcome tract. It gives in an interesting historic setting an exposition of the modern point of view in geometry. Long as has been the history of geometry, the present highly fruitful era dates only from 1854, the year of Riemann's famous Dissertation on the problems of comparative geometries.

The current of thought due to the inspiration of Riemann, and the interesting and characteristic ideas of Klein, formulated in his Erlanger programme of 1872, have together dominated the subsequent development of geometrical thought. It is interesting historically to see how the coming of the Theory of Relativity has compelled mathematicians to realize the importance of the Riemannian concept, that a space is a manifold having a certain structure.

This tract has a useful introductory chapter on linear independence, and another upon the Theory of Groups. It sets out to formulate a comprehensive set of axioms upon which differential geometries can be based. It is an interesting exposition of the modern point of view in geometry and is to be heartily welcomed, both by American students to whom the important work of its senior author is already well known, and by English students, who will welcome the entry of the junior author into the geometrical field, to which important contributions were made by Professor Whitehead many years ago.

Fig. 1.

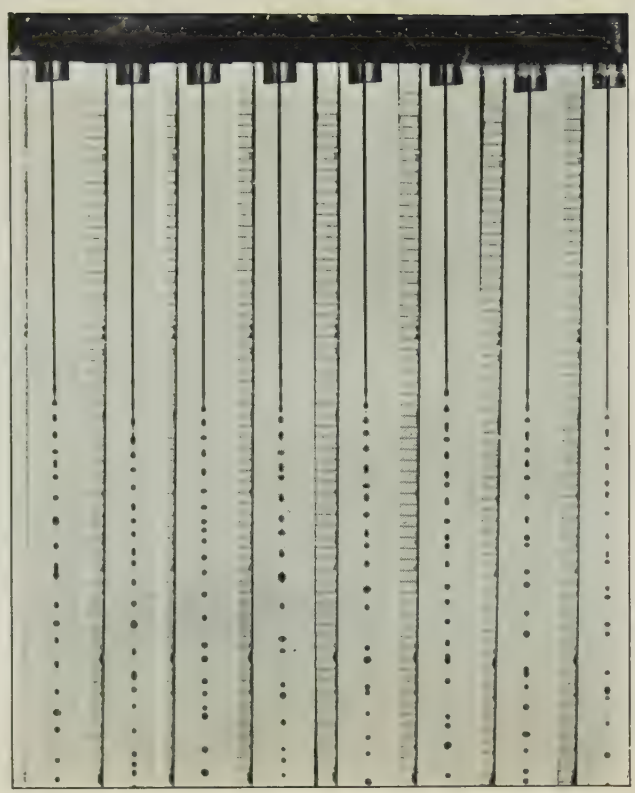

Mercury jets in air. Cylindrical nozzle.
$d = \cdot 30$ mm.

Fig. 2.

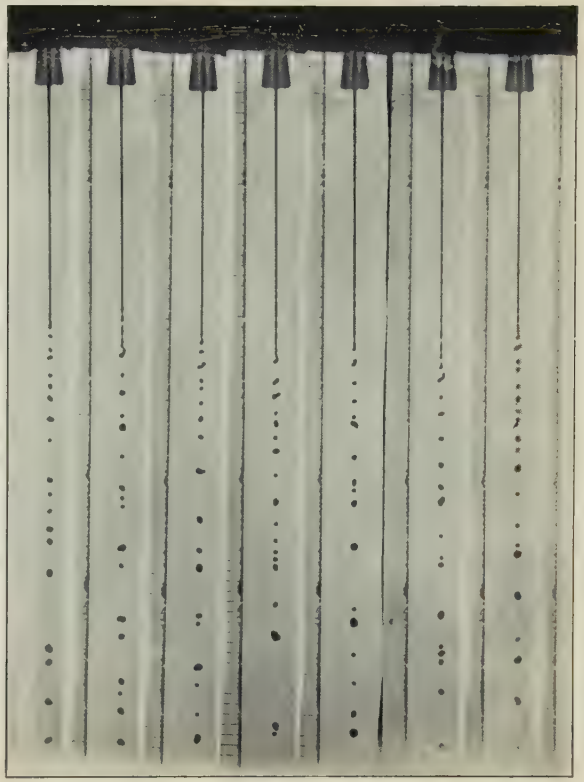

Mercury jets in air. Diverging nozzle.
$d = \cdot 403$ mm.

Fig. 3.

Aniline jets in air at constant speed.
$d = \cdot 501$ mm.
$V = 136$ cm./sec.
L = 2·01 cm. (Average)

Fig. 4.

Aniline jets in water at constant speed.
$d = \cdot 501$ mm.
$V = 52{\cdot}0$ cm./sec.
L = [illegible] (Average)

FIG. 5.

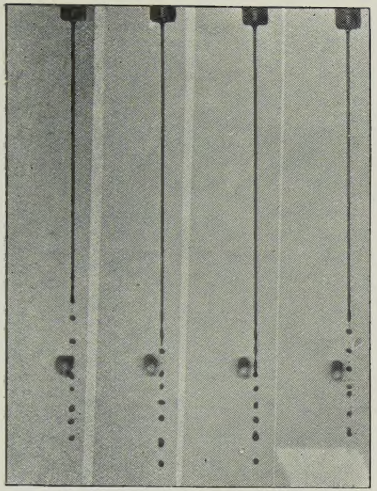

Water jets in air, constant speed.
$d = \cdot 501$ mm.
V = 220 cm./sec.
L = 3·79 cm. (Average).

FIG. 6.

Water jets in paraffin oil.
$d = \cdot 501$ mm.
Various speeds.

(1)	V = 72 cm./sec.	L = ·985 cm.
(2)	V = 95 ,,	L = 2·05 ,,
(3)	V = 97 ,,	L = 2·19 ,,
(4)	V = 228 ,,	L = 1·59 ,,

Critical Velocity 145 cm./sec.

FIG. 7.

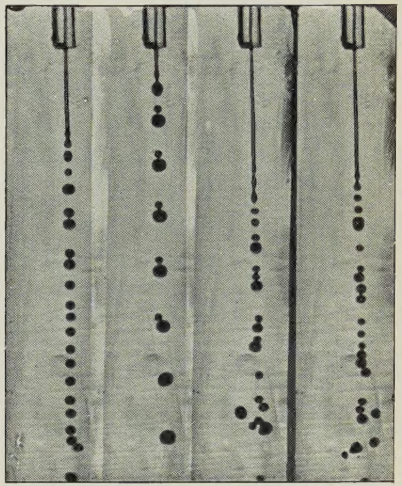

Water jets in turps.
$d = \cdot 501$ mm.
Various speeds.

(1)	V = 72 cm./sec.	L = 1·29 cm.
(2)	V = 60 ,,	L = ·51 ,,
(3)	V = 90 ,,	L = 2·06 ,,
(4)	V = 84 ,,	L = 1·80 ,,

Critical Velocity 125 cm./sec.

FIG. 8.

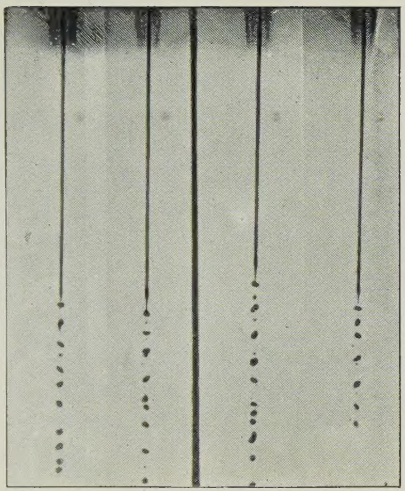

Water jets in air, constant speeds.
d=·650 mm.
V=148 cm./sec.
L=4·57 cm. (Average).

FIG. 9.

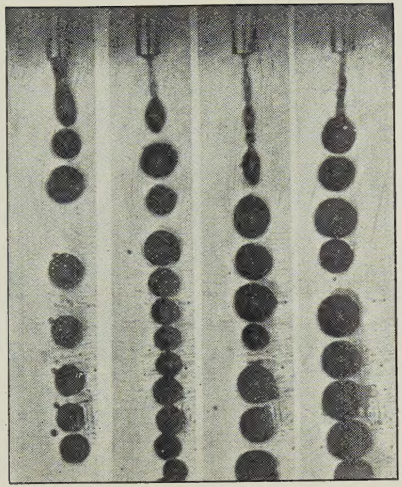

Water jets in warm castor oil.
Different speeds.
d=·650 mm.

FIG. 10.

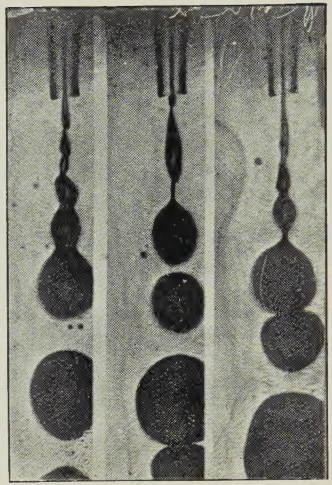

Water jets in cold castor oil.
Different speeds.
d=·650 mm.